
ESRF
The European Synchrotron

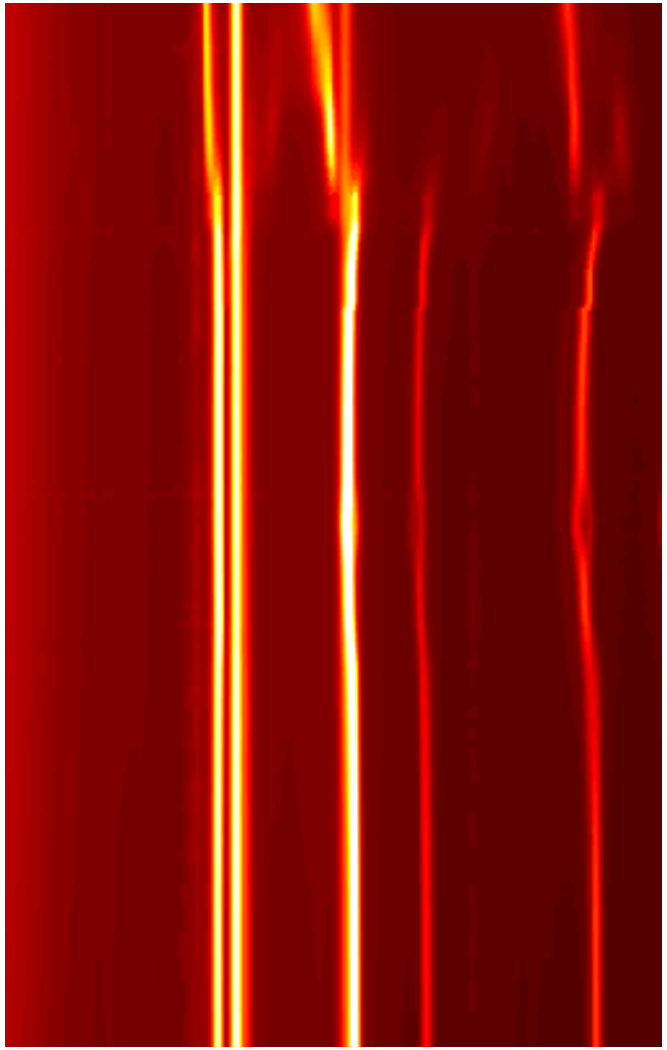

Synchrotron and Neutron Scattering for the study of amorphous materials

G. Cuello & G. Vaughan

X-RAY AND NEUTRON SCATTERING

- **Neutron** scattering is from the nucleus (and magnetic fields)
- **X-rays** scatter (mostly) from electrons

- When describing X-rays scattered from a solid
  - In the crystallographic case, consider that scattering comes from valence electrons = atomic positions,
  - is approximately elastic
  - Scattering from the nucleus and bonding electrons is ignored to the first approximation.

When scattering centres are arranged periodically, the scattering is strongly enhanced at particular angles corresponding to spacings and directions within the crystal

The diffraction peak intensity I is determined by the arrangement of atoms in the crystal and properties of their electron distributions:

$$I_{hkl} \propto |F_{hkl}|^2$$

$$F_{hkl} = S_j N_j f_j e^{2\pi i (hx + ky + lz)}$$

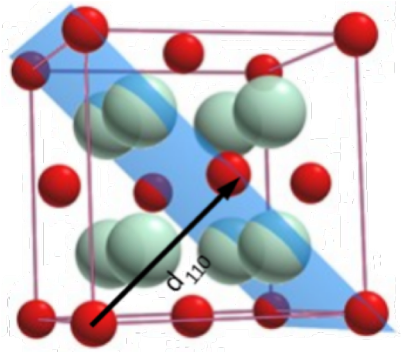

The structure factor F_{hkl} expresses the amplitude of the scattered radiation is thus a function of the type and location of the atoms involved from the (hkl) planes

$f_j \propto \exp(-\sin\theta_{hkl}/\lambda)$, $\propto Z$, for X-rays. Bragg scattering is from valence electrons, diffuse scattering is from all electrons.

$f_j \rightarrow b_j$ = coherent scattering length for neutrons, constant with $\sin\theta_{hkl}/\lambda$ for a given chemical species and isotope..

X-RAY FORM FACTOR

The X-Ray form factor scales roughly with Z, and dies off strongly with scattering angle

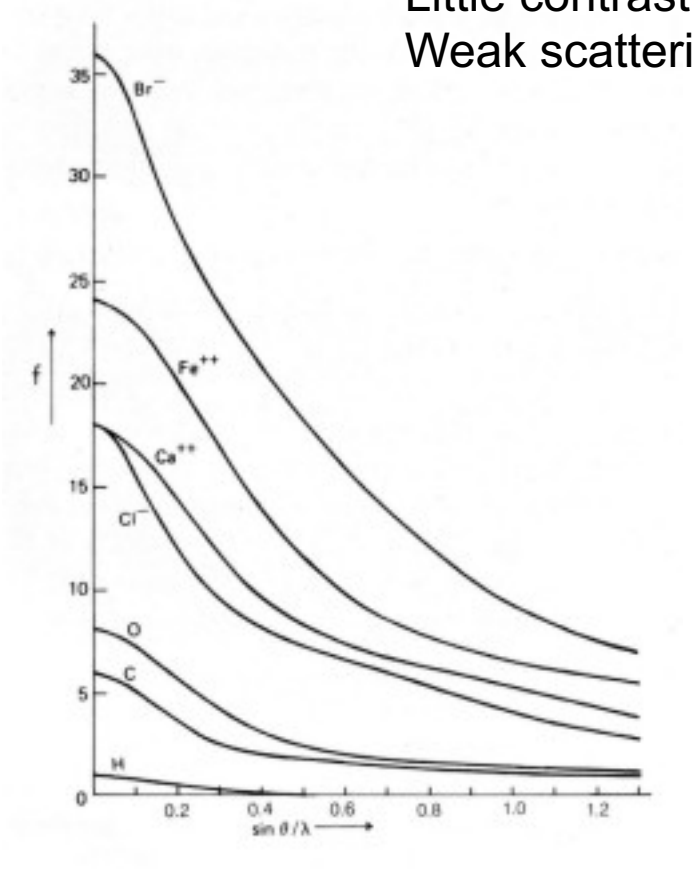

Little contrast between elements with similar Z
Weak scattering at high Q

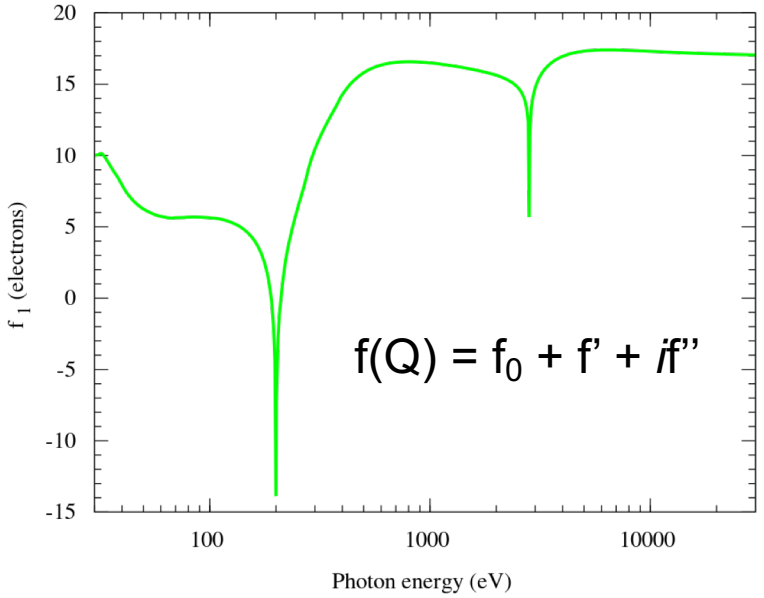

An ‘anomalous’ contribution is strongly peaked at absorption edges

SCATTERING FROM THE DIFFERENT STATES OF MATTER

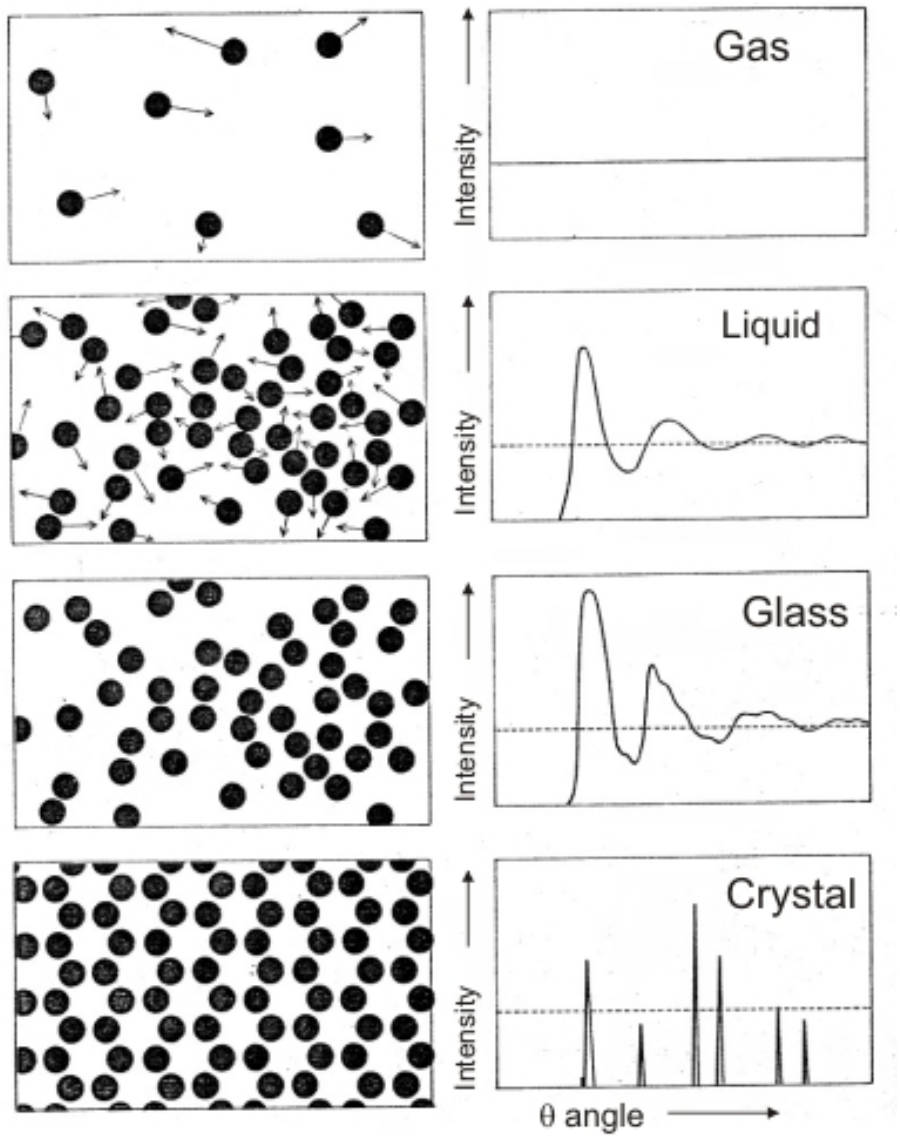

The scattering pattern directly reflects the state of positional order in the material

BRAGG'S LAW

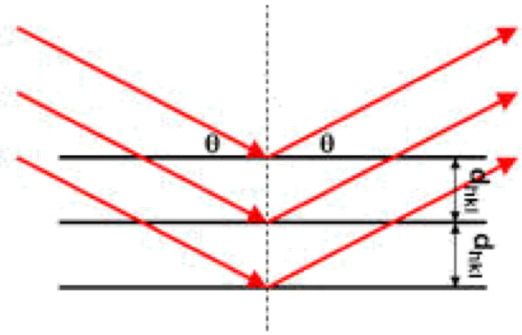

$$\lambda = 2d_{hkl} \sin\theta$$

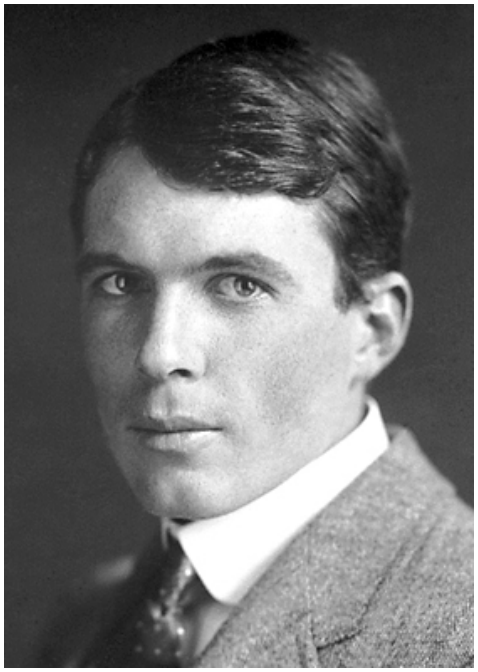

SINGLE CRYSTAL AND POWDER DIFFRACTION

The pattern of the scattered radiation is essentially the Fourier transform of the atomic arrangement (unfortunately we measure the square, however).

If the sample is composed of a **single crystal**, the scattering is highly concentrated into spots corresponding to scattering from particular planes in the crystal.

If the sample is composed of many crystals in a large variety of orientations (a "**powder**"), those spots are distributed in rings at given angles corresponding to the families of planes. These peaks are generally treated with empirical models to extract their intensity, with all the other scattering ignored.

If the sample is amorphous, it's a perfect powder.

CRYSTALLINE AND AMORPHOUS MATERIALS

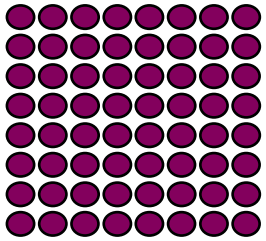

ordered crystal

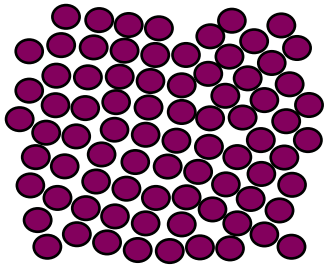

?

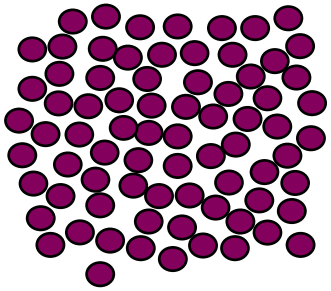

amorphous / liquids

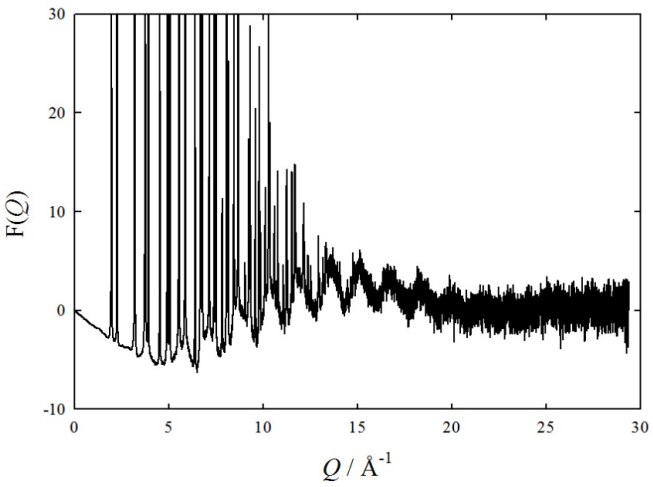

Nanoscale information appears as diffuse scattering underneath the Bragg-peaks in a diffraction pattern

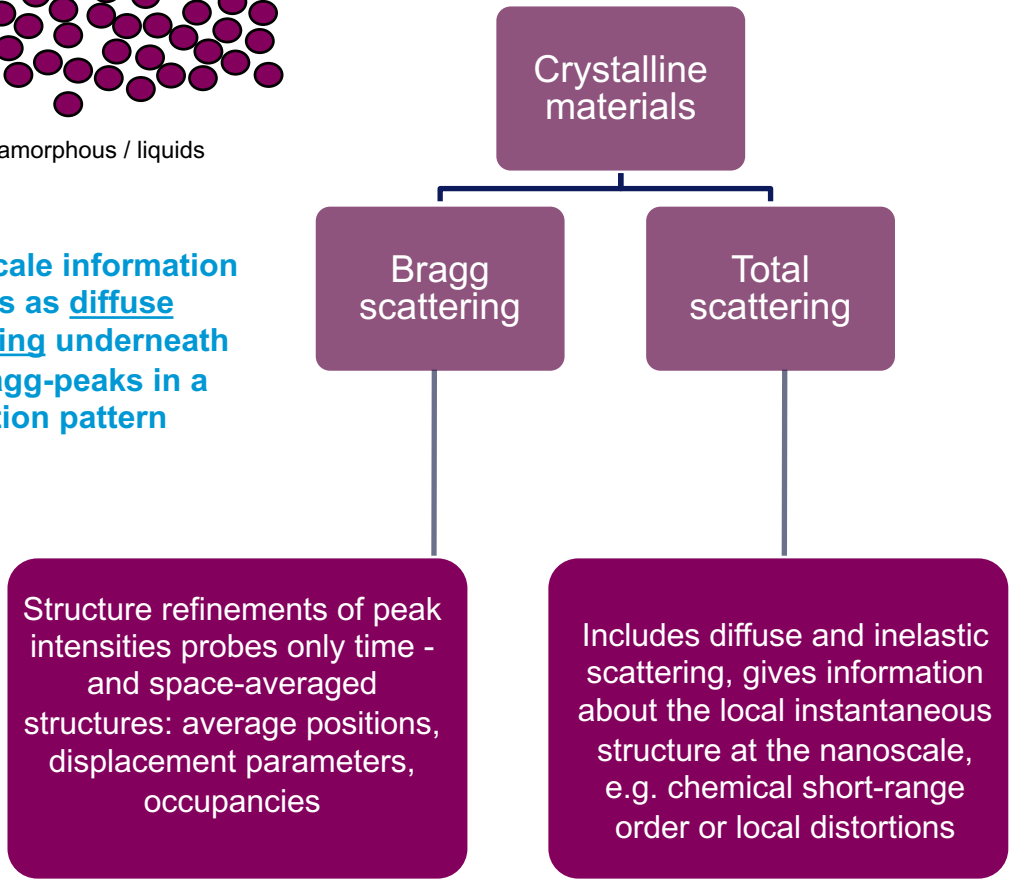

WHAT IF IT'S NOT CRYSTALLINE AT ALL?

The pair-distribution function (PDF) is essentially the Fourier transform of the scattering, and gives a model-free histogram of inter-atomic distances

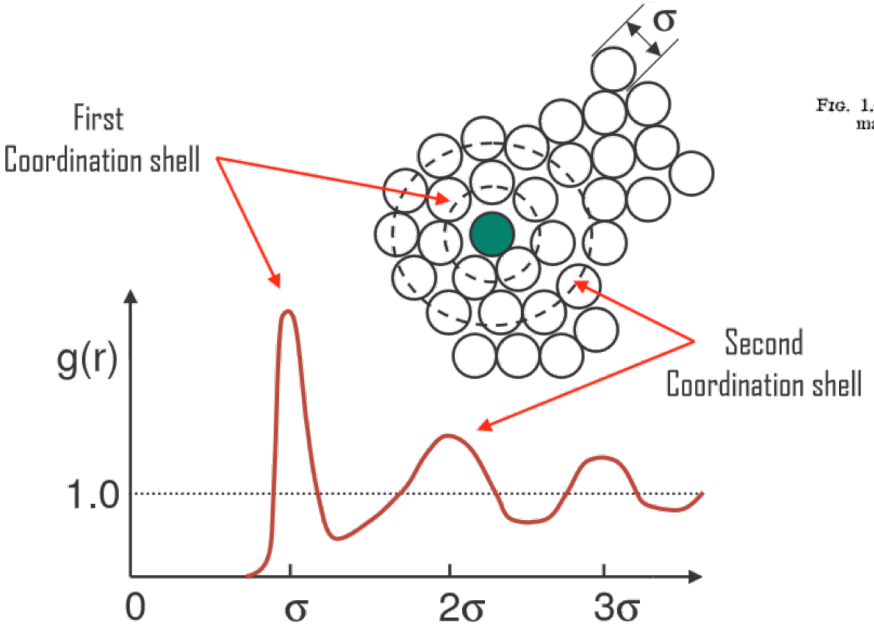

The PDF has been around for a long time

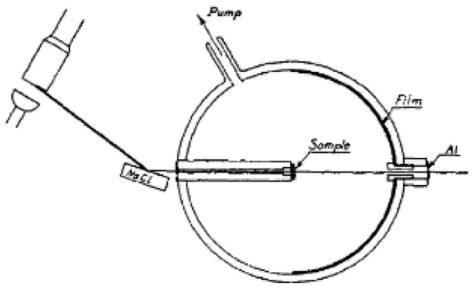

FIG. 1.—Vacuum camera with monochromator for making X-ray diffraction patterns of glass.

Bertram Warren

Needs very high-Q data for clean g(r) (high energy synchrotron, neutron) – now becoming very popular

PDF ANALYSIS

1st PDF

Direct methods

Rietveld methods

Computers

Synchrotrons & Spallation Sources

H E + Area Detectors

1930 1940 1950 1960 1970 1980 1990 2000

liquid Na

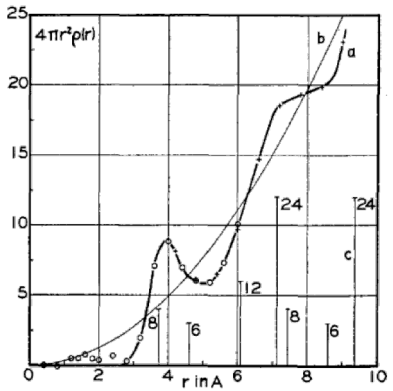

Tarasov & Warren J.Chem.Phys.(1936)

Graphitic Carbon

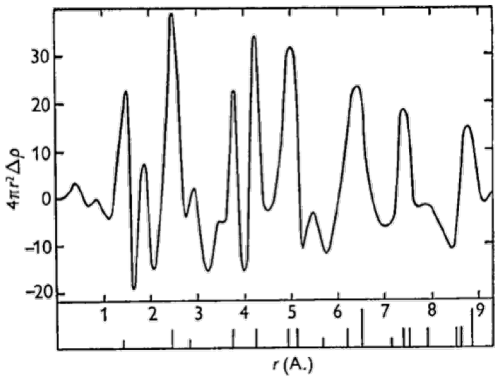

RE Franklin Acta. Cryst. (1950)

Zeolites

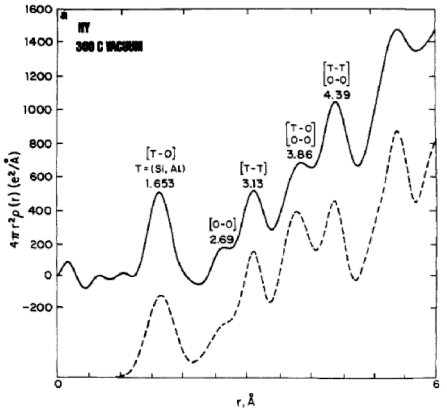

RD Shannon J.Phys.Chem.(1985)

Courtesy of M. Brunelli

GETTING THE PDF FROM THE DIFFRACTION DATA

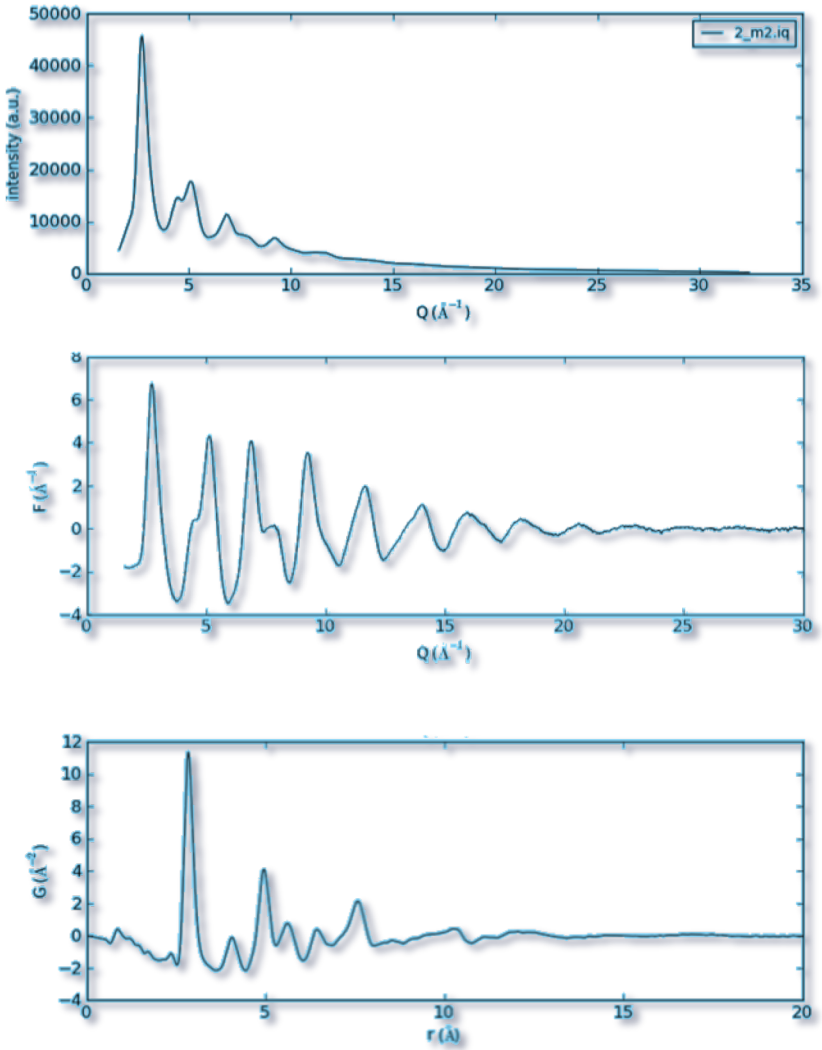

$$S(q) = \frac{I(q) - \langle f(q)^2 \rangle}{\langle f(q) \rangle^2} + 1$$

$$F(q) = q(S(q) - 1)$$

Debye Equation:

$$F(q) = \frac{1}{N\langle f(q) \rangle^2} \sum_{i \neq j} f_i(q)\, f_j(q) \frac{\sin qr_{ij}}{r_{ij}}$$

$$G(r) = \frac{2}{\pi} \int_{q_{min}}^{q_{max}} F(q) \sin qr \, dq$$

$$G(r) = \frac{1}{N\langle f \rangle^2} \sum_{i \neq j} f_i\, f_j \delta(r - r_{ij})$$

FORMAL DERIVATION OF THE PDF

H. E Fischer, A. C. Barnes, P. S. Salmon: “Neutron and x-ray diffraction studies of liquids and Glasses” *Rep. Prog. Phys.* 2006 69 233–299

D. A. Keen: “A comparison of various commonly used correlation functions for describing total scattering” *J. Appl. Cryst.* 2001 34 172

More in-depth information reading:

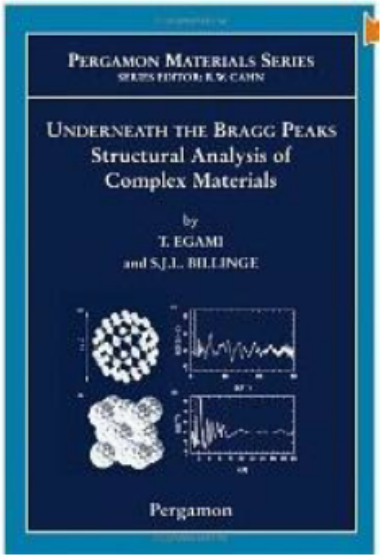

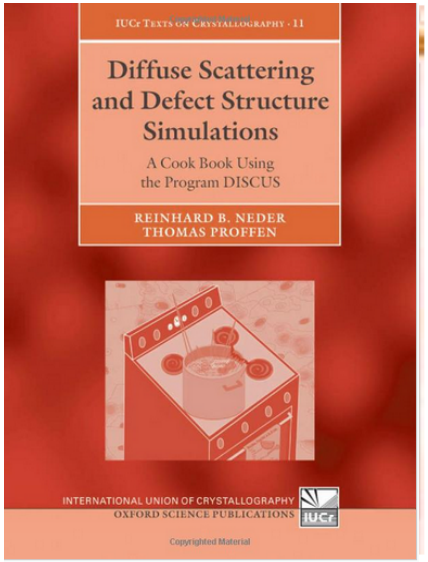

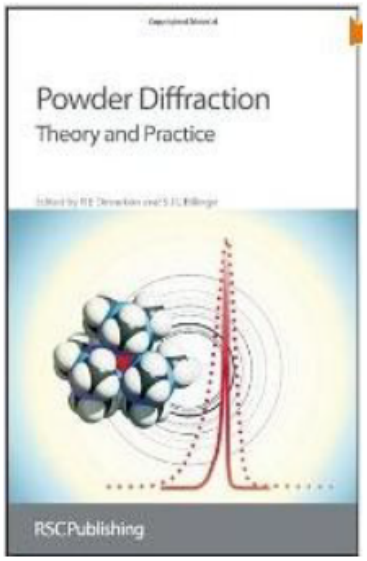

Properties of the PDF

The PDF is a real-space histogram of bond lengths in the material

$$G_c(r) = \frac{1}{r} \sum_i \sum_j \left[\frac{b_i b_j}{\langle b \rangle^2} \delta(r - r_{ij}) \right] - 4\pi r \rho_0$$

The bond lengths are model-independent

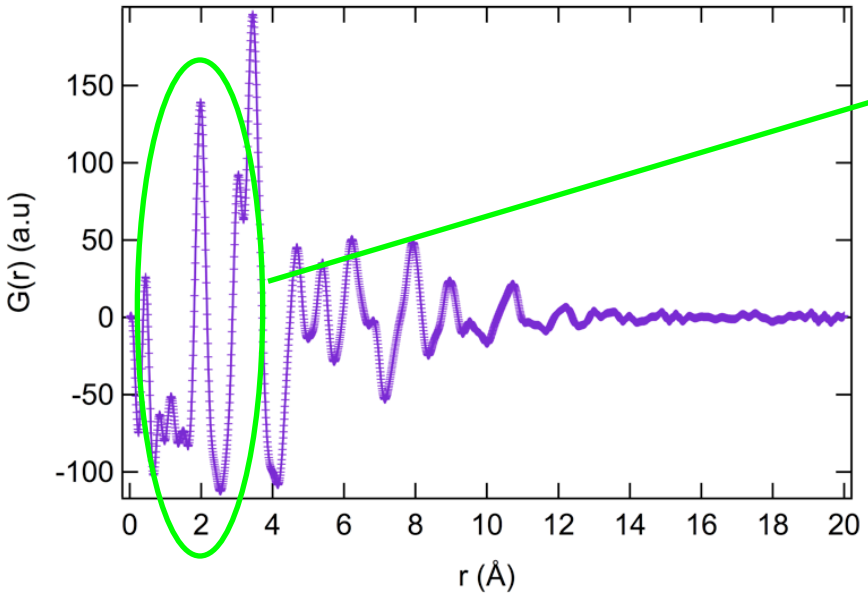

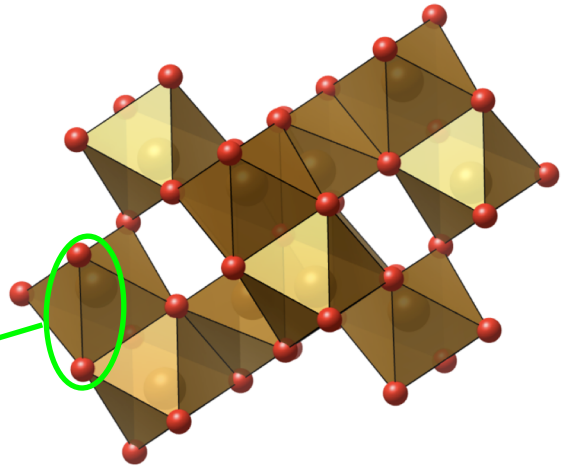

TYPES OF PDFS – MOLECULAR (PLASTIC) CRYSTAL

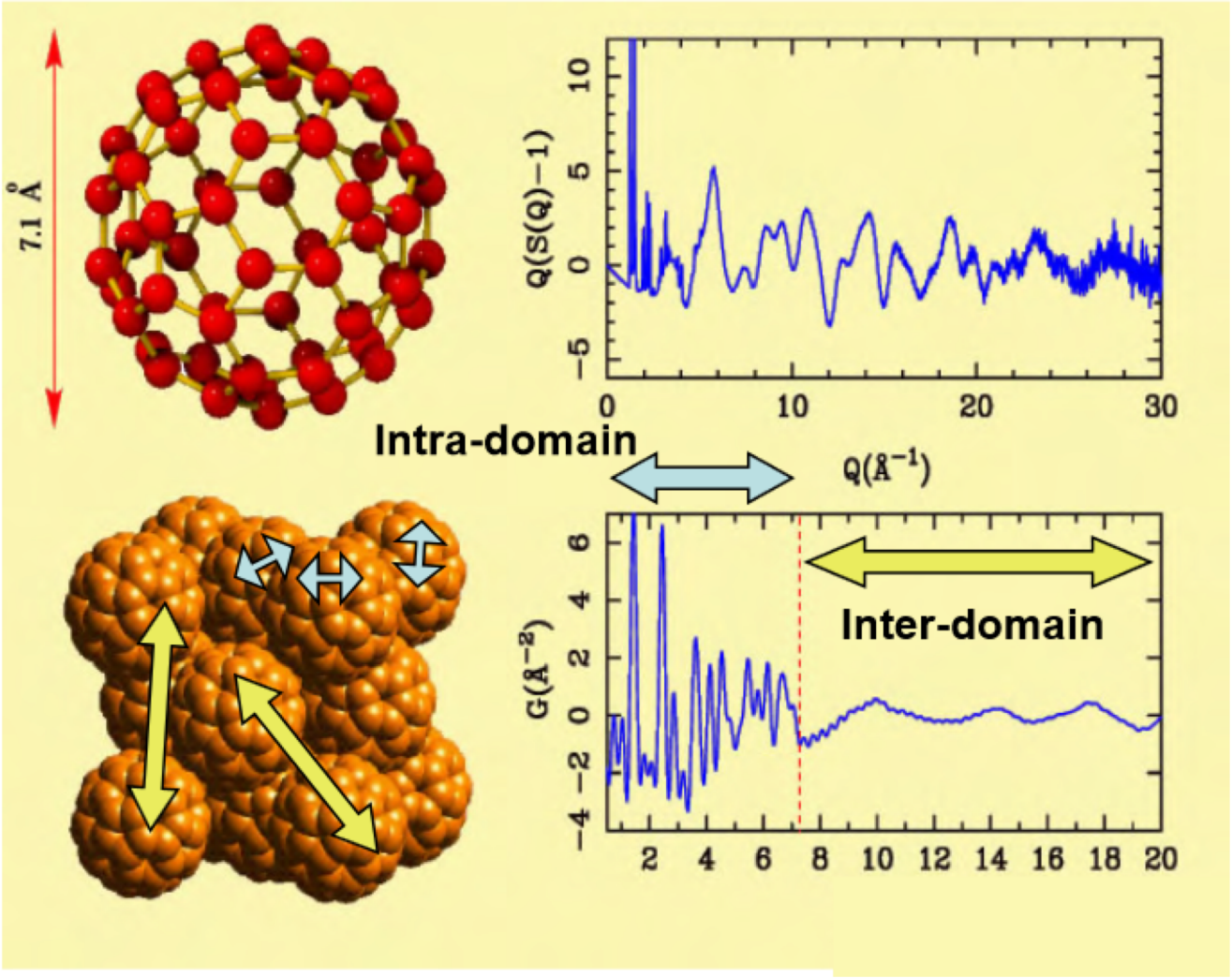

S.H.J. Billinge, Nature 2010

EFFECT OF QMAX

$$G(r) = 4\pi r[\rho(r) - \rho_0] = \frac{2}{\pi}\int_0^{\infty} Q[S(Q) - 1]\sin(Qr)\,dQ \quad \text{(upper limit } Q_{max}\text{)}$$

The ideal F(Q) is multiplied by a step function ⇒ G(r) gets convoluted with a sinc function:

sinc(*r*) = *sin*(Q_{max} *r*) / *r* ⇒ *r-resolution* ≈ π/Q_{max}

good r-resolution of G requires large Q_{max}

$Q = 4\pi \sin\theta/\lambda$

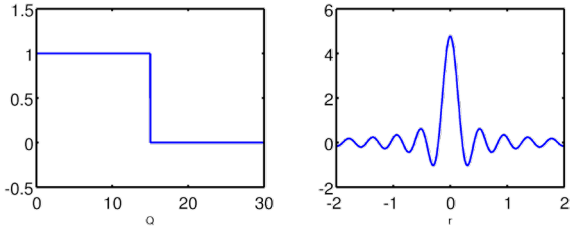

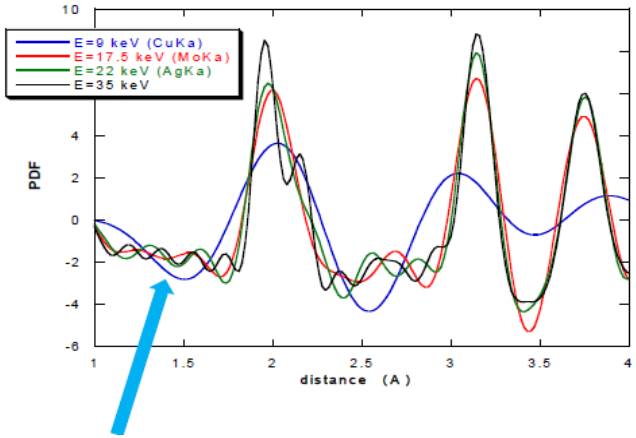

- Ripples due to FT termination at Q_{max}
- Q-position changes vs Q_{max}
- Similar effects may also be due to any correction error with a slow *Q* dependence

EFFECT OF QMAX

To get rid of ripples one should collect data up to very high Q_{max}.

- The black curve has Q_{max} = 8 Å^{-1} and corresponds to the PDF that one can obtain by employing a laboratory diffractometer equipped with a Cu anode.
- Modern diffractometers can have a Mo, or even Ag anode, which allows to access higher Q_{max}, around 20 Å^{-1}.
- Synchrotron radiation data are typically terminated to Qmax >~ 28 Å^{-1} (some ripples my be still present).
- Ripples almost disappear only reaching Q_{max} = 50 Å^{-1}.

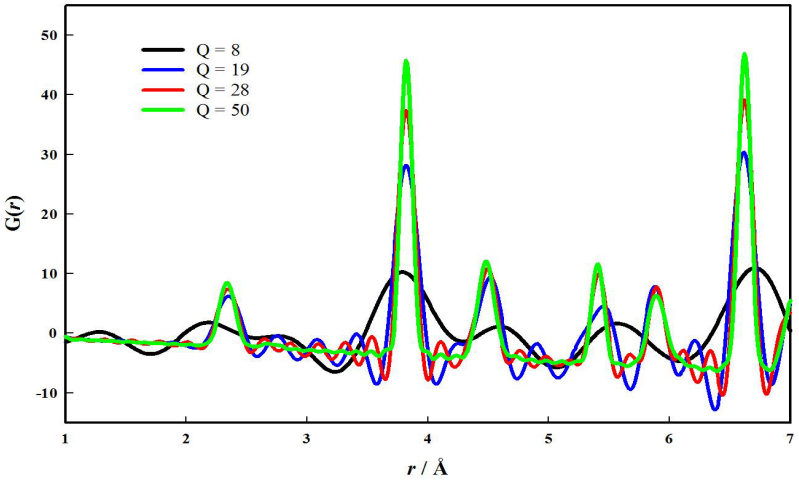

Calculated XRPD G(r) curves for CeO_2 terminating the FT at different Q_{max} values indicated in the plot in Å^{-1} units.

SYNCHROTRON BEAMLINES FOR PDF

Most synchrotrons have one or more beamlines carrying out PDF, some have dedicated stations

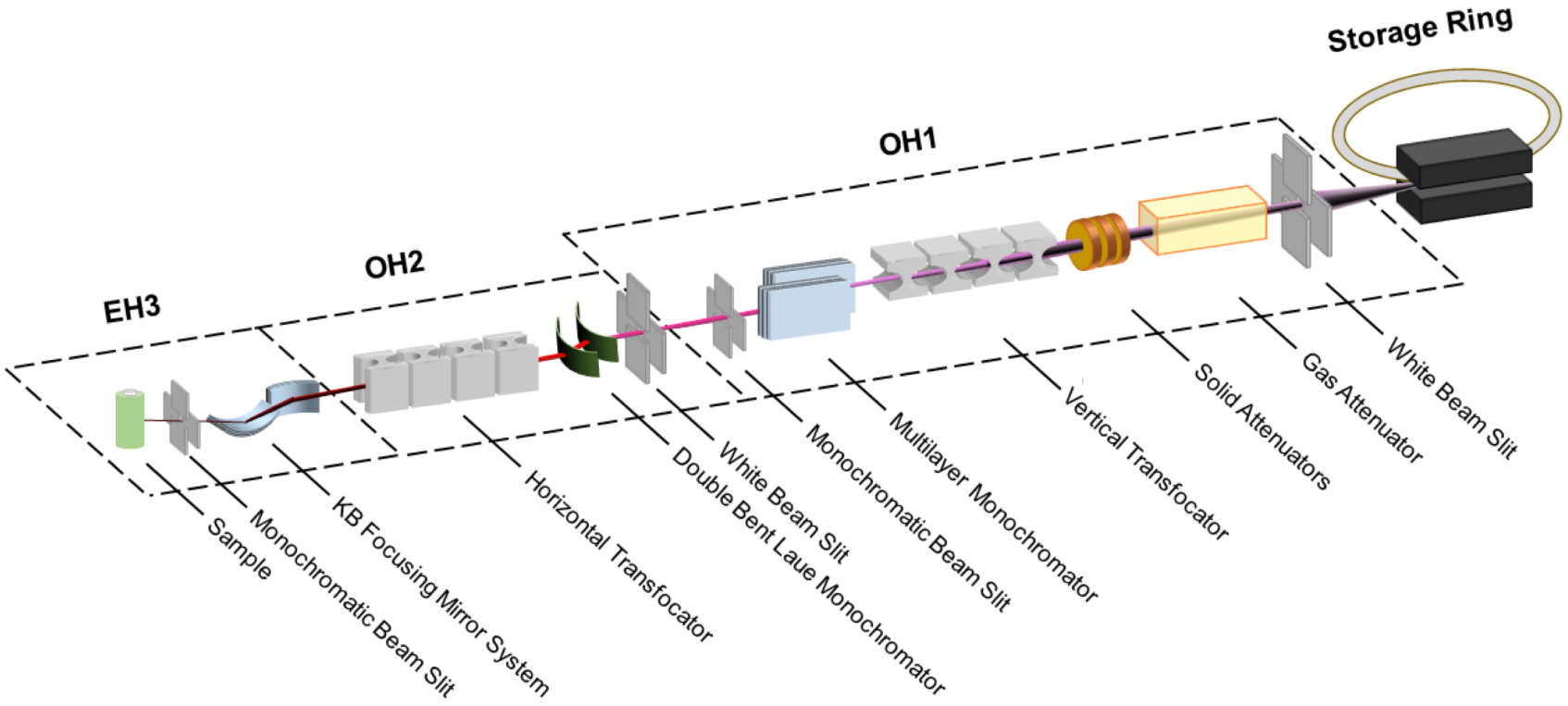

DATA ACQUISITION

Continuous Transform on finite data

- High q – implies high energy (> 70 keV)

Good statistics

- Particularly at high q; contrary to form factor behaviour

Low/well characterized background

- Minimize inelastic scattering
  - avoid absorption edges (W, Pb, …)
  - using energy discrimination
- Clean background – minimize parasitic scattering
  - sample environment
  - tomographic methods

Moderate band pass (10^{-3} $\Delta E/E$) tolerable

INELASTIC AND PARASITIC BACKGROUNDS

$$I = I_e + I_{ie} + I_p$$

$$I = I_e + \left(I_{istruct} + I_{Comp} + I_{Fluo}\right) + I_p$$

Fluorescence comes from all absorption edges below the incident energy
Fluorescence can be 80% of the signal at high Q

Jablonksi diagram depicting simple 1 photon excitation fluorescence

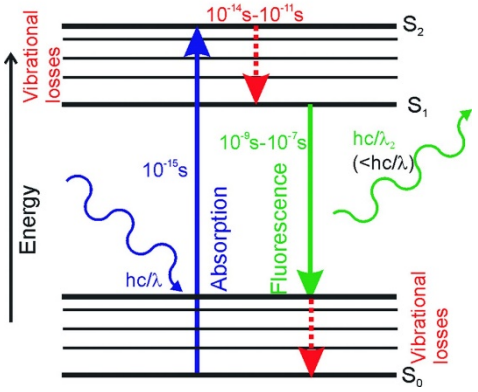

Compton scattering has a spatial and energy distribution

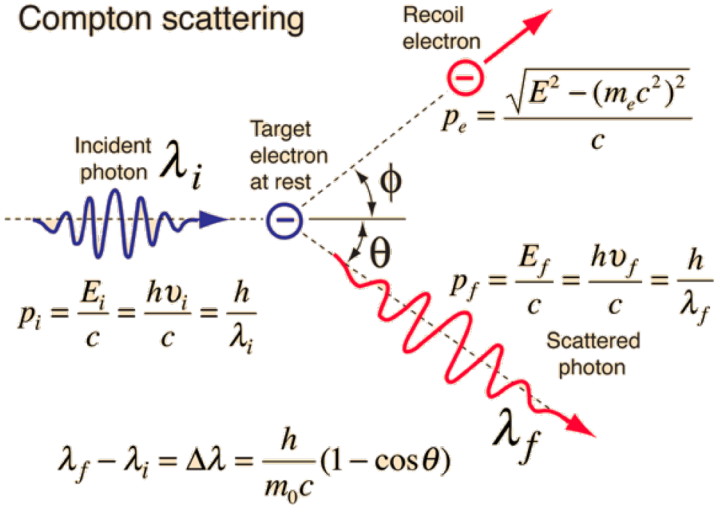

DETECTORS – POINT DETECTOR(S) AND ANALYSER CRYSTAL(S)

Scintilators and PMT

- Angle sensitive
- Energy discrimination
- Background elimination
- Good dynamic range
- Photon counting
- Very high angular resolution
- Accurate lattice parameters
- Slow

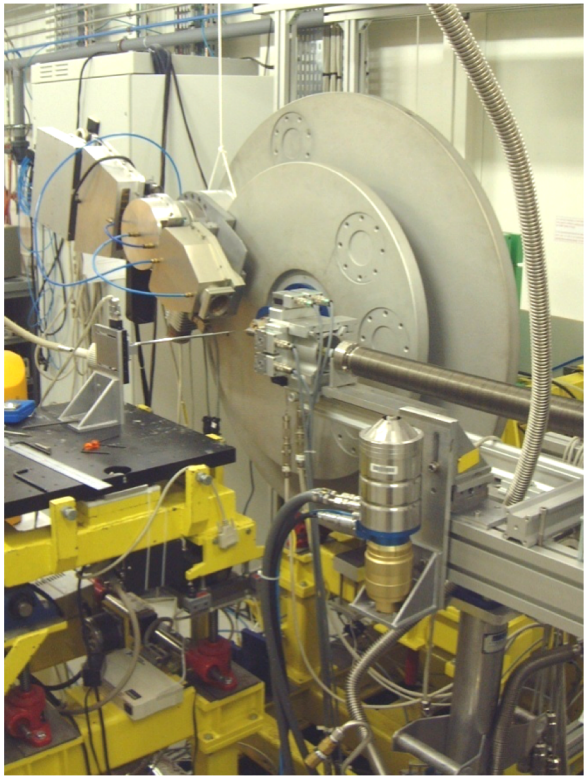

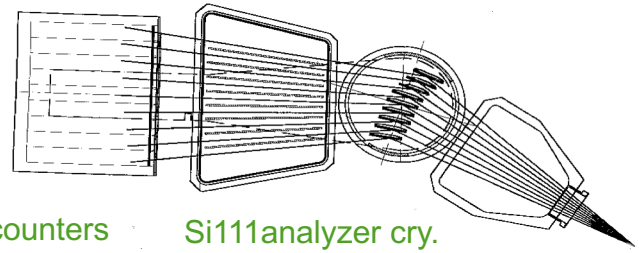

DETECTORS – 2D DETECTORS

Mostly Developed for Medical Imaging

- Flat panel detectors
- CCD/CMOS cameras coupled to scintillators
- Pixel detectors

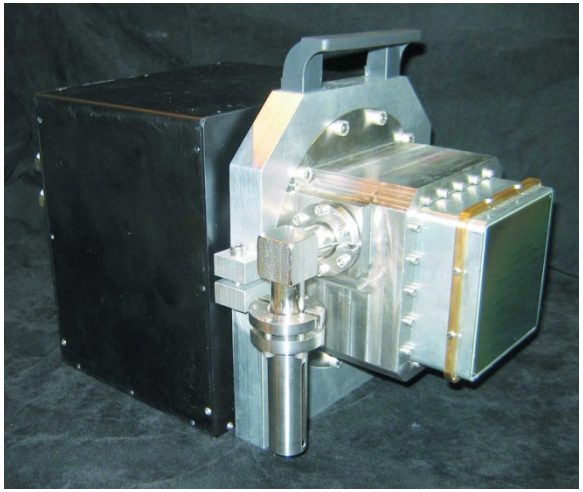

2D DETECTORS

	Advantages	Disadvantages
CCD/CMOS Cameras Phosphor coupled	Stable Background Stable Flat Field	High Background Limited Dynamic Range Large PSF Low Sensitivity Integrating
Flat Panel	High Sensitivity Stable Flat Field No PSF Cheap	Very High Background Variable Background Integrating
Pixel Detectors	High Dynamic Range High Sensitivity Photon Counting Zero Background Energy Discrimination Stable Flat Field No PSF	Price

EFFECT OF ELECTRONIC NOISE

$$I = (I_0 - D)R$$

$$I = (I_0 - D)\frac{\langle R \rangle}{R_i}$$

$$D = \frac{1}{N_D}\sum D_j = \frac{n_D}{N_D}\sum I_{0,j} = n_D I_0$$

$$\sigma_I^2 \cong \sigma_{I_0}^2\left[1 + \frac{n_D}{N_D} + \frac{(1-n_D)^2}{n_R N_R}\right]$$

$$\begin{aligned}\sigma_{\langle R \rangle}^2 &= \left(\frac{1}{N}\right)^2 N\sigma_{R_i}^2 \\ &= \left(\frac{\sigma_{R_i}^2}{N}\right) \\ &\approx 0\end{aligned}$$

COMPARISON OF FLAT PANEL AND PIXEL DETECTOR

	Pilatus3 X CdTe 2M	Perkin Elmer XRD 1621
Detection technology	Hybrid photon counting	Flat panel
Sensor material	CdTe	CsI
Pixel size [μm^2]	172×172	200×200
Total number of pixels (H × V)	1475×1679	2024×2024
Maximum frame rate[Hz]	250 (500 with ROI)	15 (30 with 2×2binning)
Point Spread Function (FWHM)	1 pixel	2 pixels
Energy threshold [keV]	8-40	none
Maximum count rate [ph/s/pixel]	5×10^6	Integrating detector
Non linearity	<2% at 10^6 counts/s/pixel	
Counter depth	20 bit	16 bit
Dynamic range	20 bit	12.8 bit
Minimum exposure [ns]	200	33000000
Image lag	0	~1% after 100ms

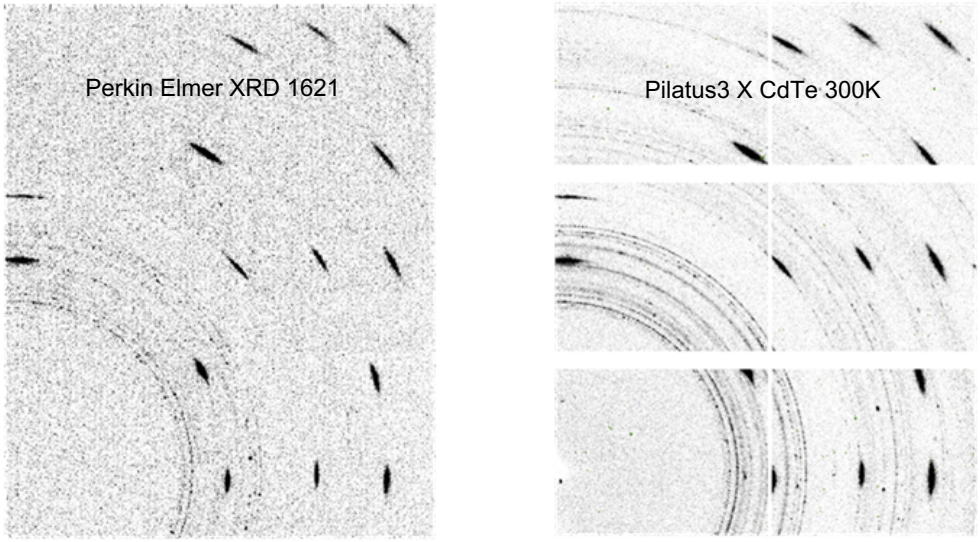

Superconducting filament, Ø50 μm, measured at 50 keV, with exposure time of 100ms with a Perkin Elmer XRD 1621 flat panel detector (left) and with the Dectris Pilatus3 X CdTe 300K prototype

REDUCTION OF XRD DATA

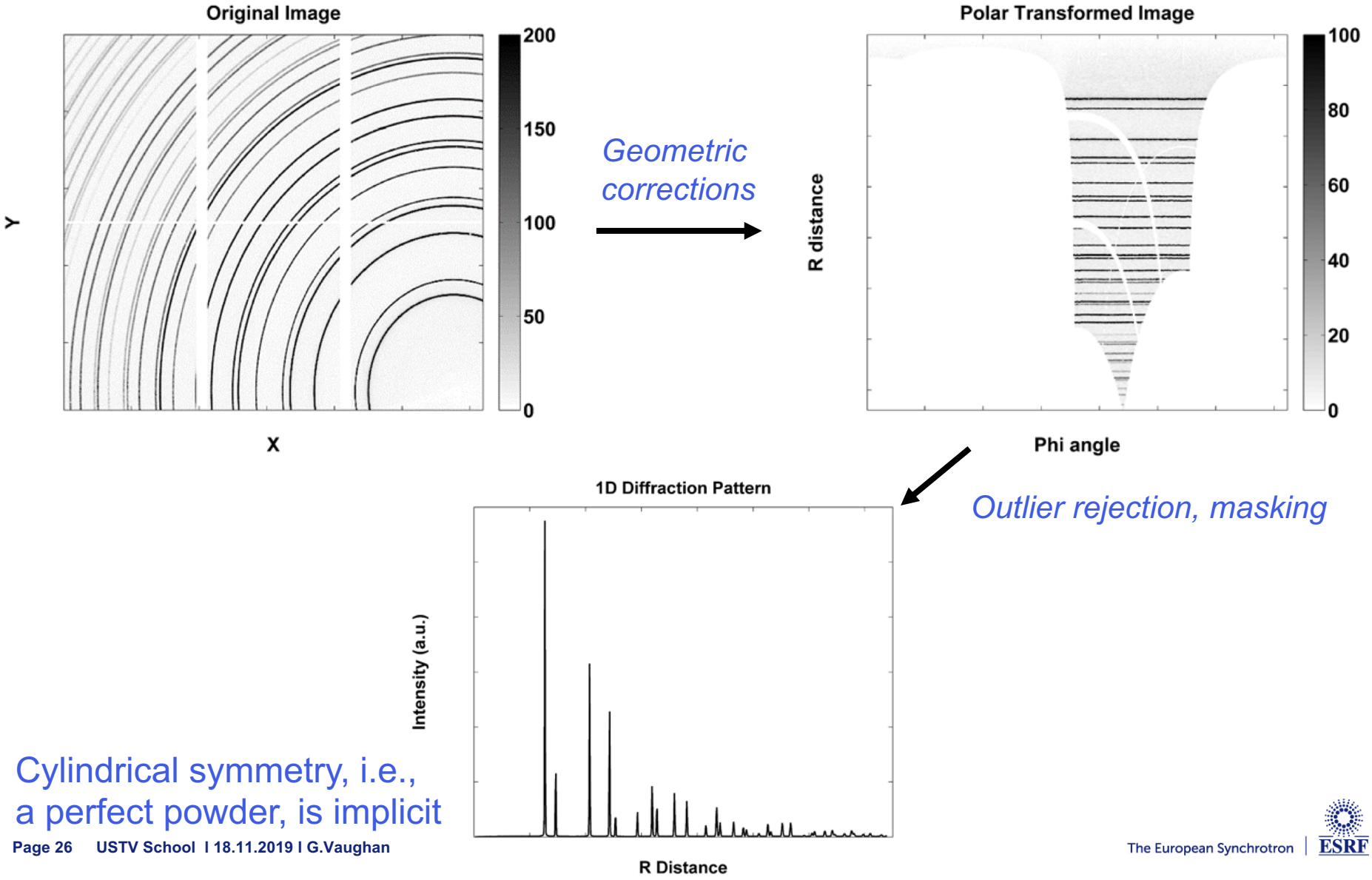

Cylindrical symmetry, i.e., a perfect powder, is implicit

EFFECTS OF SAMPLE GEOMETRY - BROADENING

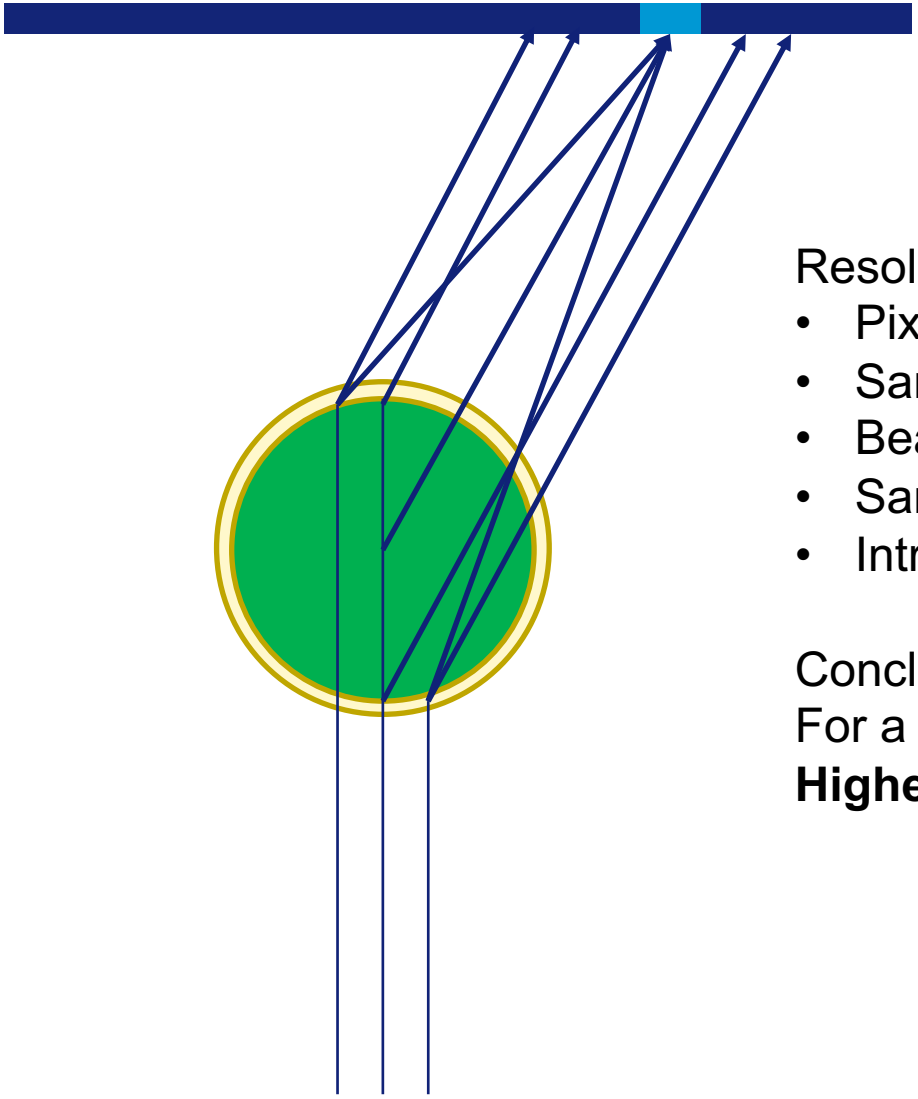

Resolution dependent on

- Pixel Size
- Sample – Detector Distance
- Beam Size
- Sample Size
- Intrinsic Broadening

Conclusion:
For a given Q-range, best to use
Higher Energy/further distance

EFFECTS OF SAMPLE GEOMETRY – ABSORPTION

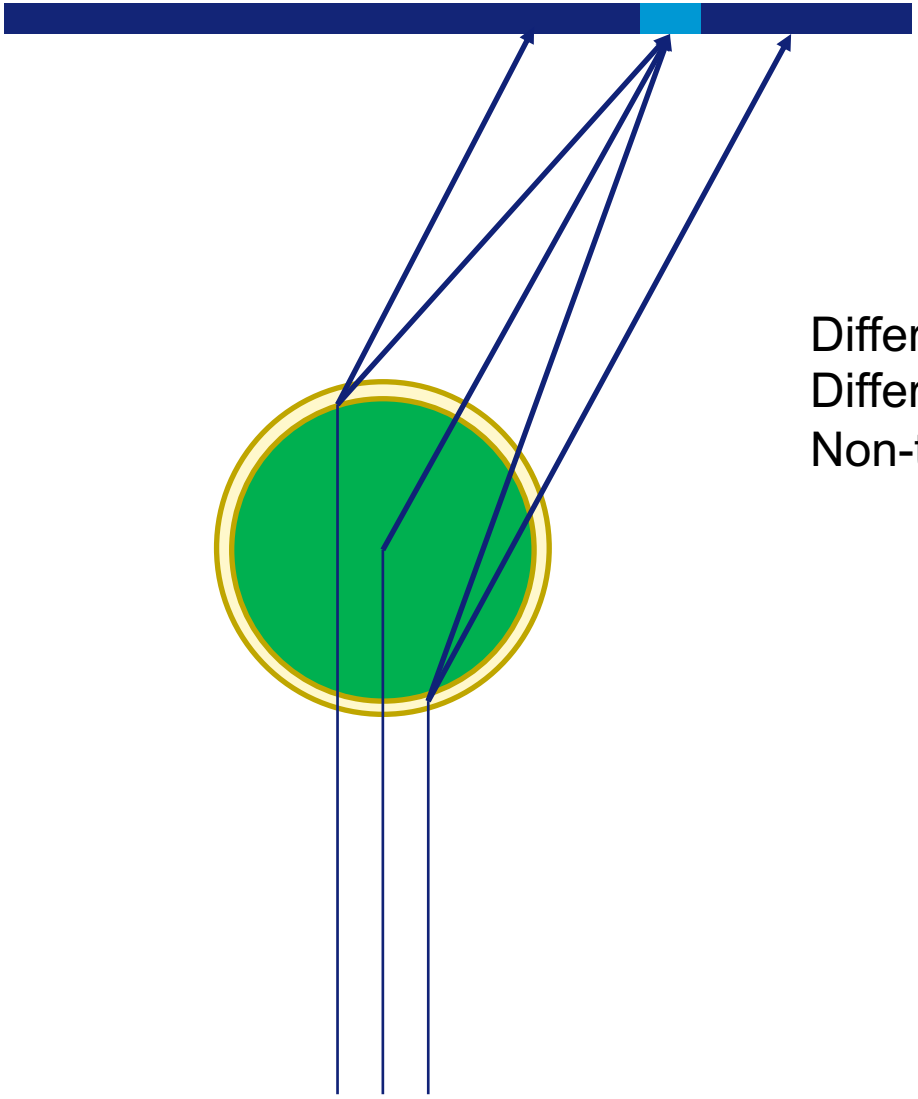

Different Rays have different pathlengths
Different angles have different signal
Non-trivial absorption correction

EFFECTS OF SAMPLE GEOMETRY – BACKGROUND SUBTRACTION

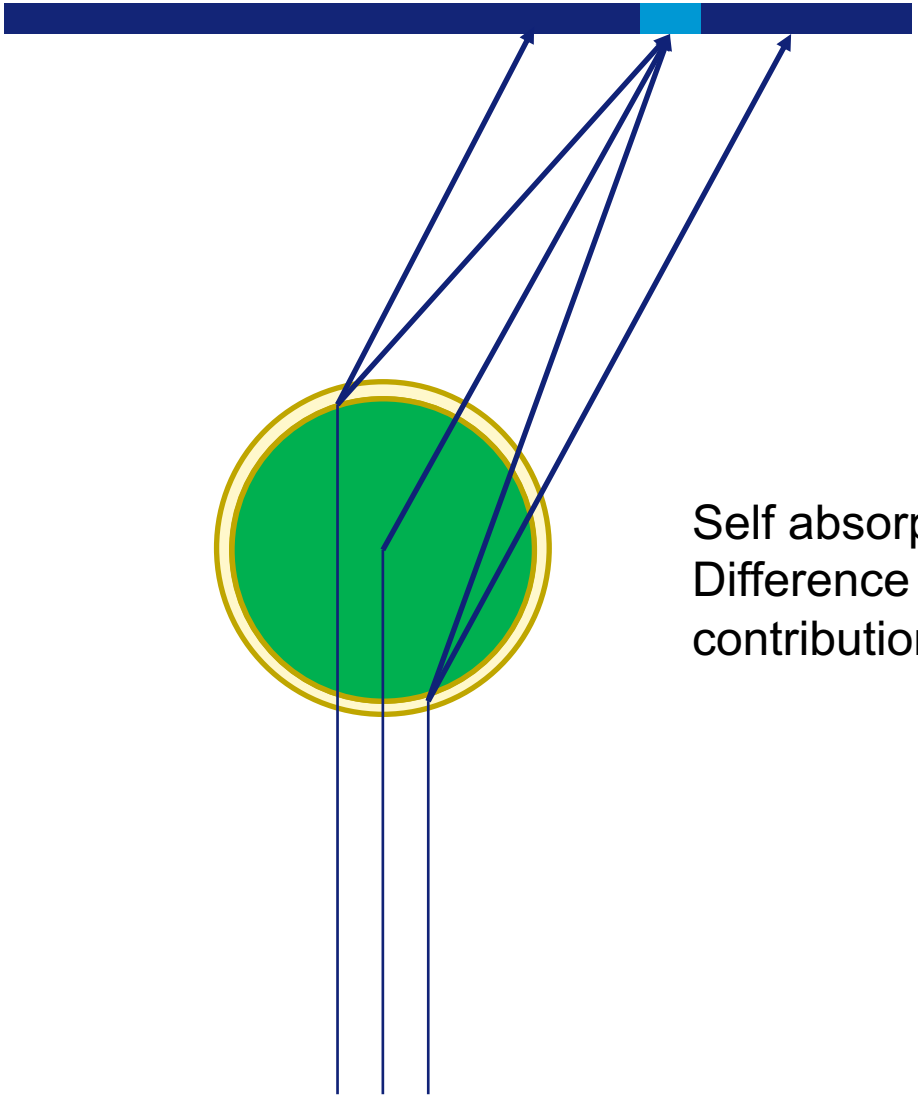

Self absorption affects background subtraction
Difference pattern will slightly oversubtract back contribution

EFFECTS OF SAMPLE GEOMETRY – 2D CASE

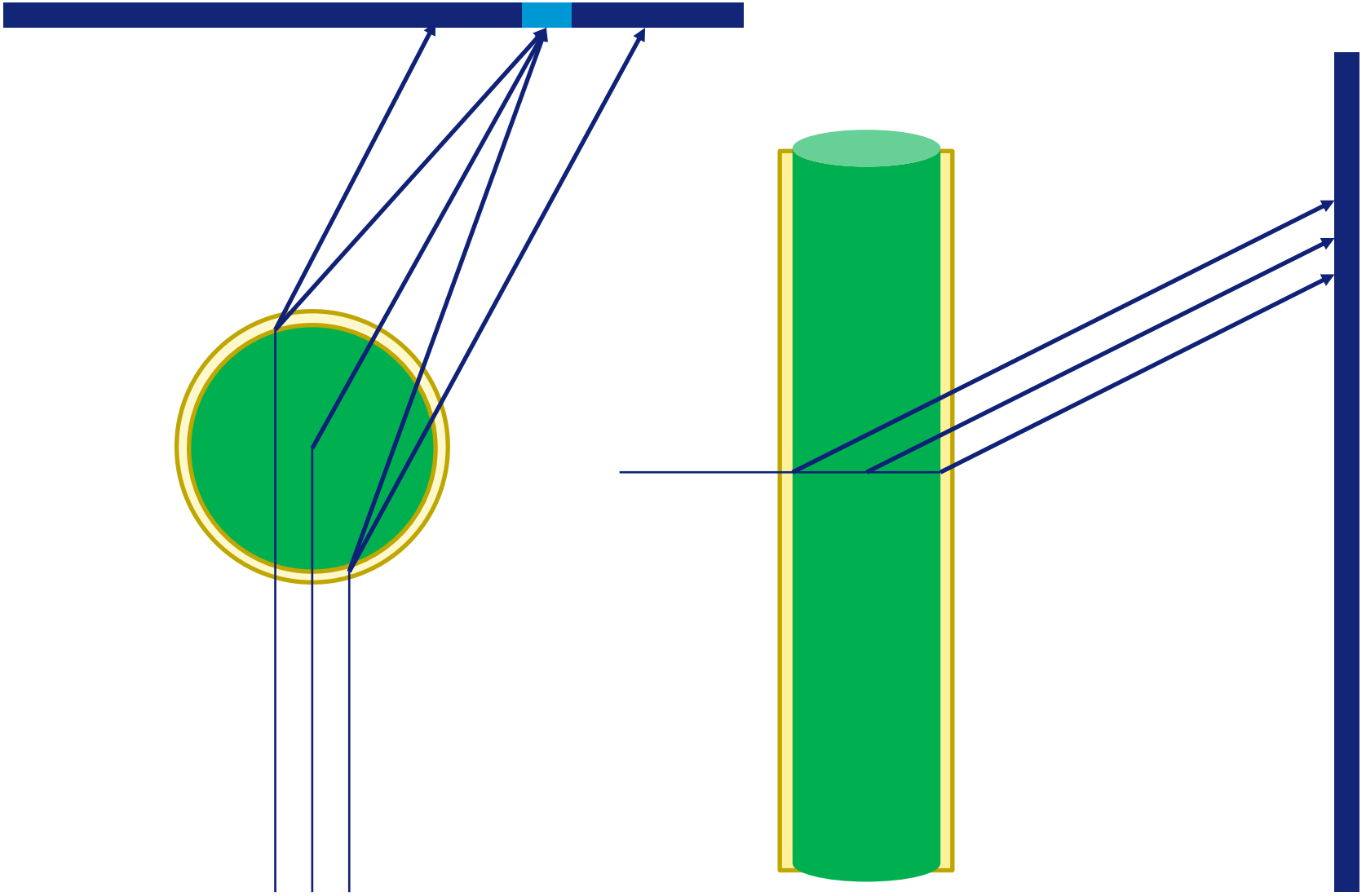

POLARIZATION CORRECTOIN

Polarization correction depends on

- **Scattering angle**
- **Azimuthal angle (synchrotron plane polarized)**
- **Optical and sample configuration**
  - Every scattering event affects the polarization
  - Right/left symmetry broken by sample scattering

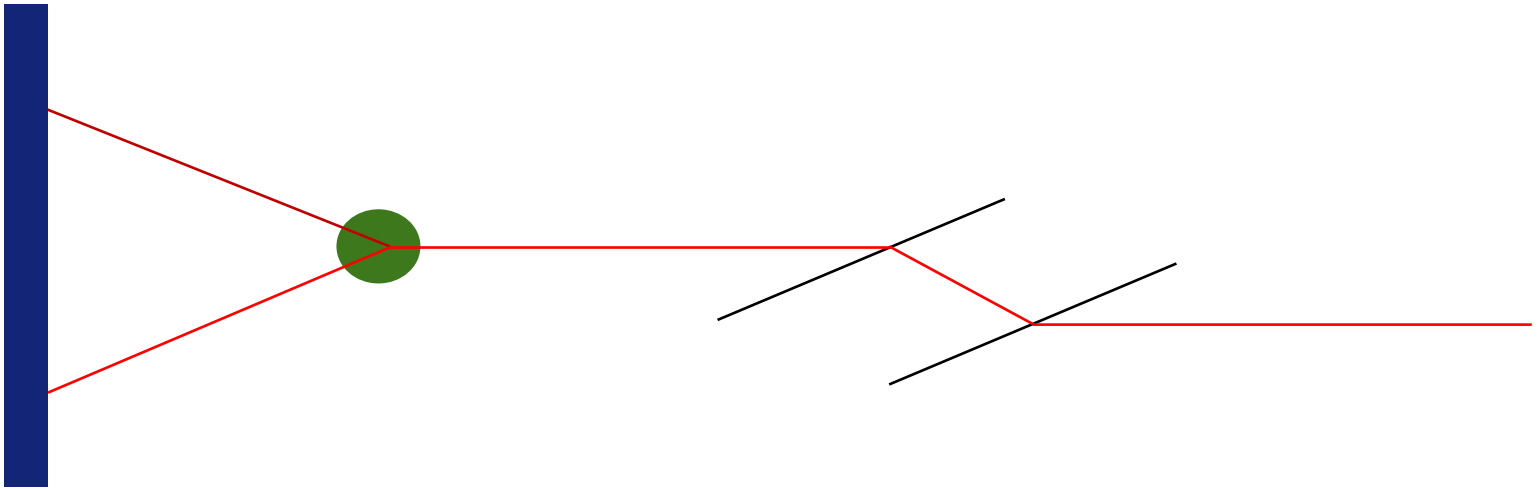

EFFECT OF SAMPLE GEOMETRY

Sample Geometry affects

- **Angular Resolution**
- **Absorption correction**
- **Background subtraction**

Convolution of (rapidly-varying) scattering pattern means that a proper treatment would require ray-tracing (algebraic reconstruction)

Achievable (in progress) but not in general plausible

- **Tomographic data collection**
- **Iterative computation**

Precise polarization correction difficult to implement

- **This can be seen with noiseless detectors and good statistics at high Q**

"Solution" ← i.e., work-around to hide the problems

- **Use either 90 or 360 azimuthal degrees**

EXAMPLE OF A BMG - MASKING

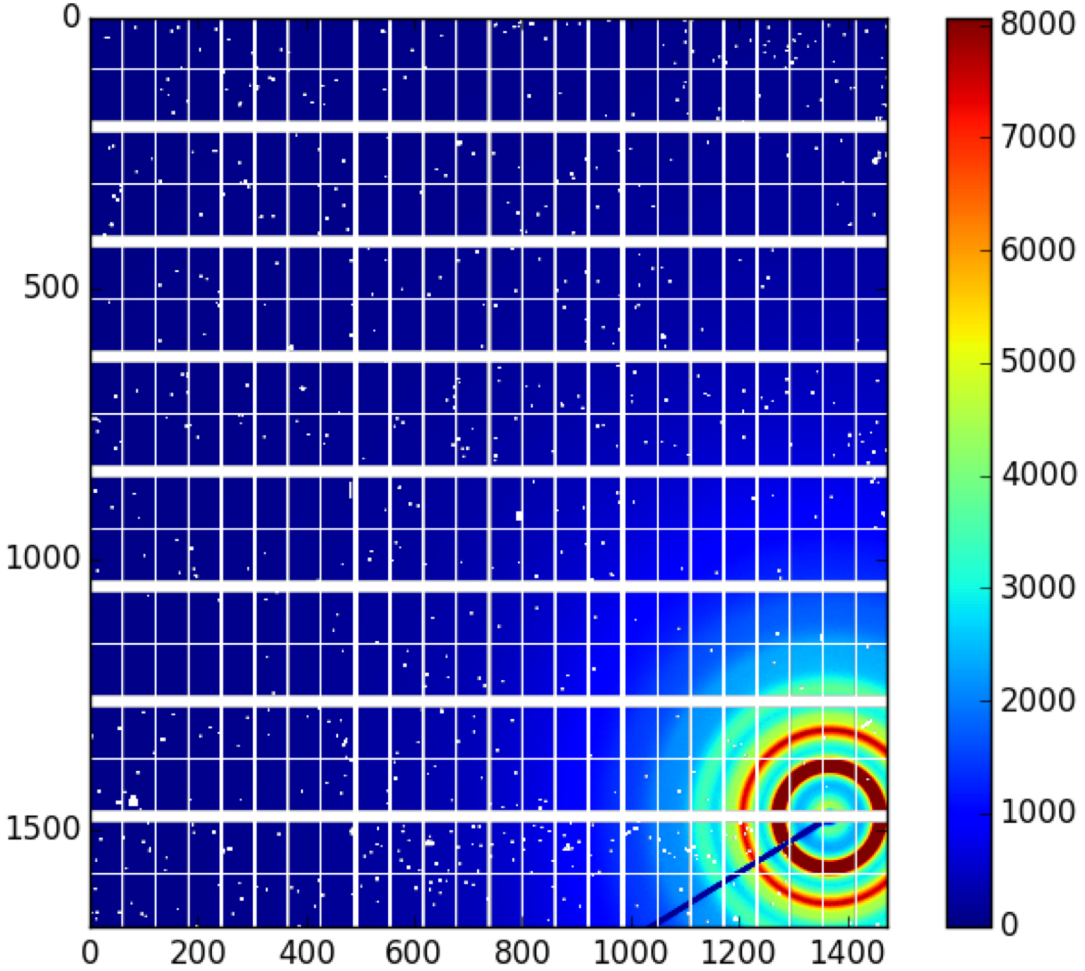

BMG

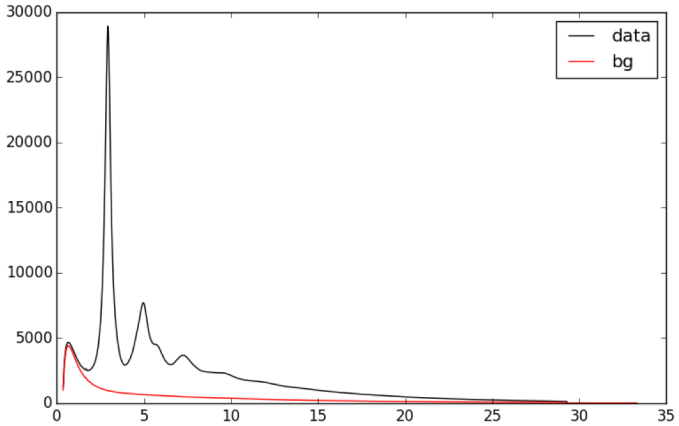
data
bg

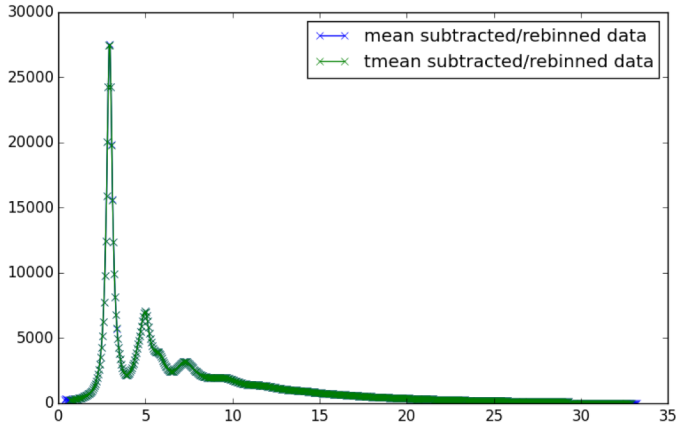
mean subtracted/rebinned data
tmean subtracted/rebinned data

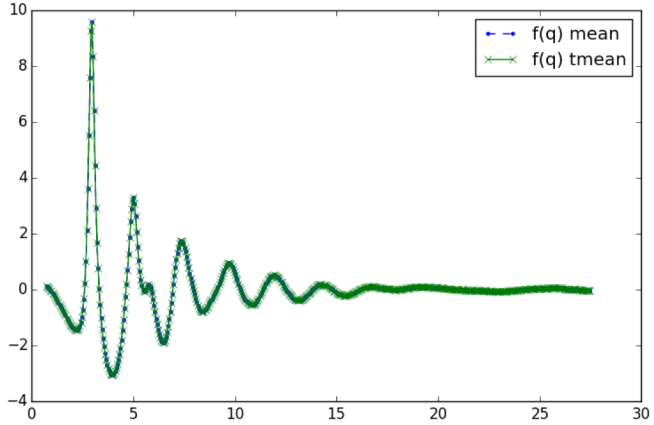
f(q) mean
f(q) tmean

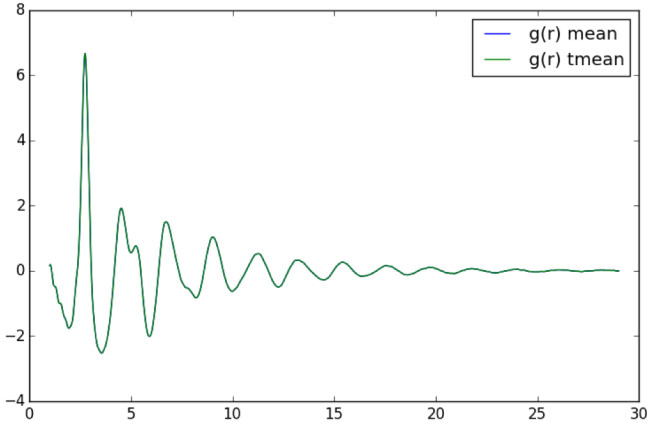
g(r) mean
g(r) tmean

EFFECT OF NOISE ON G(R)

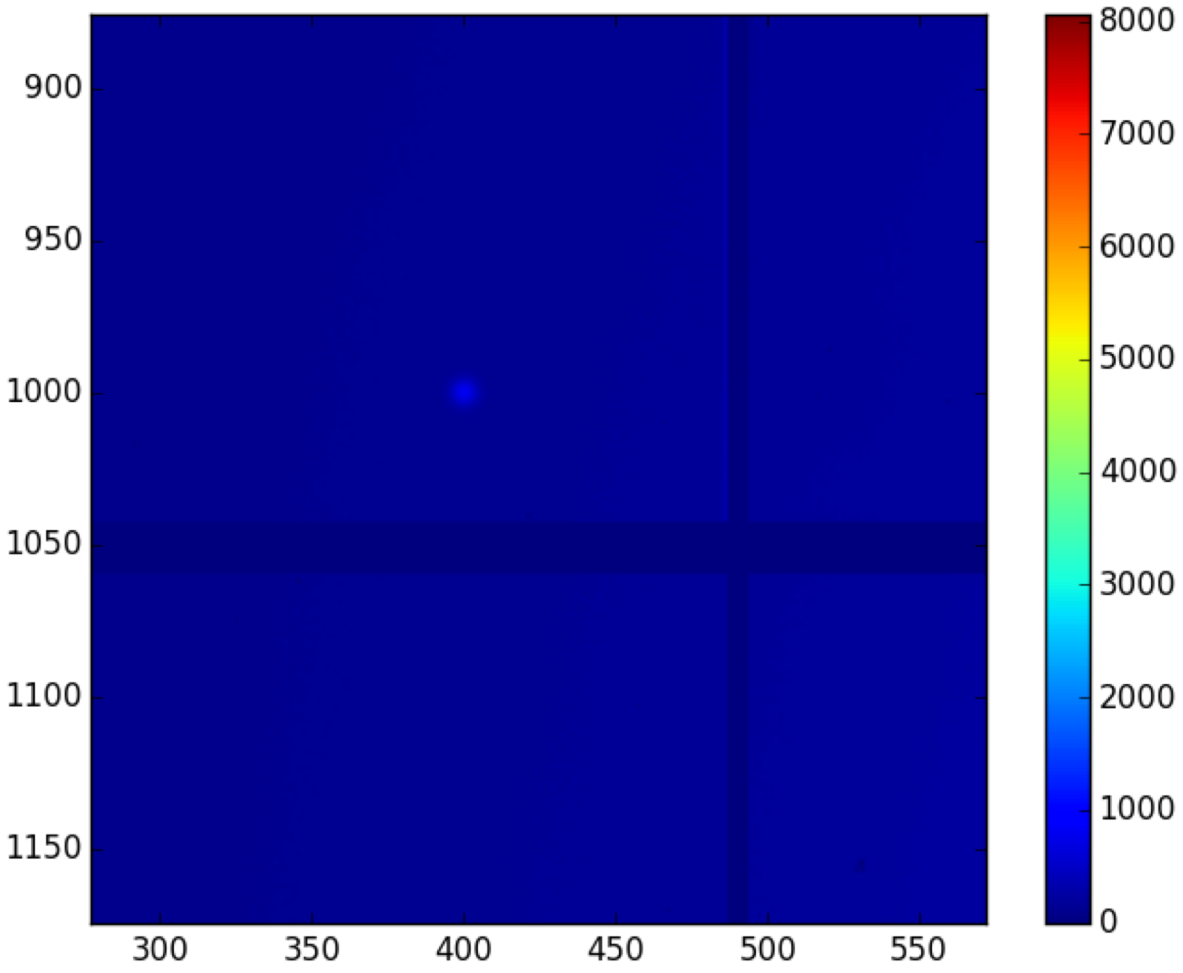

EFFECT OF NOISE ON G(R)

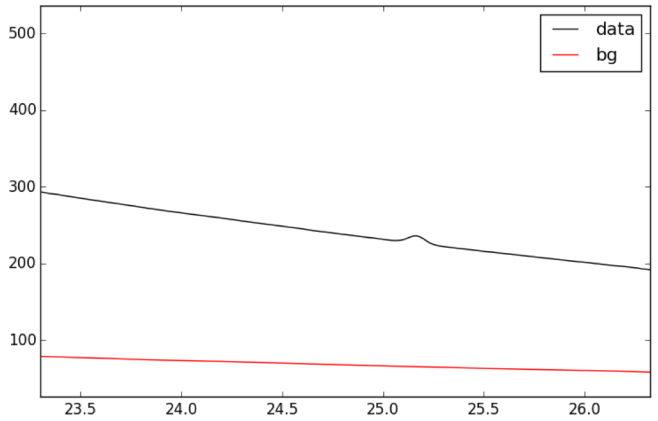

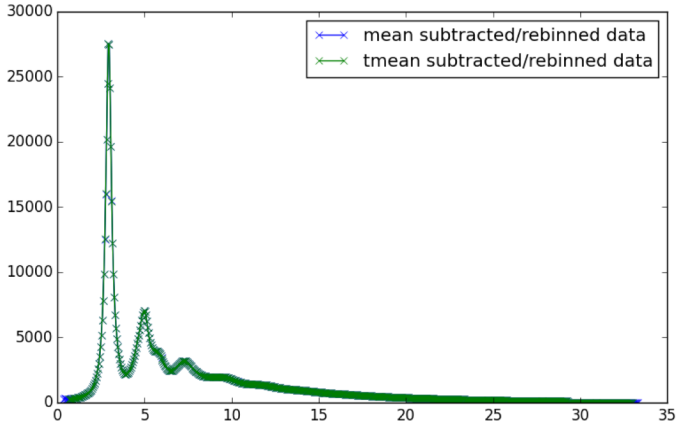

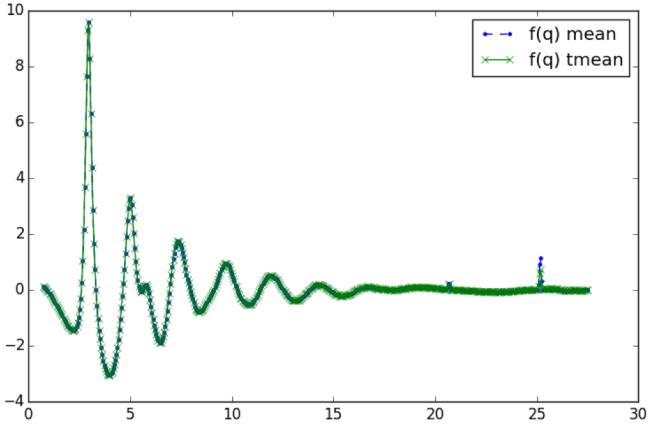

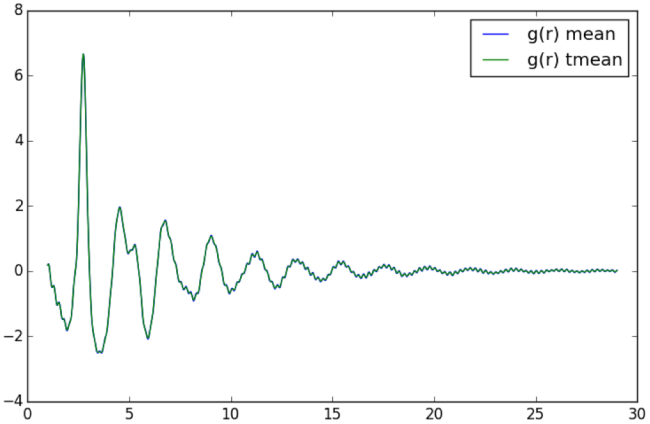

THE DREADFUL F(Q) ISSUE

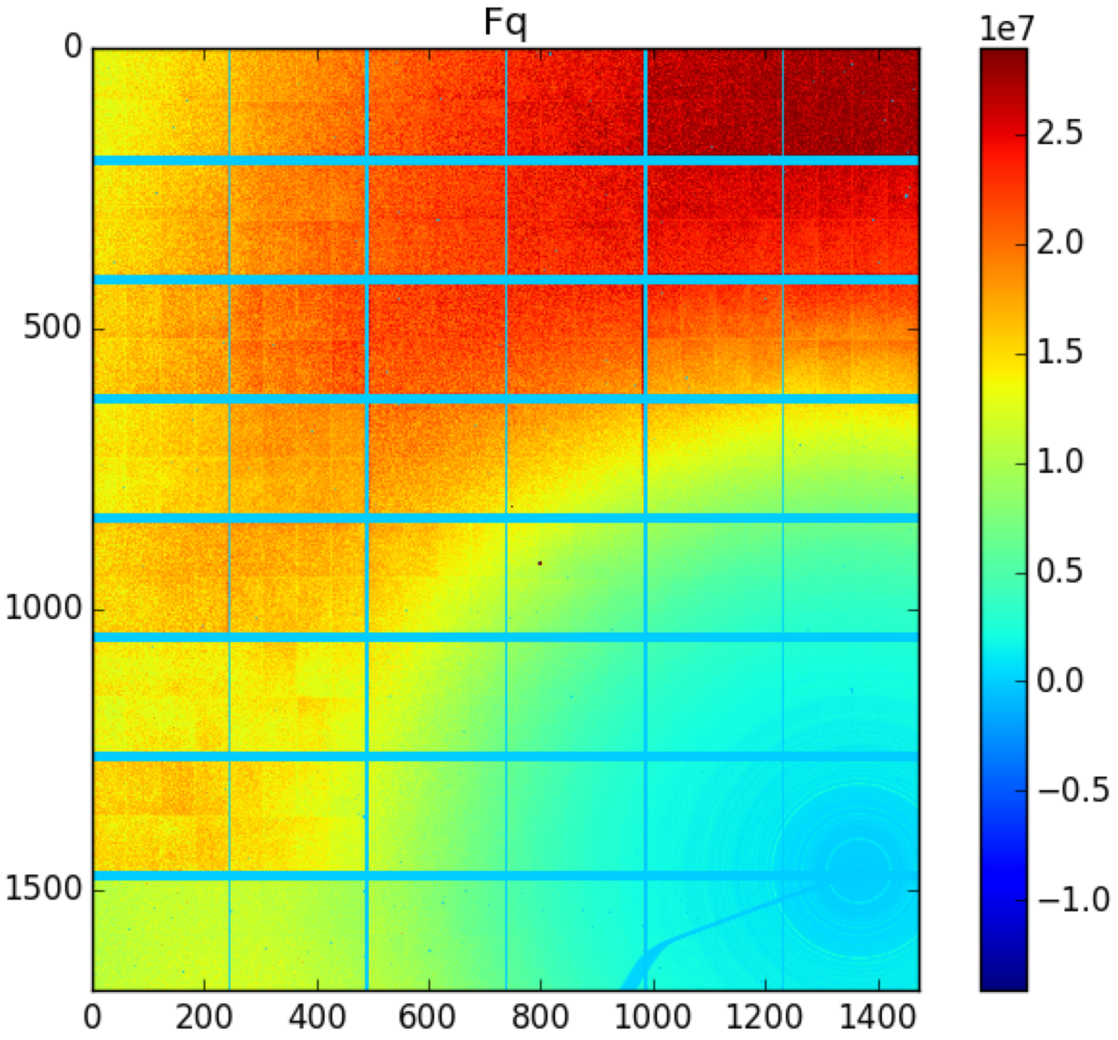

ANALYTICAL VS. SEMI-EMPIRICAL BACKGROUND SUBTRACTION

Inelastic Backgrounds can be subtracted by either

- **Analytical**
  - Correct form calculated and removed
- **Semi-Empirical**
  - Polynomial or spline representation for the effects
  - Form of the function respects analytical form

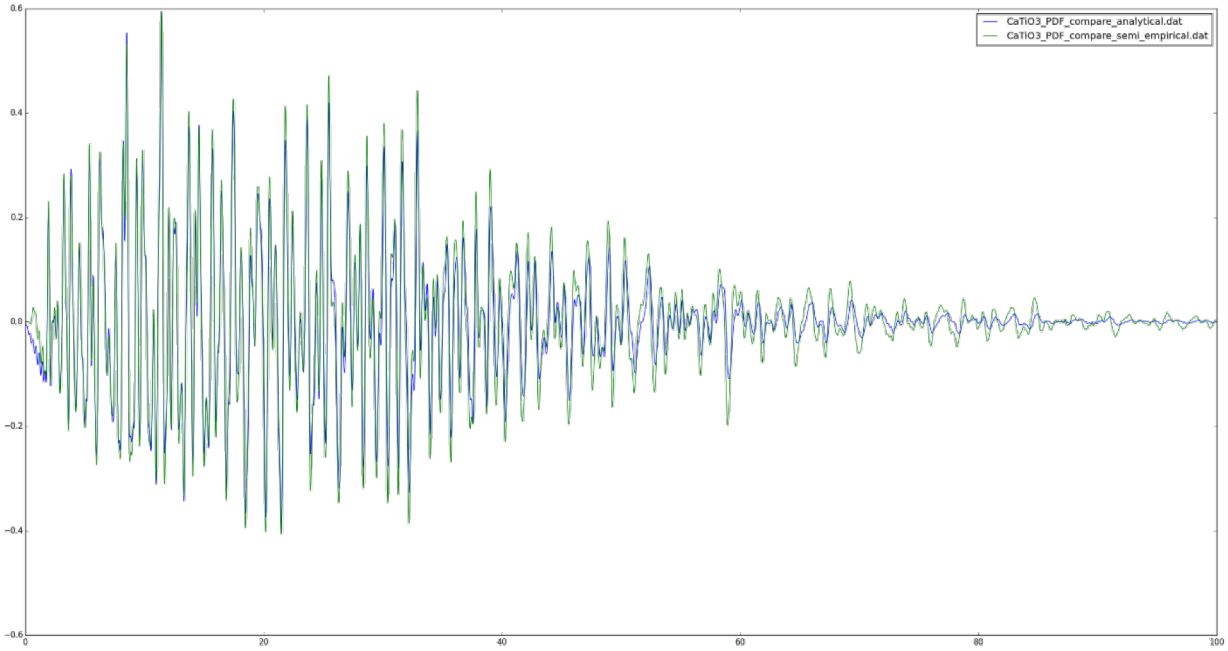

EXTRACT G(R) FROM THE SPLINE OF F(Q)

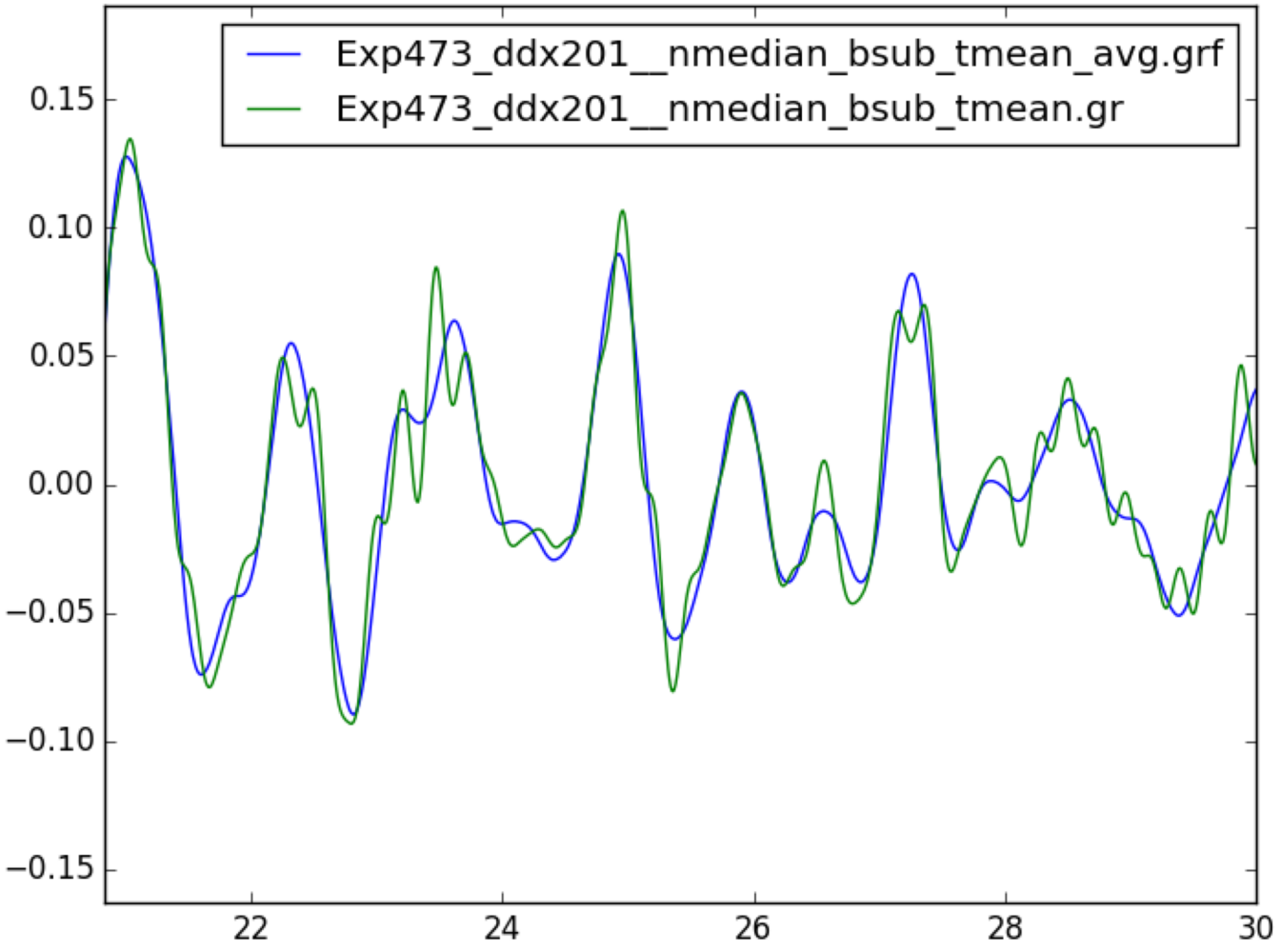

Calculate G(r) from the spline of the data, respecting the physical shape

EXTRACT G(R) FROM THE SPLINE OF F(Q)

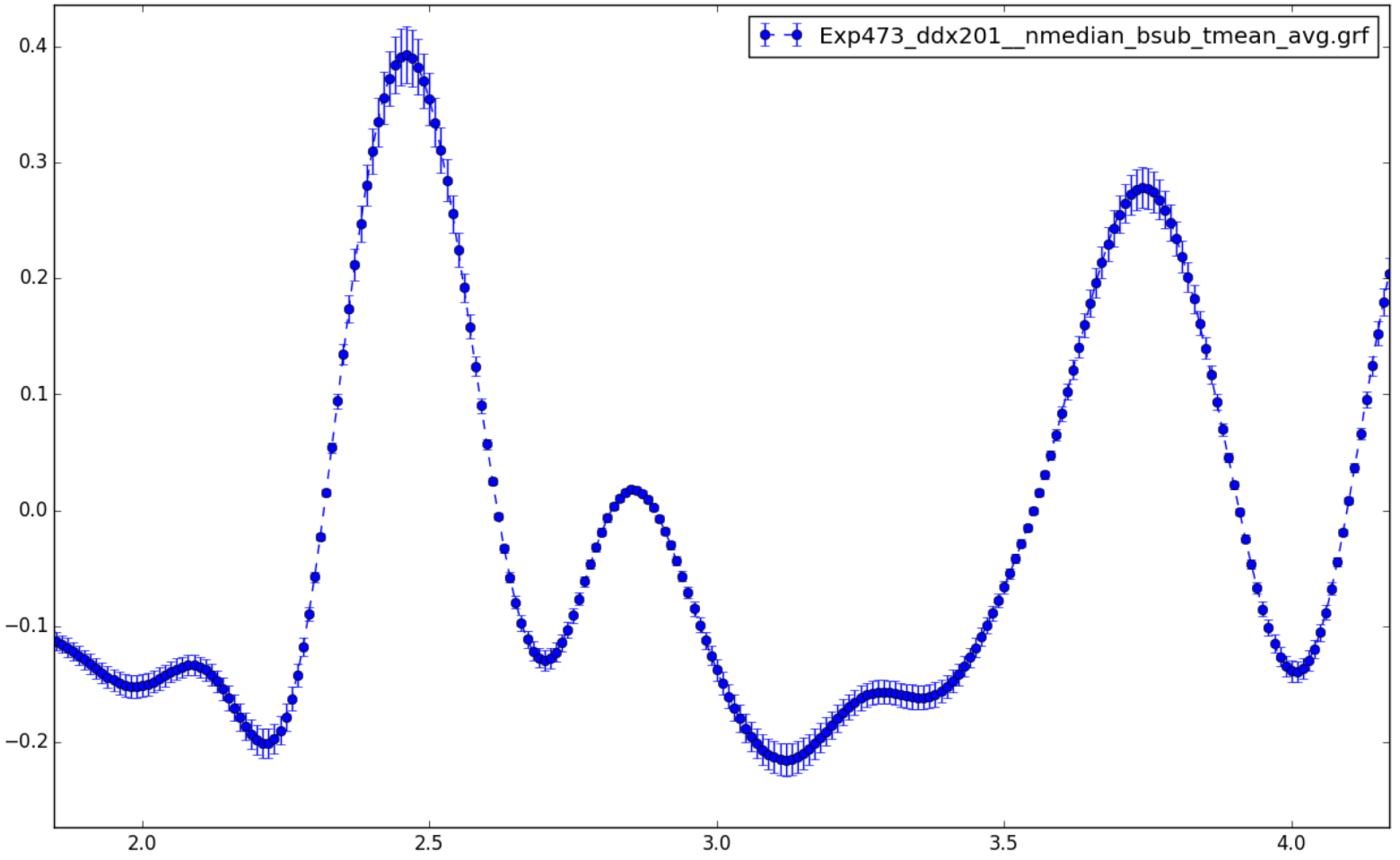

Calculate statistics on G(r) from weighted simulations

MEASUREMENT OF TG AND FREE VOLUME BY X-RAY SCATTERING

By simply measuring nearest-neighbor distances the instability of atomic vacancies in glasses could be demonstrated

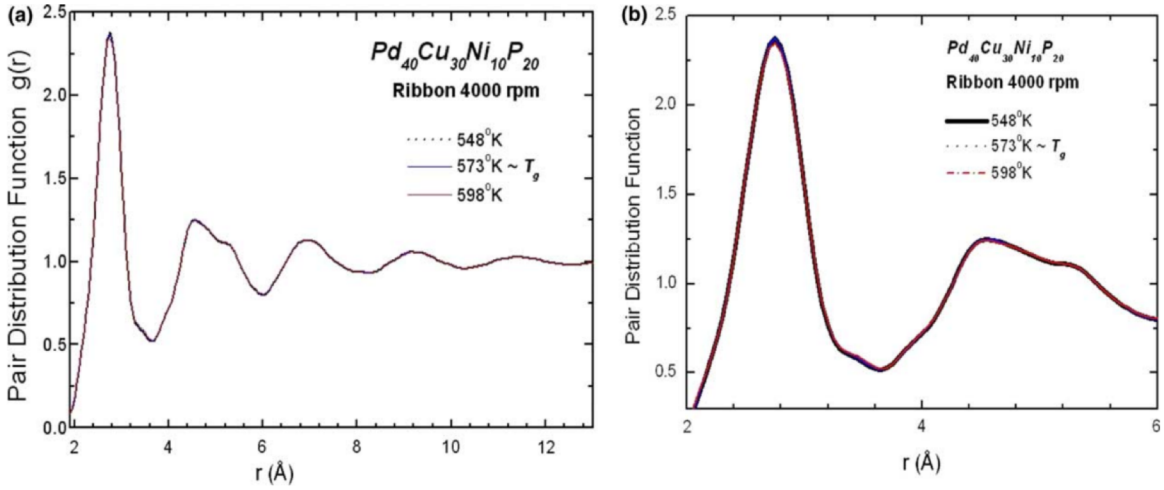

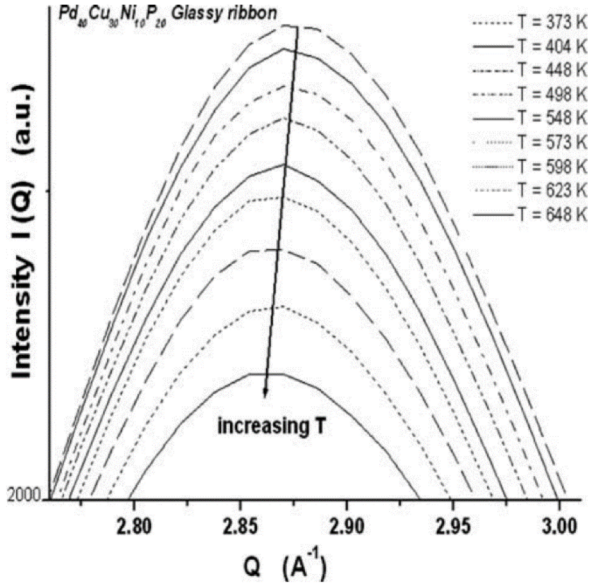

MEASUREMENT OF TG AND FREE VOLUME BY X-RAY SCATTERING

The activation energy could be measured by the slope of the relaxation

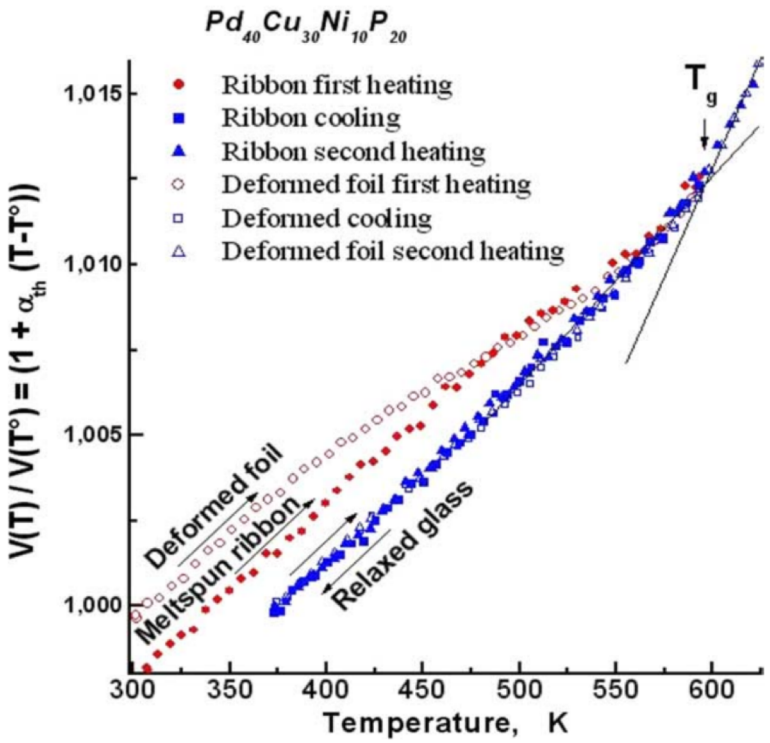

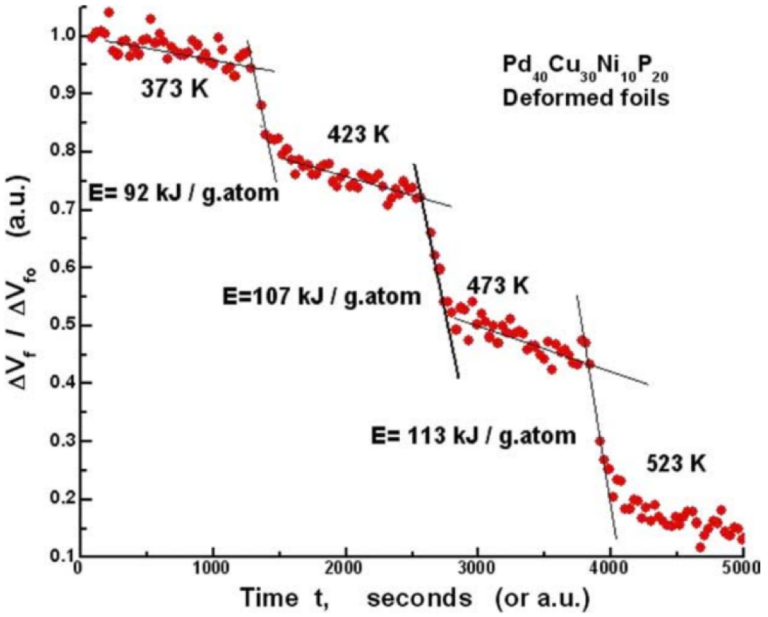

MEASUREMENT OF TG AND FREE VOLUME BY X-RAY SCATTERING

Regardless of the means that free volume was introduced, the glass always relaxed to the same structure with vacancies annealed out, with a measurable activation energy.

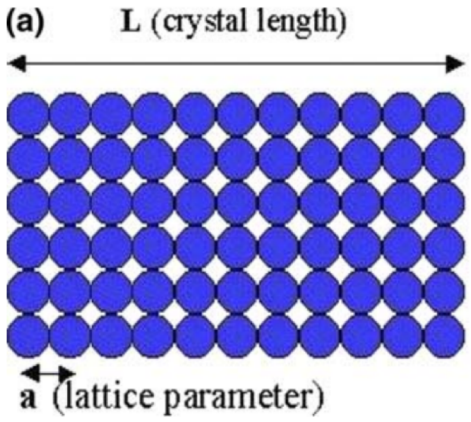

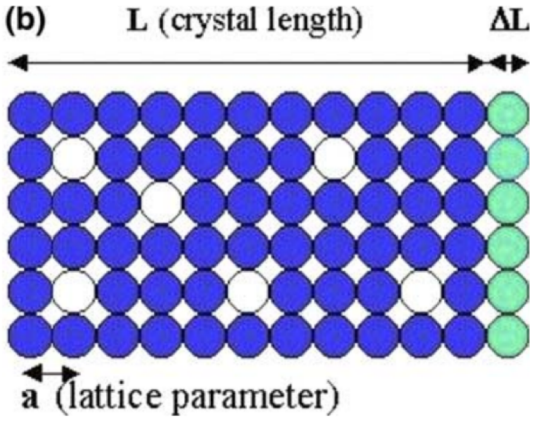

$$C_v(T) = \left[\frac{\Delta L(T)}{L_0} - \frac{\Delta a(T)}{a_0}\right]$$

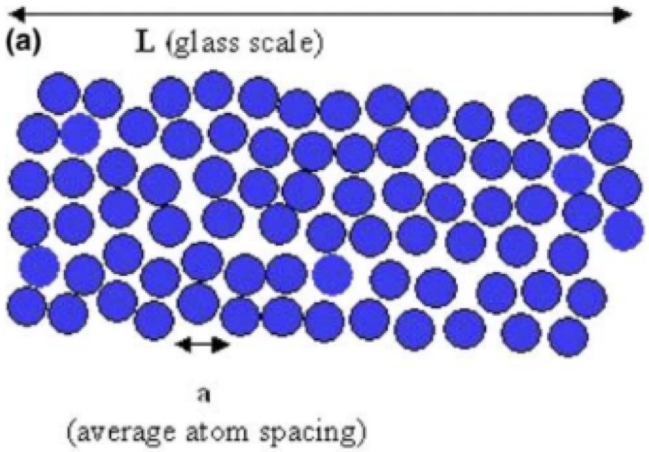

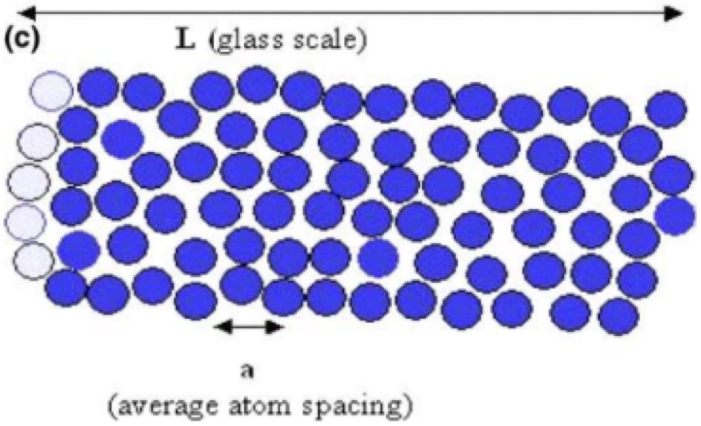

$$\frac{\Delta L(T)}{L_0} = \frac{\Delta a(T)}{a_0}$$

$$C_v(T) = 0$$

Yavari et al., Acta Mater. 2005

DETECTION OF POLYMORPHS IN AMORPHOUS STATE

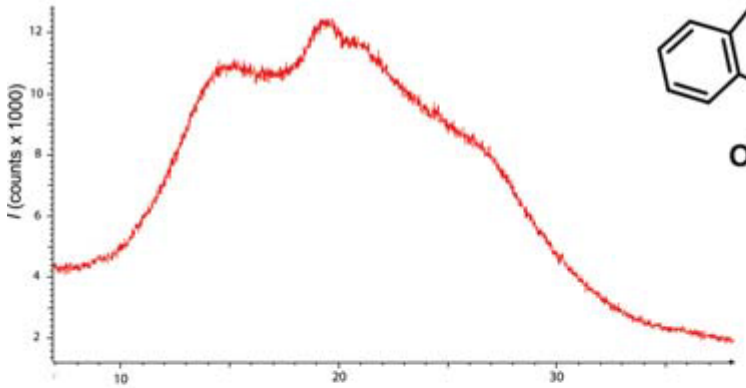

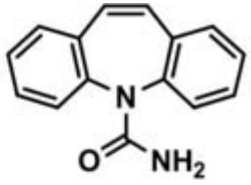

CBZ

Can the polymorph present in an amorphous sample be identified?

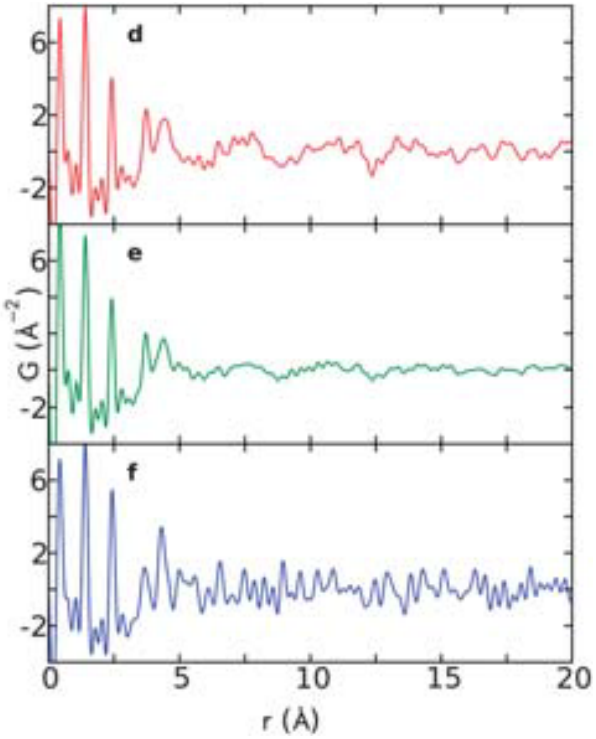

Carbamazepine polymorph III

Melt-quenched carbamazepine

Carbamazepine polymorph I

Billinge et al CrysEngComm 2010

Fingerprinting in organic or pharmaceutical molecular compound

Amorphous content

References:

- ✓ T. Davis, M. Johnson, S. J. L. Billinge. Cryst. Growth Des. 2013, 13, 4239−4244.
- ✓ Sheth, A. R., Bates, S., Muller, F. X. & Grant, D. J. W. (2005). Cryst. Growth Des. 5, 571–578.
- ✓ Billinge, S. J. L., Dykhne, T., Juhás, P., Božin, E., Taylor, R., Florence, A. J. & Shankland, K. (2010). CrystEngComm, 12, 1366–1368.
- ✓ D. Prill, P. Juhás, S.J.L. Billinge, M.U. Schmidt. Acta Cryst. (2016). A72, 62–72.

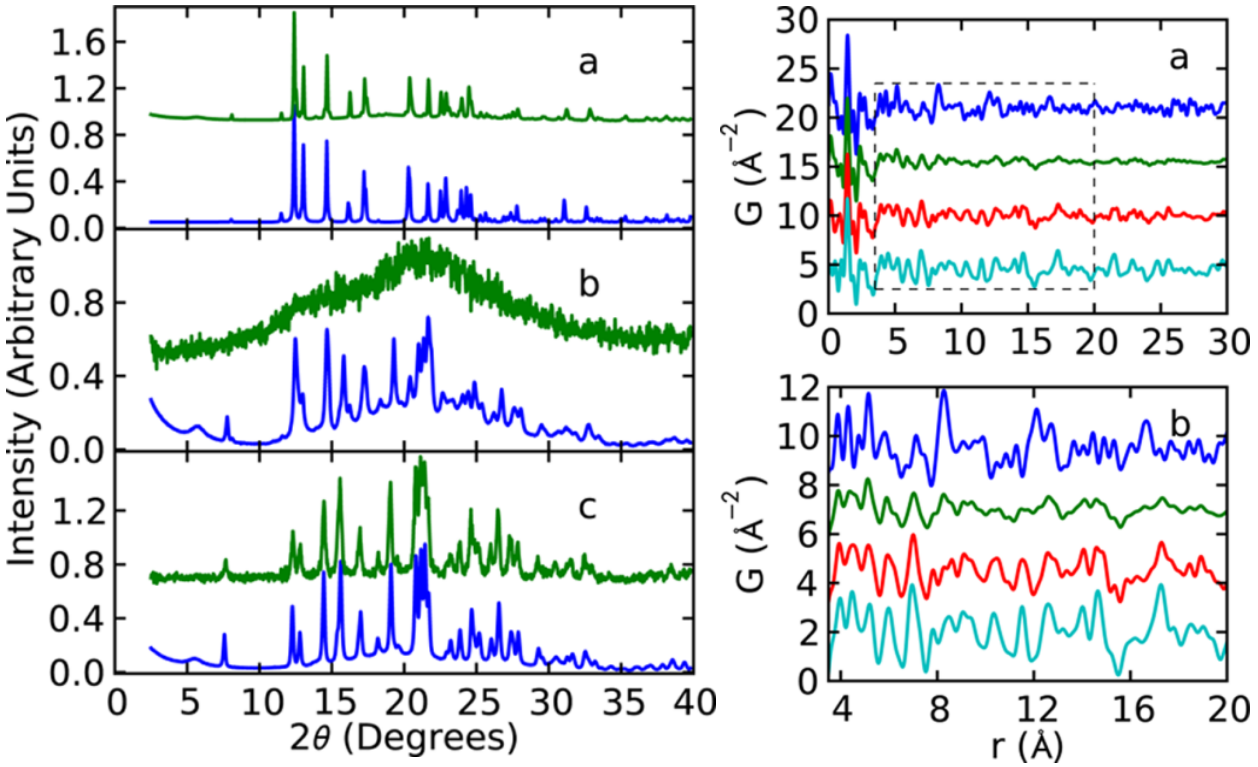

INFORMATION IN THE PDF

Peaks Positions: interatomic distances

Peak Intensity: coordination number

Peak widths: disorder (thermal, static)

Attenuation with r: size of coherent domains

This information is all model-Free

Ultimately, the entire structure is described by the PDF, but it is an inverse problem…

- Fit to PDF using a periodic model, and local disorder (“Small box”)
- Fit to PDF using a Debye model
- Fit to PDF via reverse Monte Carlo (“Big Box”)

The fits are usually poorly convergent; additional information is of great use.

More common is to do the reverse, to compare the measured data with models derived from simultations.

SOFTWARE FOR CALCULATING AND MODELLING PDFS

- **Small box methods**
  - consider a periodic structure, introduce disorder
  - Typically applied to characterize disorder in crystalline materials
  - **`PDFGUi (Diffpy-CMI), Topas, Fullprof`**…
  - Simple, approximate model
- **Big box methods**
  - Consider and large ensemble of atoms, refine against scattering data and possibly energetic constraints (“Reverse Monte-Carlo”)
  - Mine the result to characterize local structure
  - Typically used for extended networks such as glasses
  - **`RMCProfile`**
  - Very detailed but possibly over-refined model
- **Debye methods**
  - Fit data to an explicit model
  - Typically used for *e.g.* clusters
  - Quantitative, but requires model building (extreme inverse problem)
  - **`Diffpy-CMI`**

STRUCTURE OF COMPLEX CLUSTERS FROM PDF

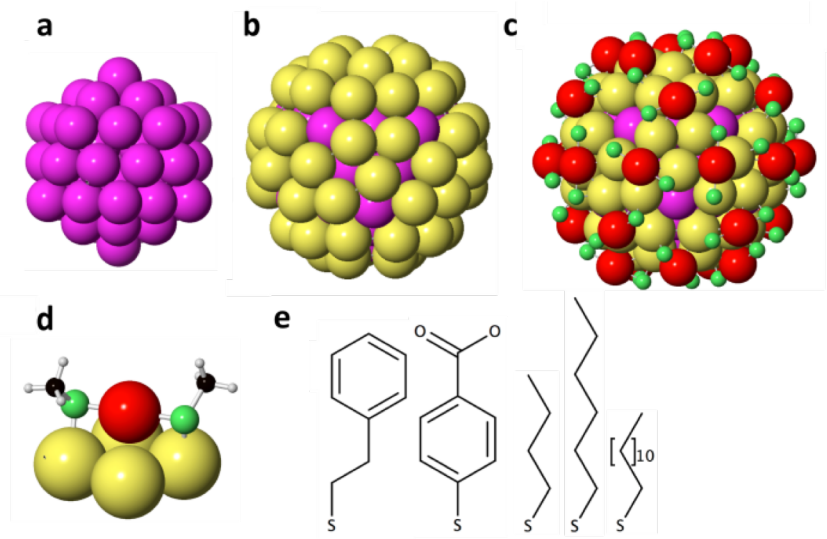

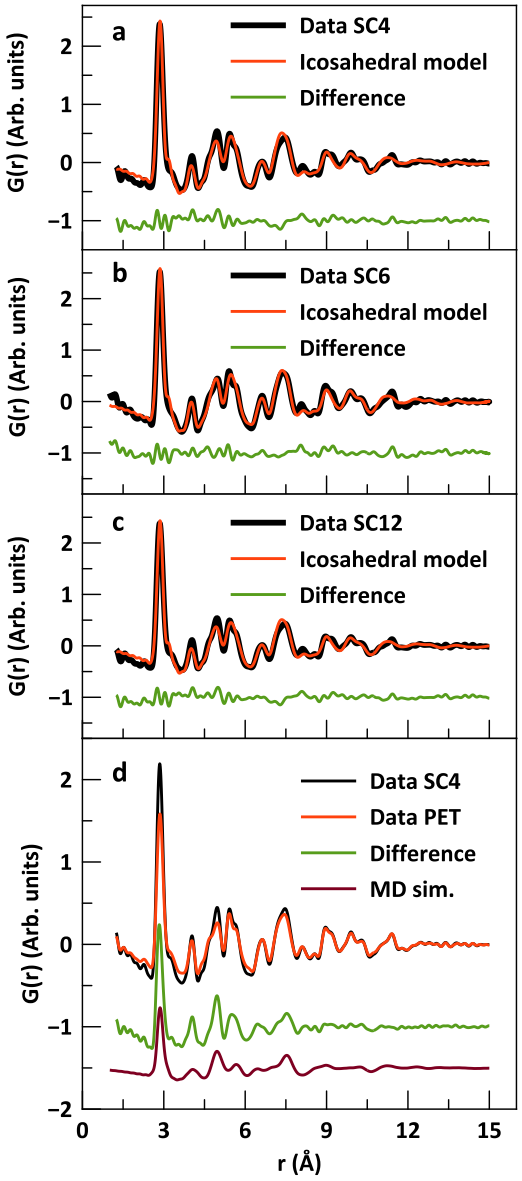

- Even complex, multi-component systems in solution might be characterized

- Easier to verify the plausibility of a proposed structure than to actually solve that structure *a priori* from the data, *i.e.,* P ≠ nP (probably…)

Jensen et al., Nature Comm 2016

Brookite nanoparticles refined without a model yield symmetry "naturally"

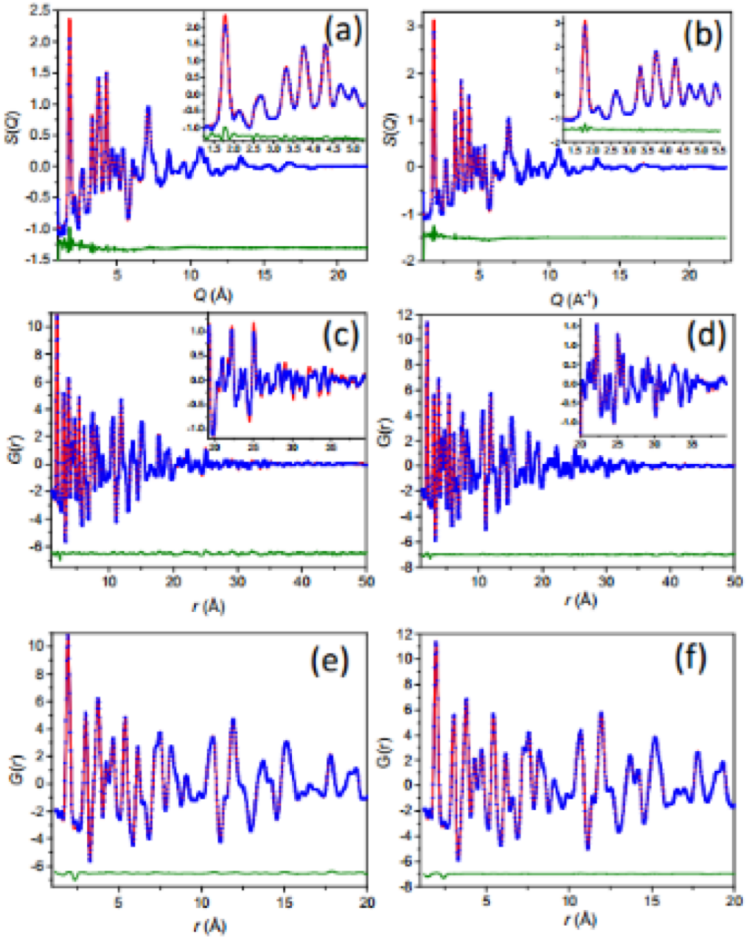

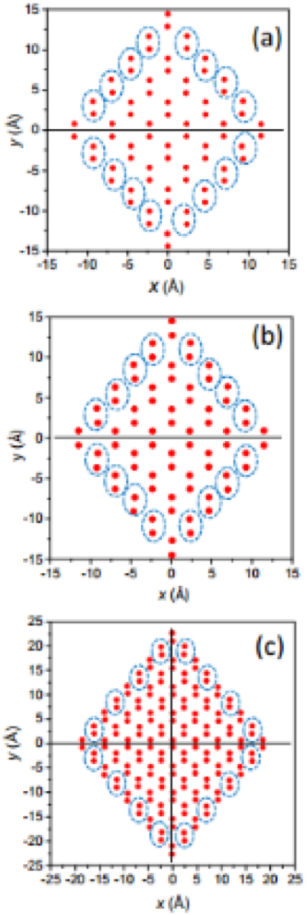

RMC structure (Sample A)

DFT Model

RMC structure (Sample B)

Krayman et al., Chemistry of Materials, in press

PDF OF ULTRATHIN GLASSES

Thin films of CVP deposited metallic glasses show anomalous instability compared to normal glasses

Luo et al, Nature Comm. ***9****, 1389 (2018)*

PDF OF ULTRATHIN GLASSES

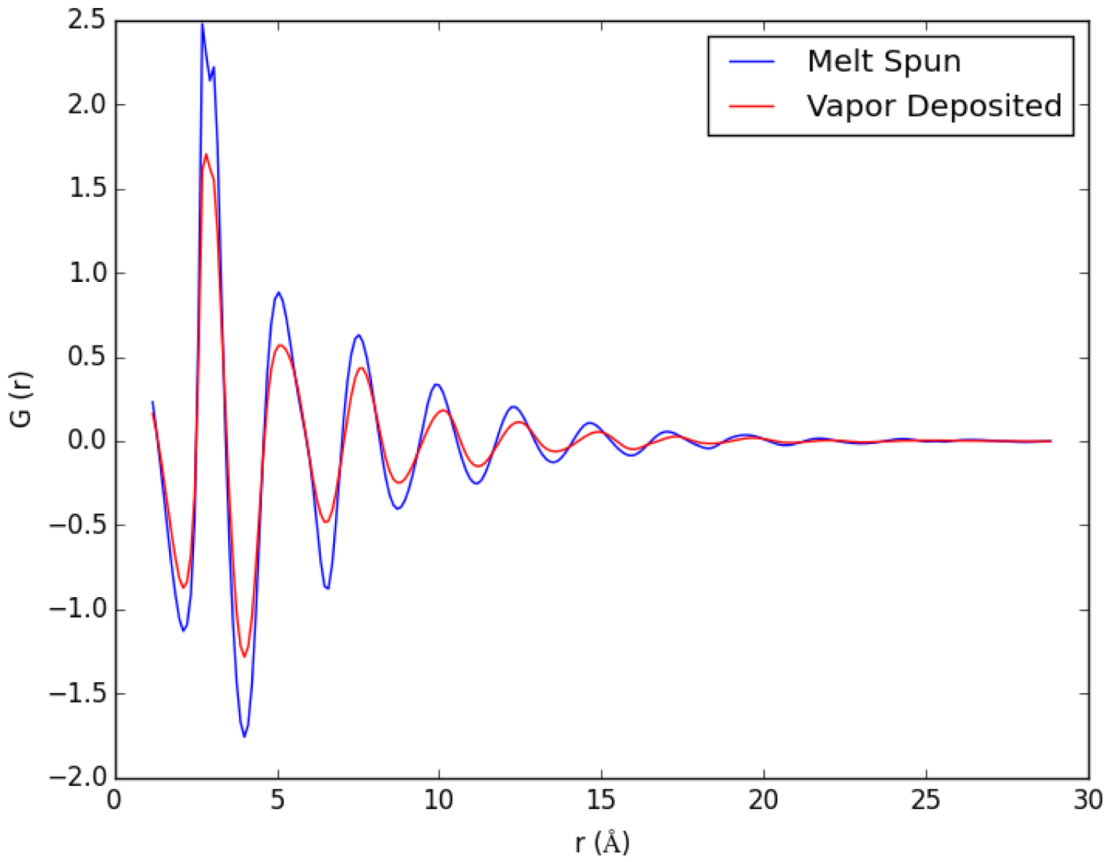

The G(r) obtained from very thin (ca. 2 micron) thick films of BMG show the microstructural origin of the ultrastability of the CVP glasses lies in greater quenched in disorder

Luo et al, Nature Comm. ***9****, 1389 (2018)*

TIME RESOLVED STUDIES OF LEVITATED SAMPLES

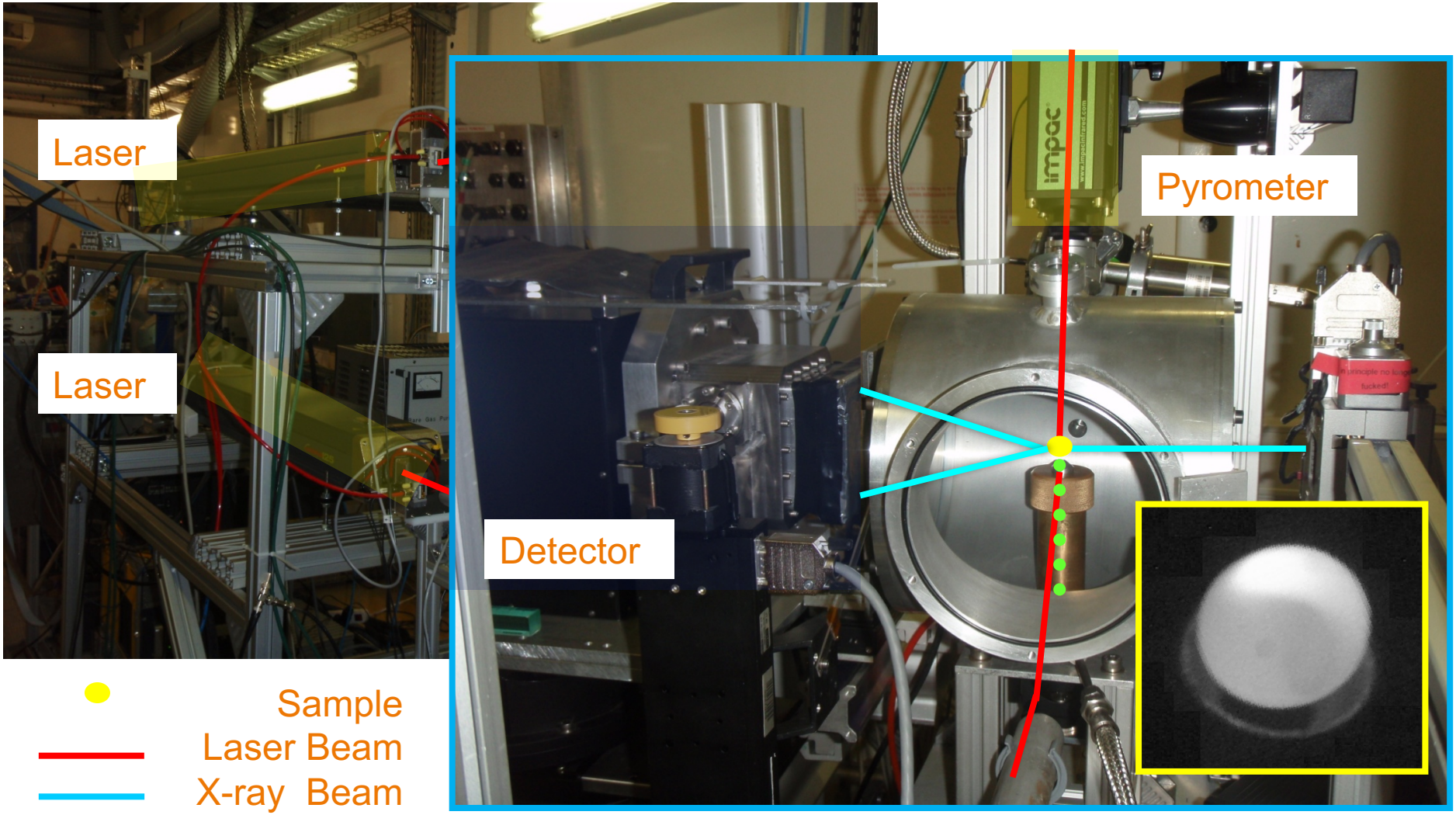

TIME RESOLVED – LASER HEATED AND LEVITATED

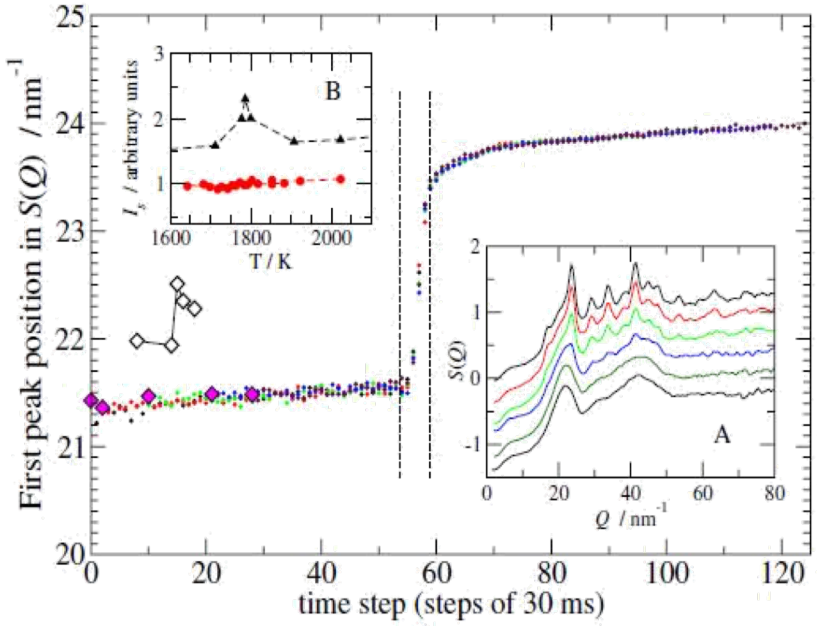

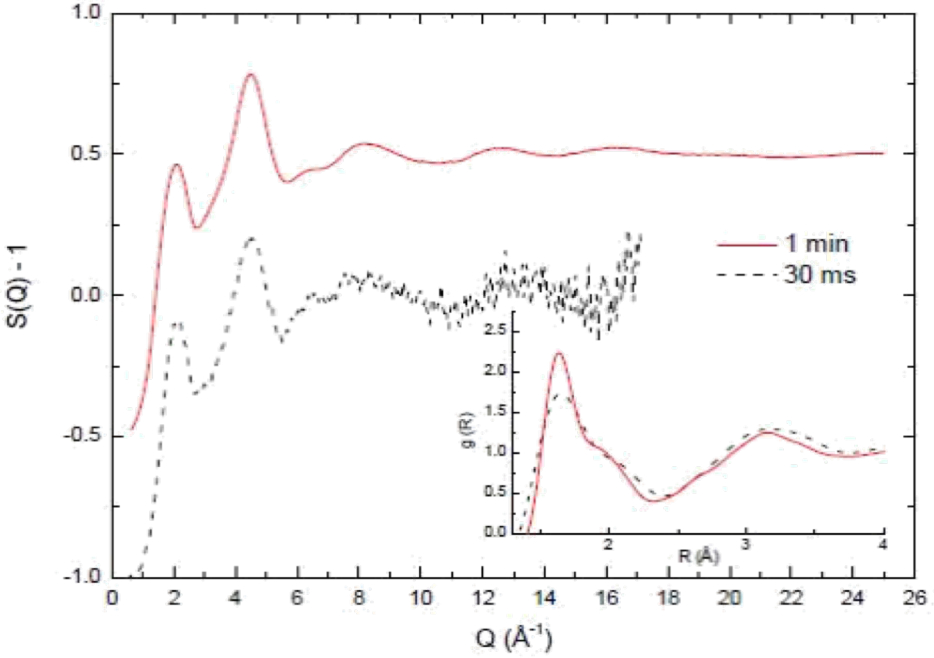

Ultrafast PDF in extreme conditions (levitated, lasar heated liquids)

Barnes et al., PRL 2009

FAST MEASUREMENT OF AMORPHOUS MATERIALS

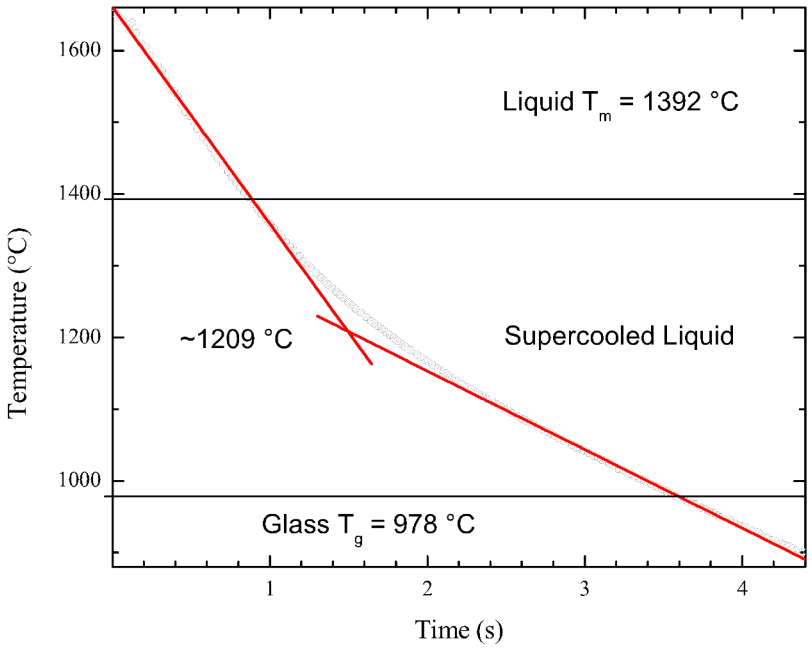

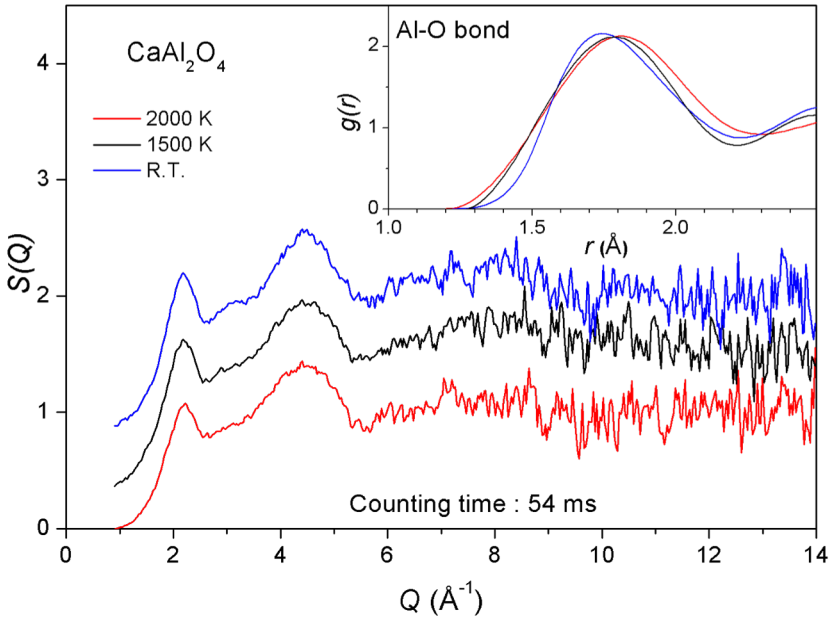

Bytchkov et al JCCP (2013)

Hennet et al European Physical Journal 196, 151-165 (2011)

Bytchkov et al PRB 83, 144201 (2011)

Barnes et al. PRL 103, 225702 (2009)

Hennet et al JNCS 354, 5104 (2008)

PDF – COMPLETE STUDY OF NANOCRYSTALLIZATION OF YSZ

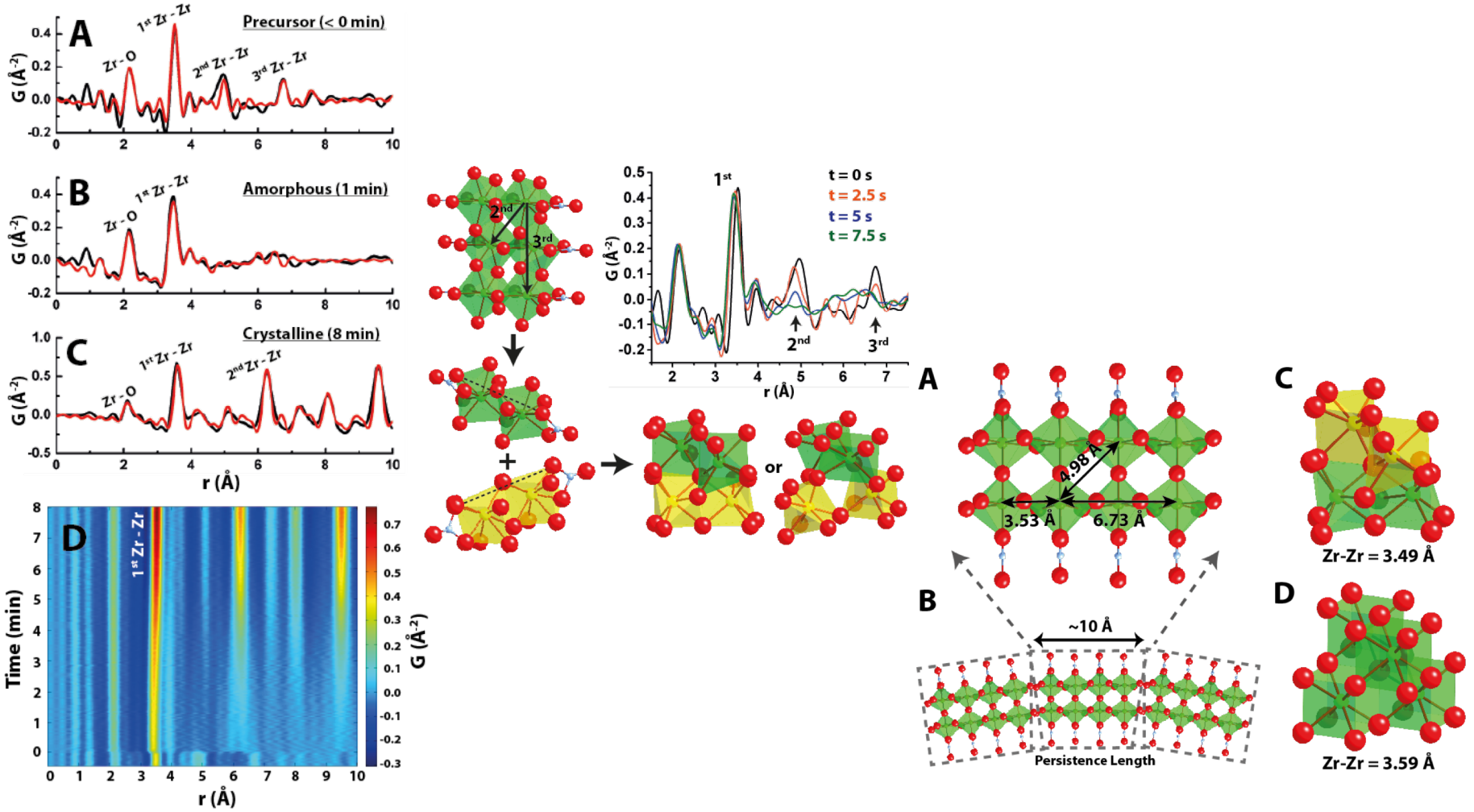

The entire process from initial crystallization from solution through nanocrystallization to macroscope crystallization could be followed with sub-second TR

Tyrsted et al., IuCr-J (2014)

PDF IN DIFFICULT CIRCUMSTANCES

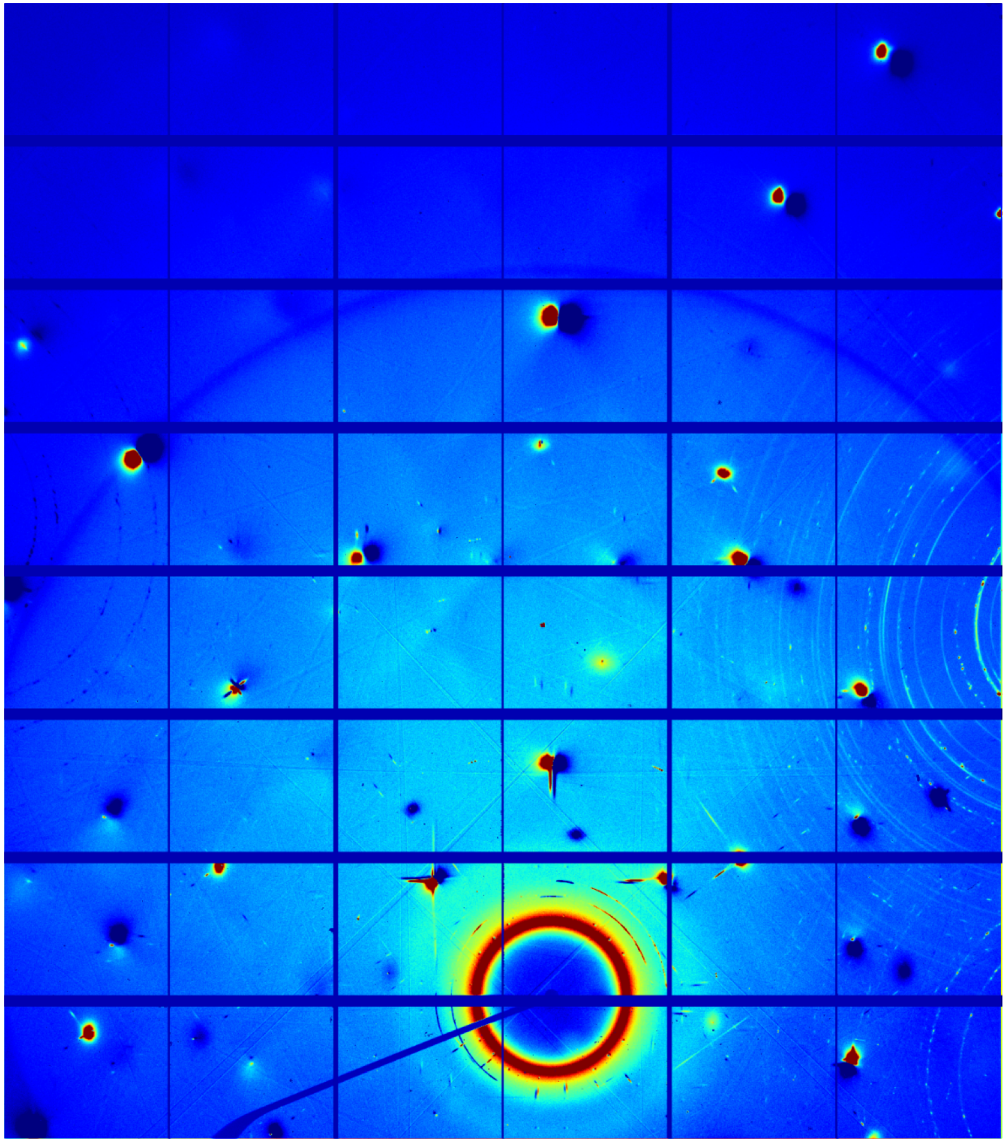

PDF IN DACS

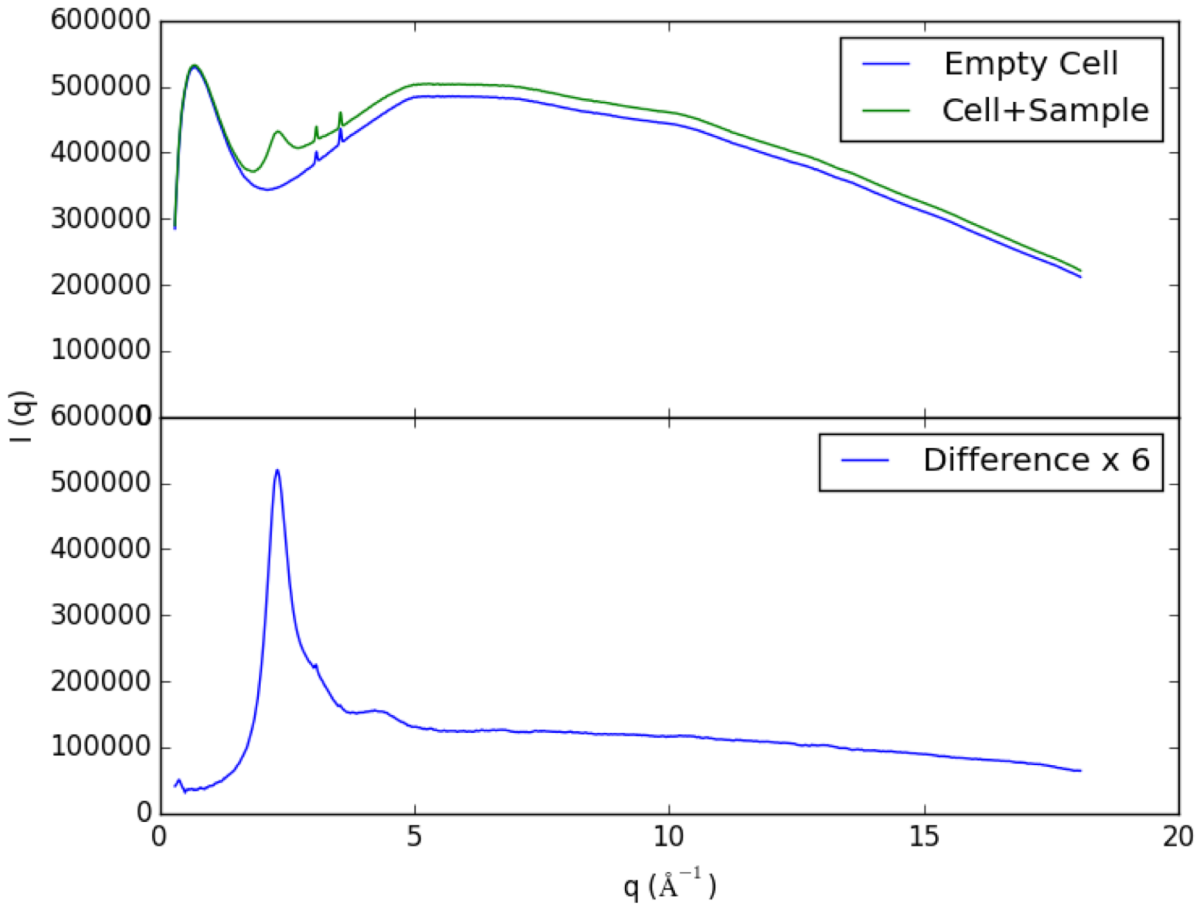

Signal from the material of interest is a small fraction of the total signal

SPLINES TO DATA

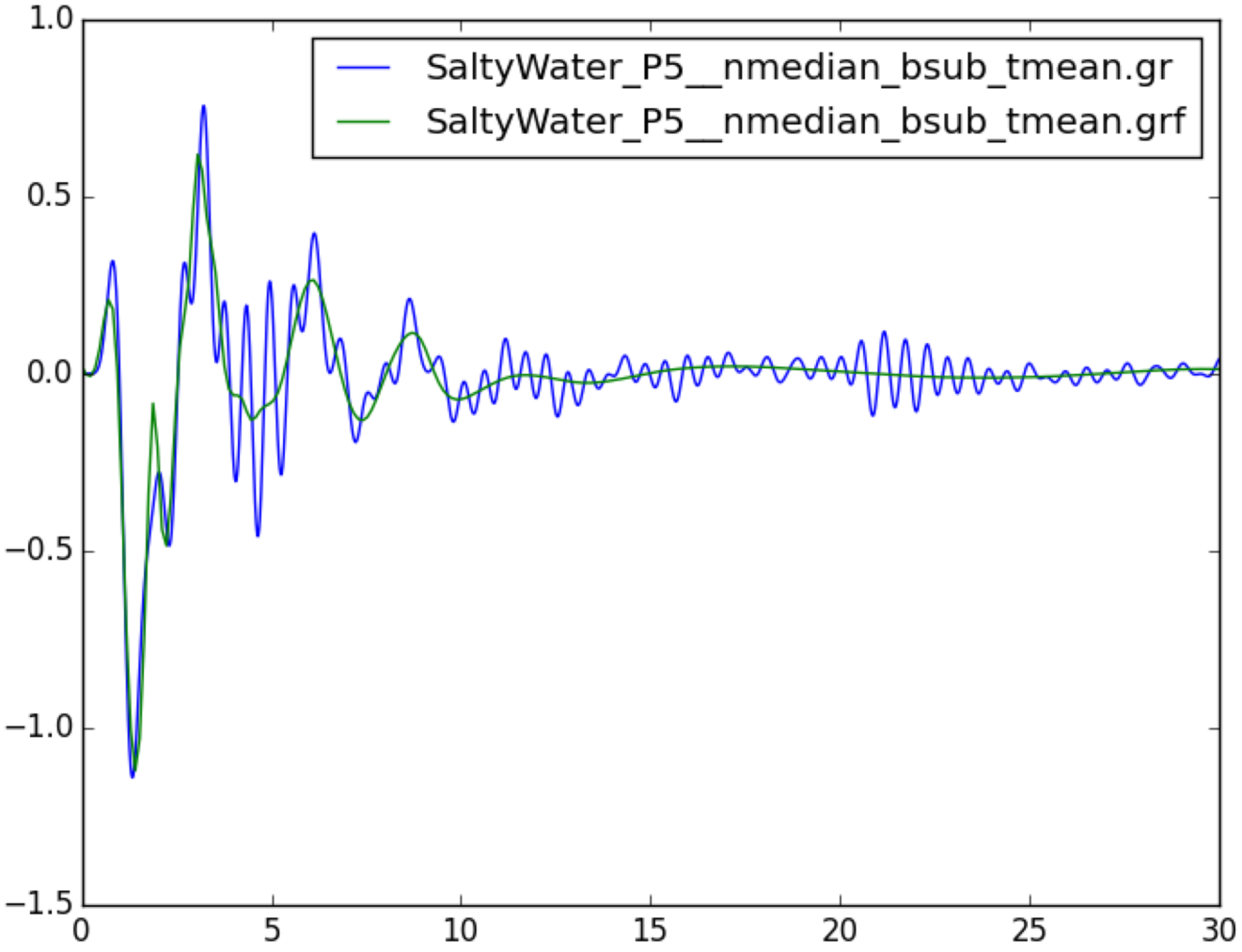

PDF OF SALTY WATER IN A DAC

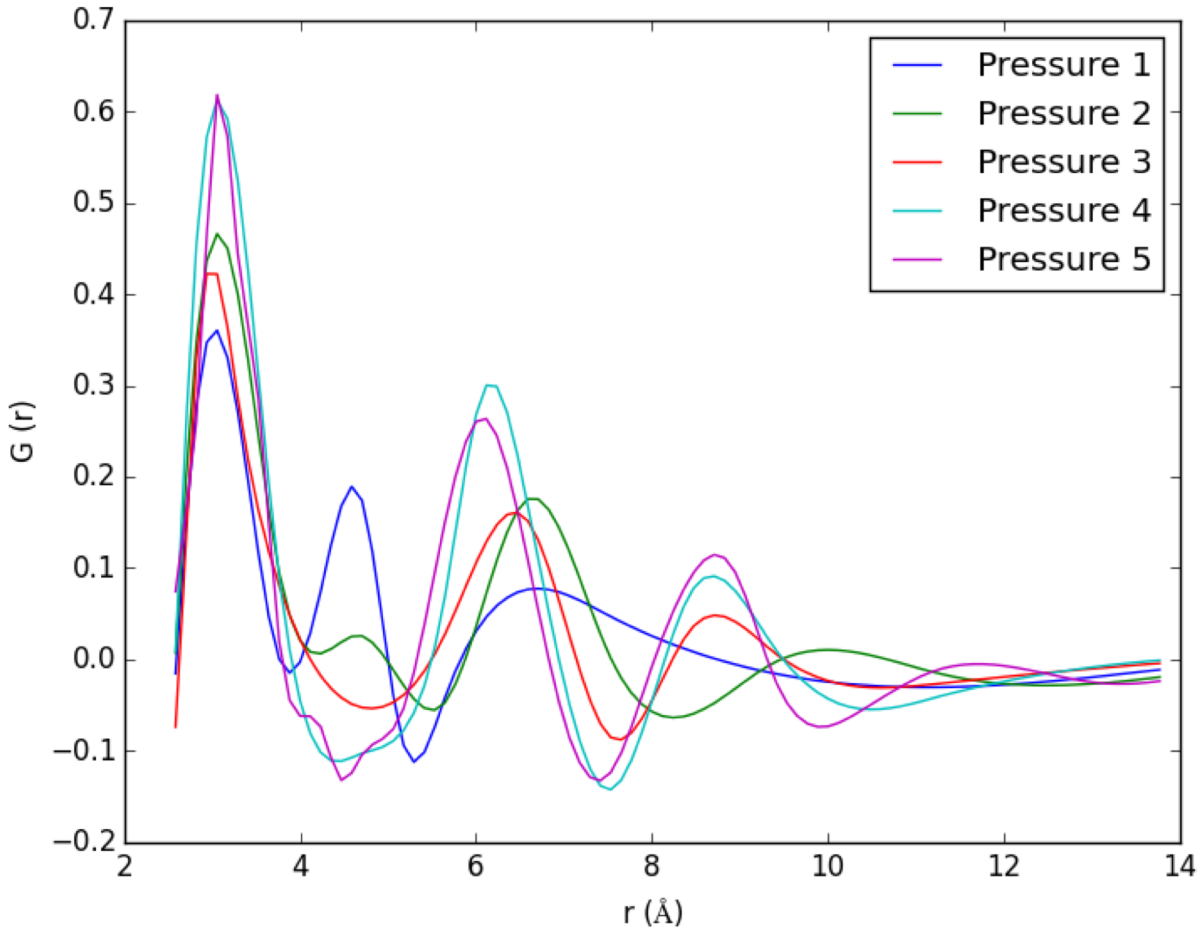

Clear changes in local environment can be seen with pressure

Petitgirard et al, in prep.

"LOCAL" LOCAL STRUCTURE

•Measure local variations in local structure with a local rather than as an average probe, even in amorphous materials

•Strain fields

•Spatially and orientationally resolved PDF

•With resolutions from microns to 100 nm

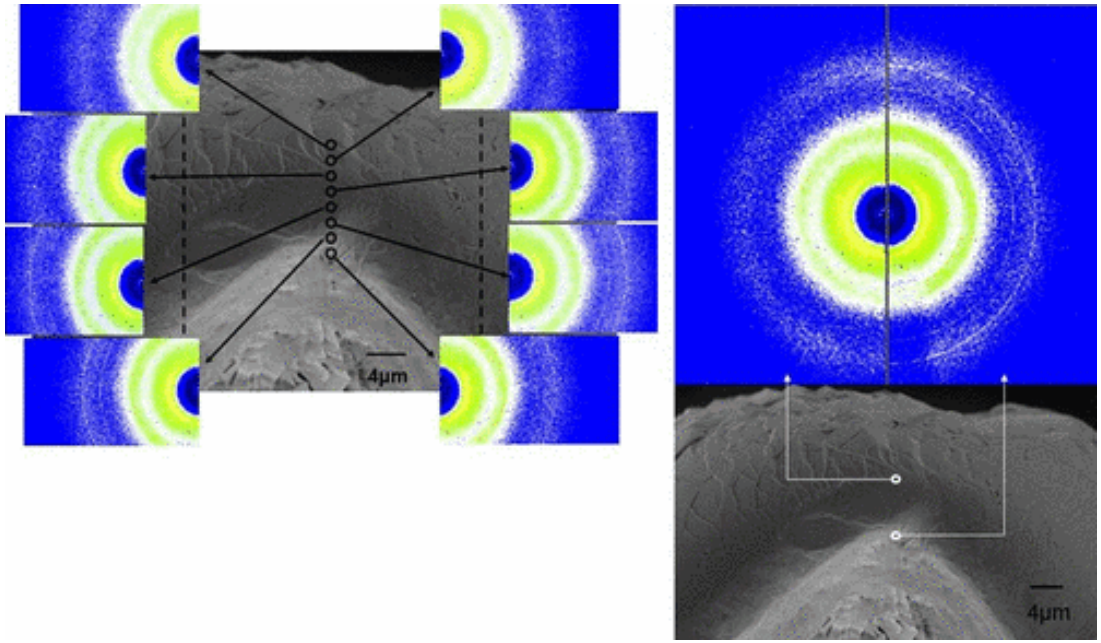

Bending induced crystallization could be measured local on a BMG

Yavari et al, PRL 2012

"LOCAL" LOCAL STRUCTURE

•Measure local variations in local structure with a local rather than as an average probe, even in amorphous materials

•Strain fields

•Spatially and orientationally resolved PDF

•With resolutions from microns ….to 100 nm

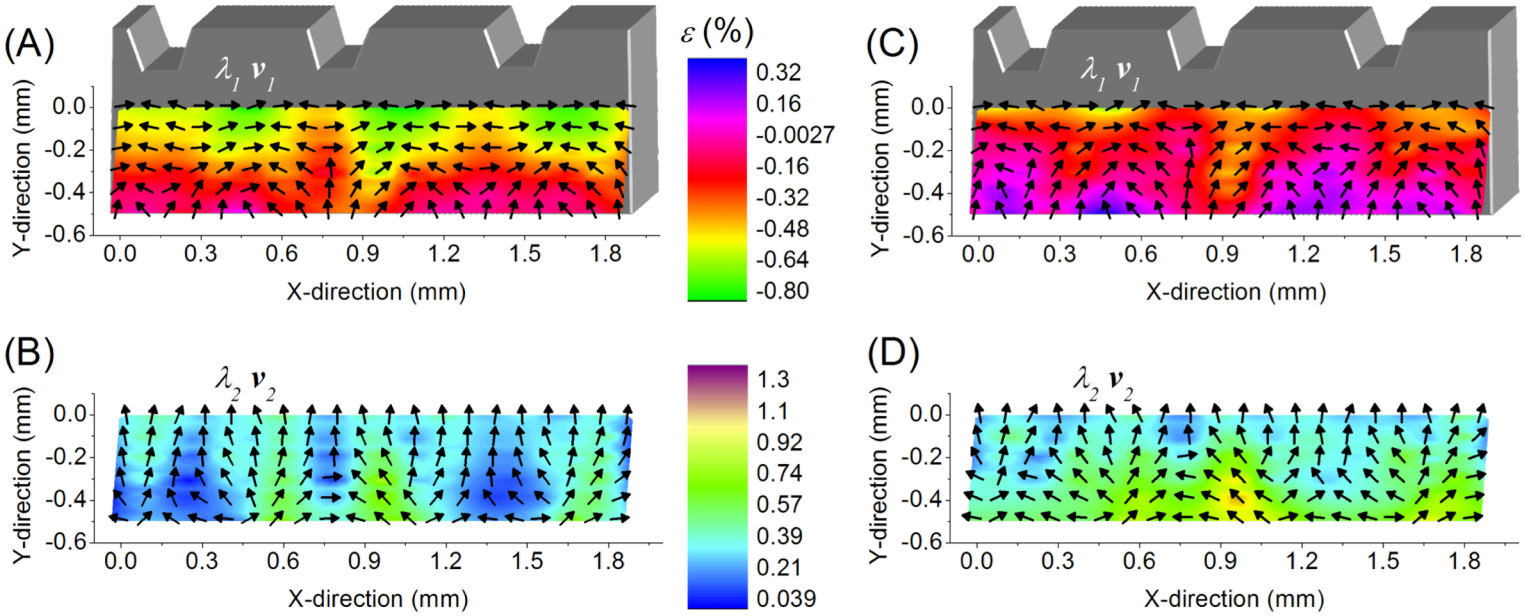

Scudino, et al., APL (2015), Shahabi et al., Acta Mater (2016)

“LOCAL” LOCAL STRUCTURE

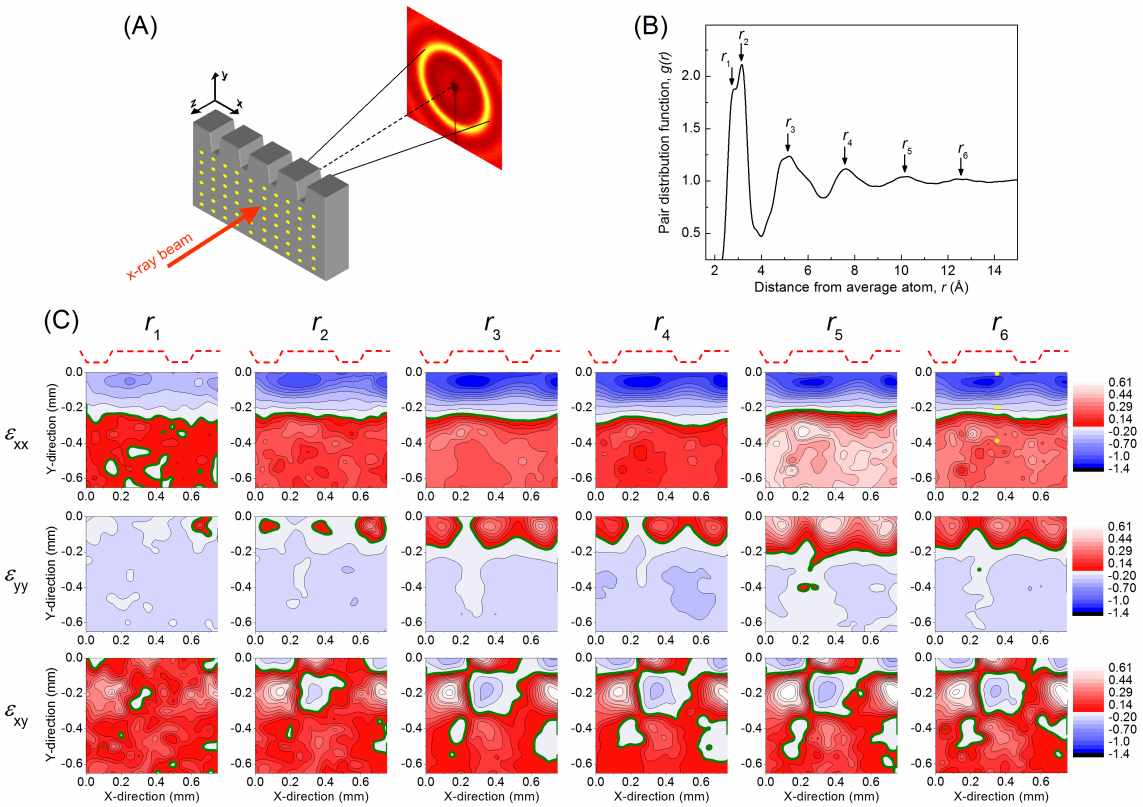

Length dependence of the strain components as seen from the nn distances in the g(r)

“LOCAL” LOCAL STRUCTURE

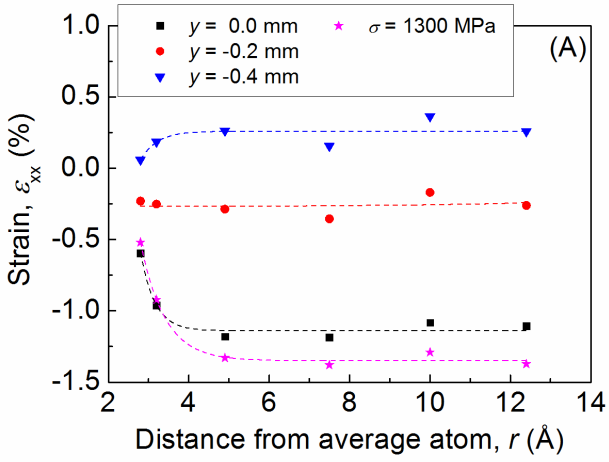

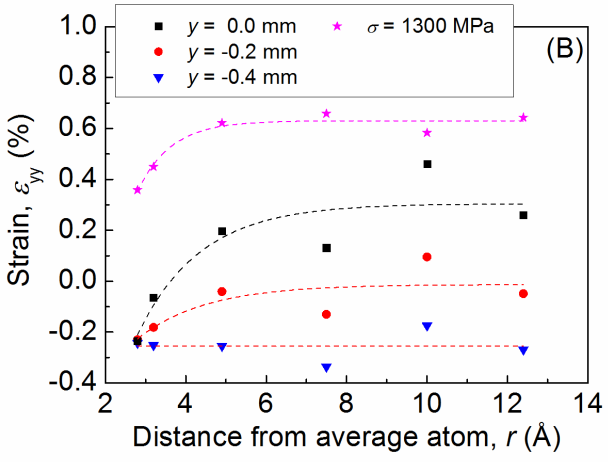

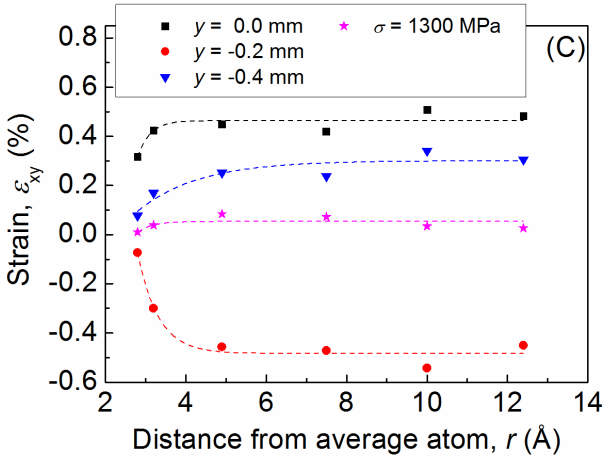

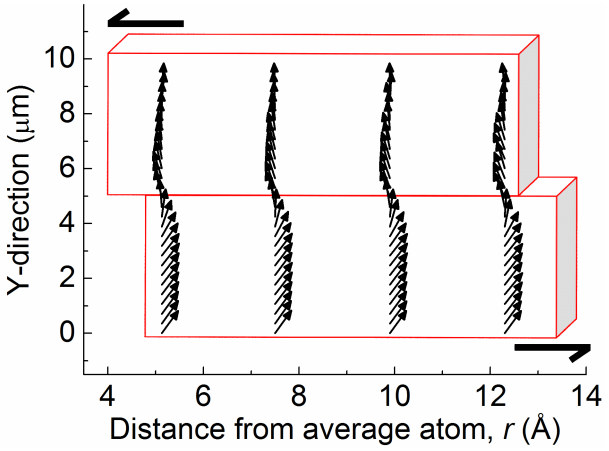

Highly contrasting strain in different coordination shells is the signature of the shear bands

TOMOGRAPHY

- Measure spatially and angularly resolved projections (radiograms)
  - Each pixel of the projection is a line integral at a particular position/angle
  - Absorption Tomography: spatial resolution given by detector
  - Result called sinogram

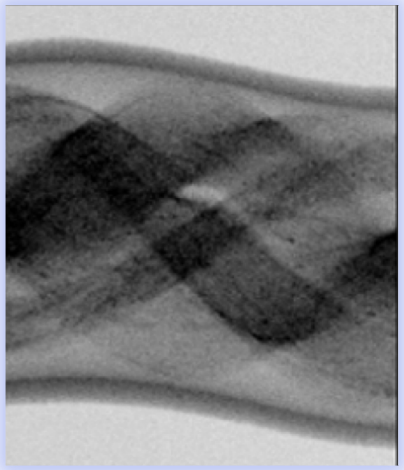

Sinogram of one layer

Inverse Radon transform

Reconstructed object

- Theorem exists to do exactly what we want: Inverse Radon Transform
- Different methods to clean/make more robust (discrete/finite/noisy) data
  - Filtered-back Projection, Algebraic reconstruction, ...

3D RECONSTRUCTION OF WORKING BATTERY

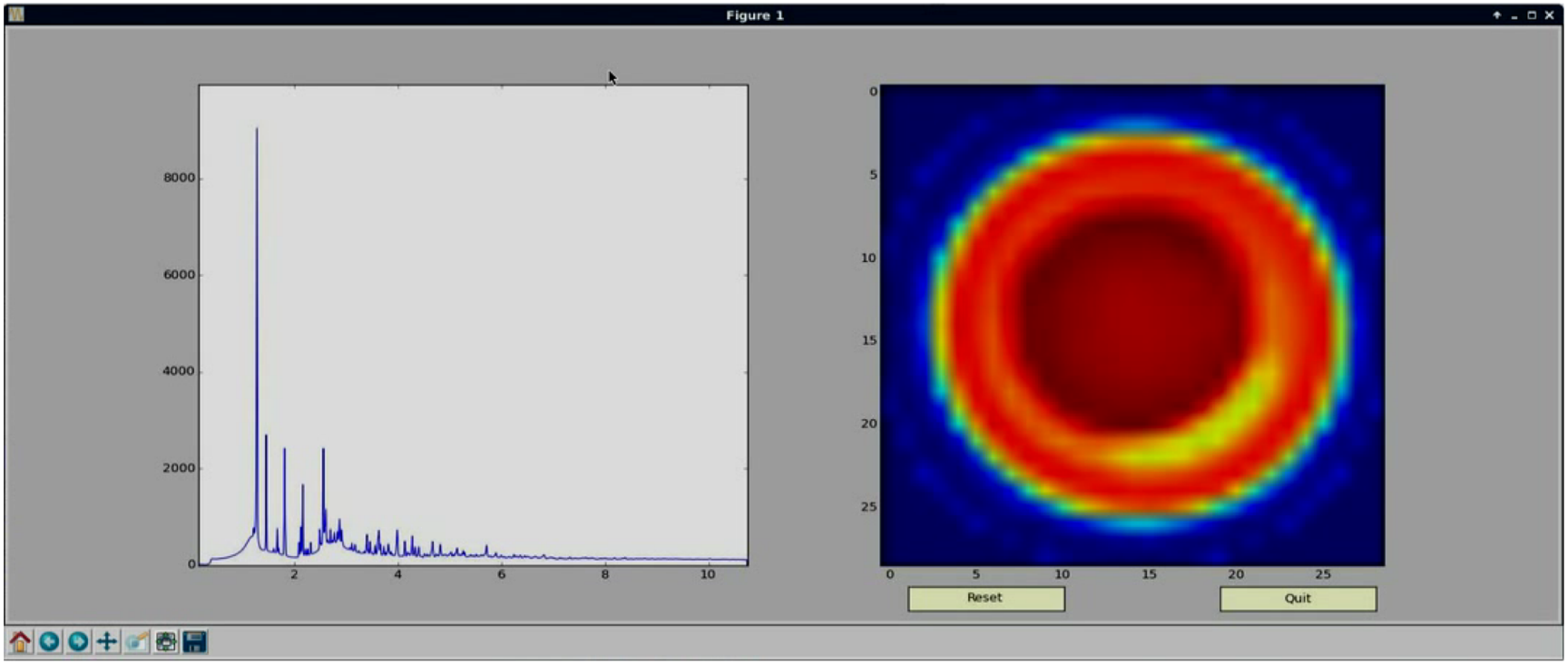

Liu et al, ACS interfaces 2019.

G(r) taken from *reconstructed voxels* can be fit to multiphase models of amorphous, nano-cluster, and crystalline states

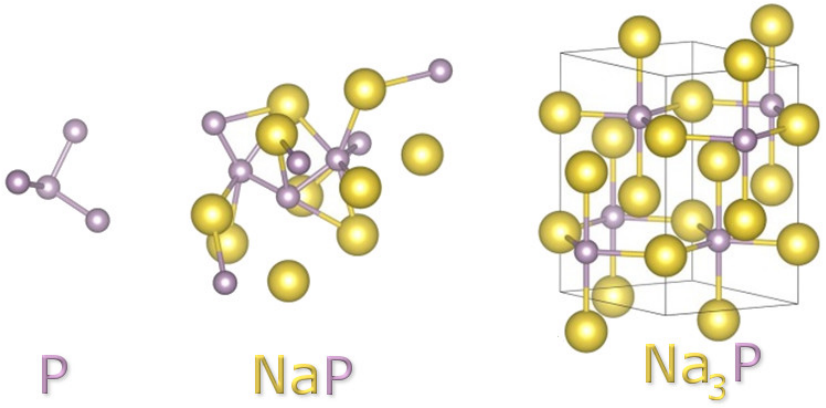

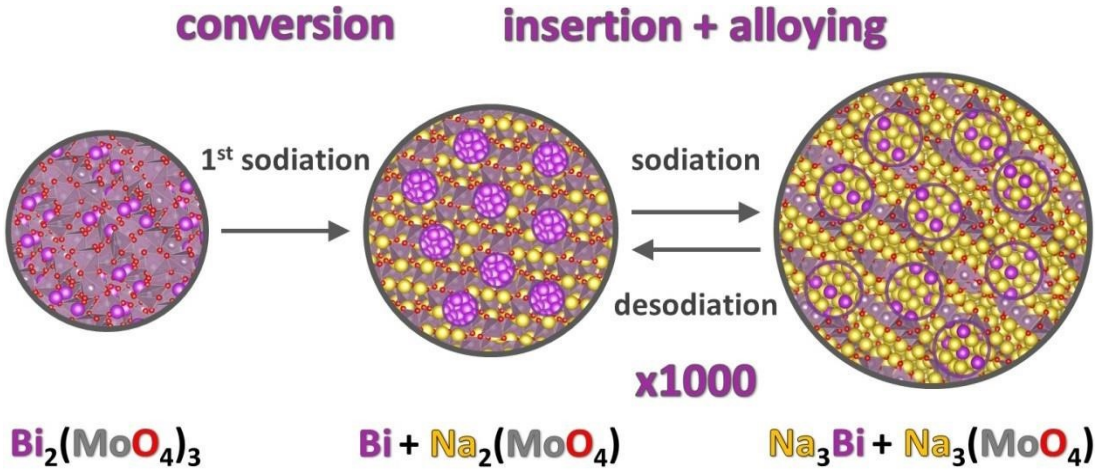

G(r) taken from reconstructred voxels can be fit to multiphase models of amorphous, nano-cluster, and crystalline states

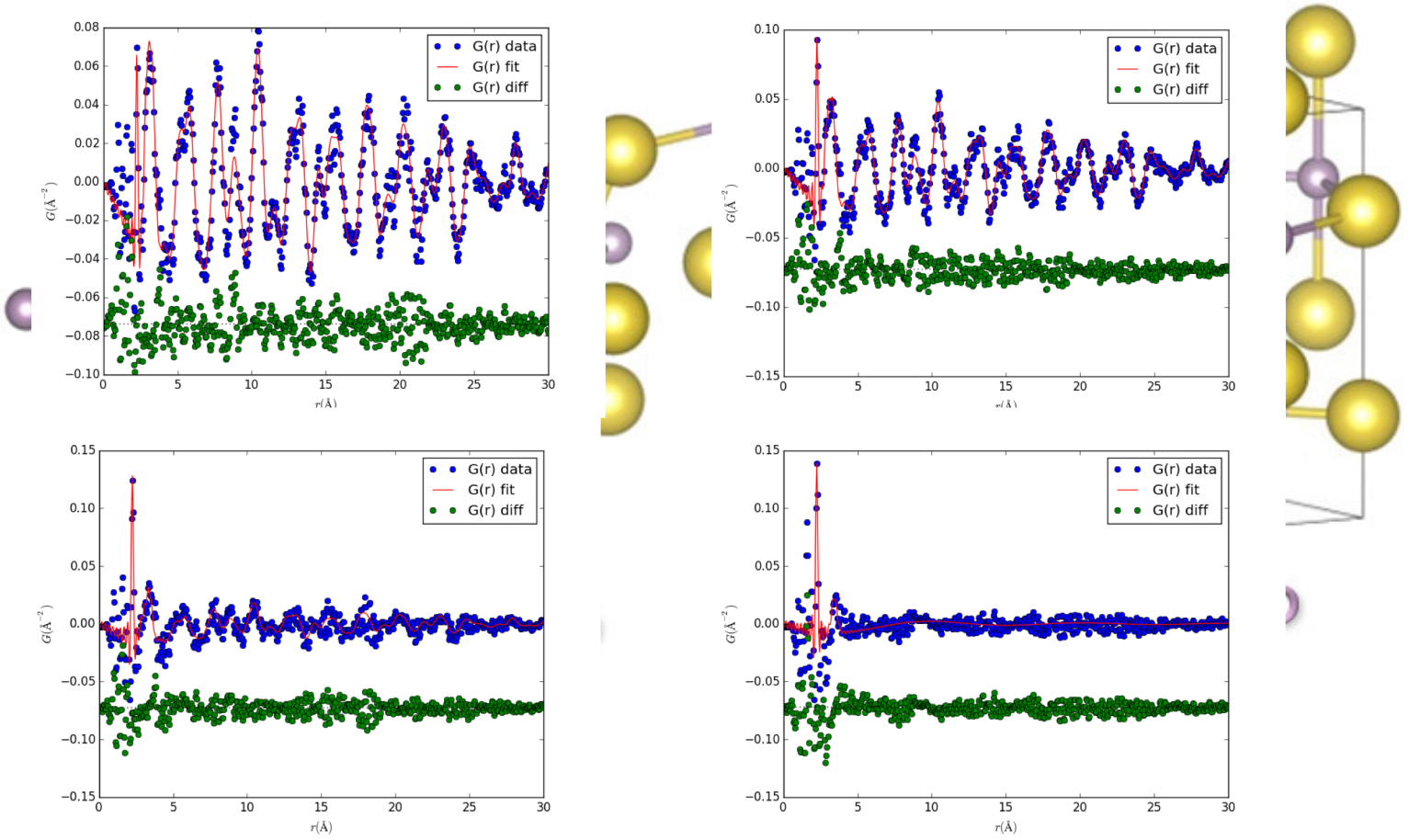

EVOLUTION OF STRUCTURE

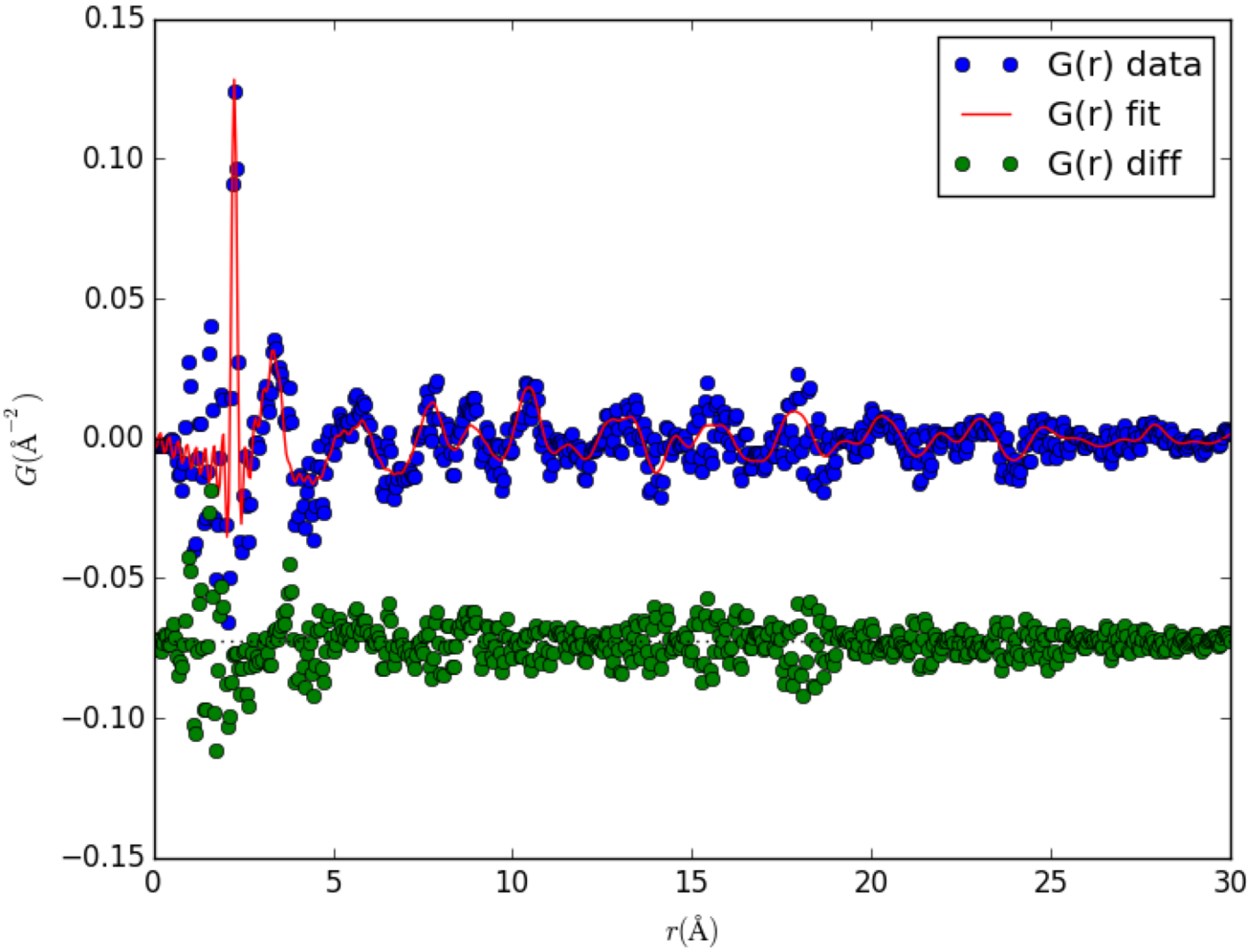

FOLLOW PHASE EVOLUTION

Using the G(r), it is possible to follow the phase evolution of multiphase systems, whether the phases are crystalline, nano-crystalline or amorphous

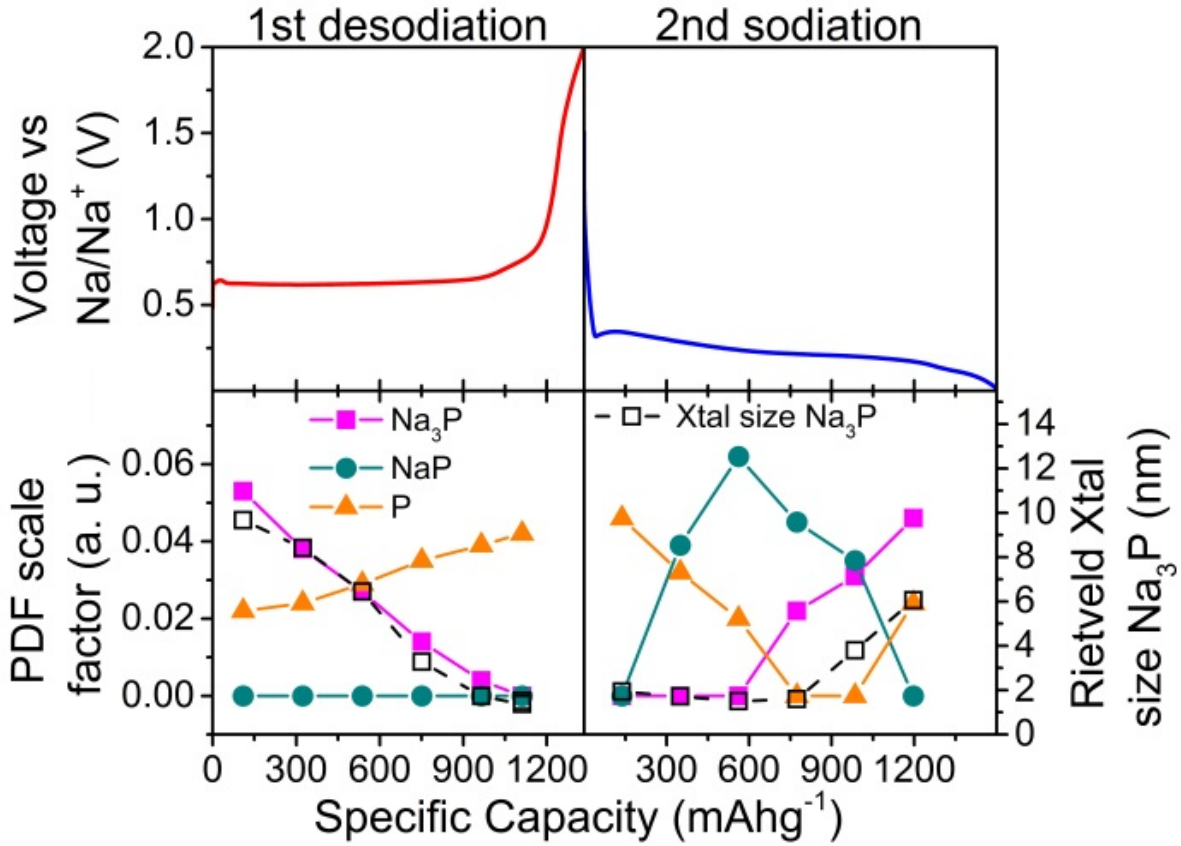

The observed voltometric behaviour can be understood via the supression of phase formation depending on rate

Sottman et al Angw. Chem. 2017.

POST ID15A REFURBISHMENT DATA (6 PHASES/MORPHOLOGIES)

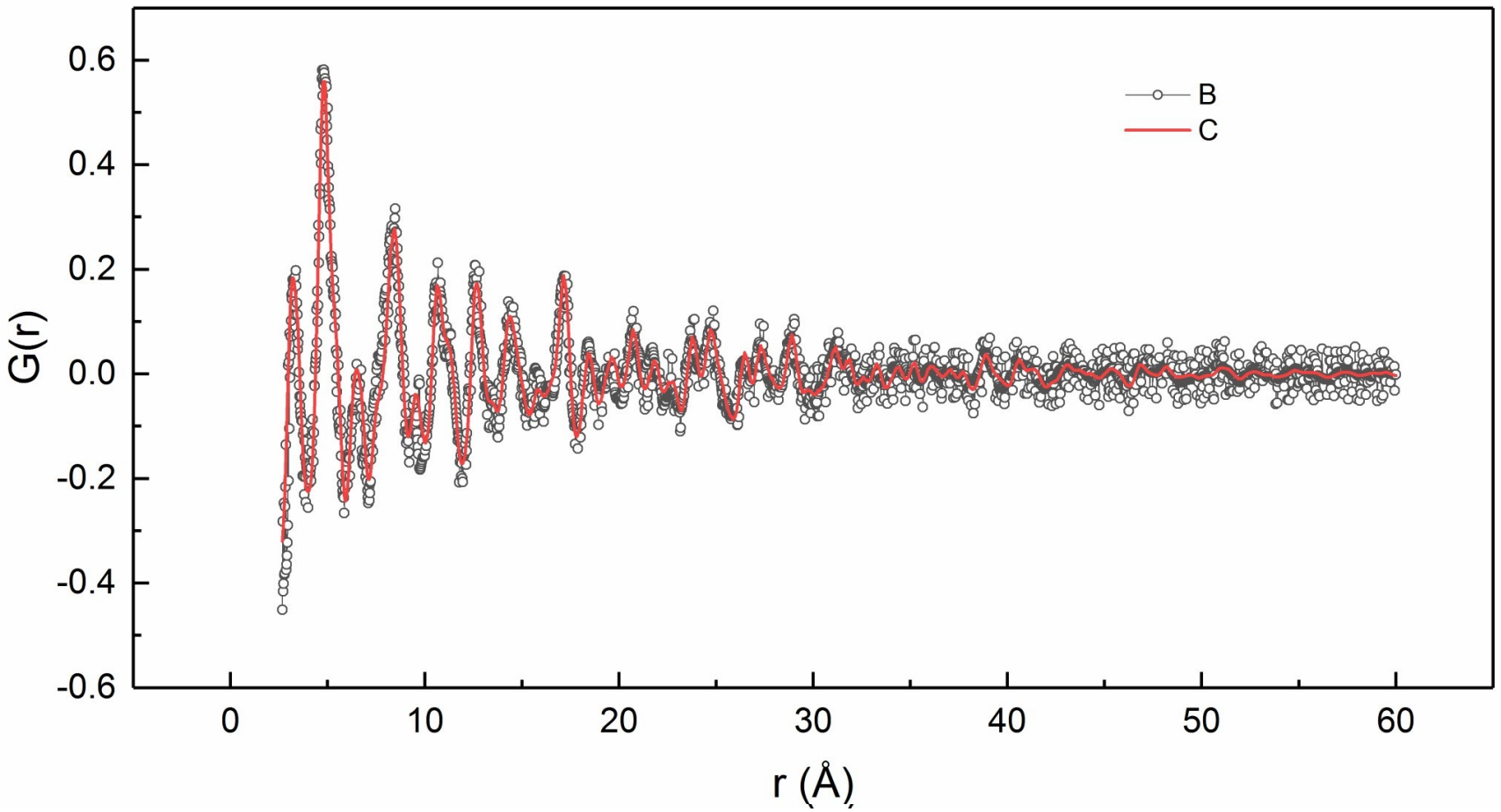

Wragg et al. in preparation

FIT TO G(R) IN RECONSTRUCTED VOXEL (6 PHASES/MORPHOLOGIES)

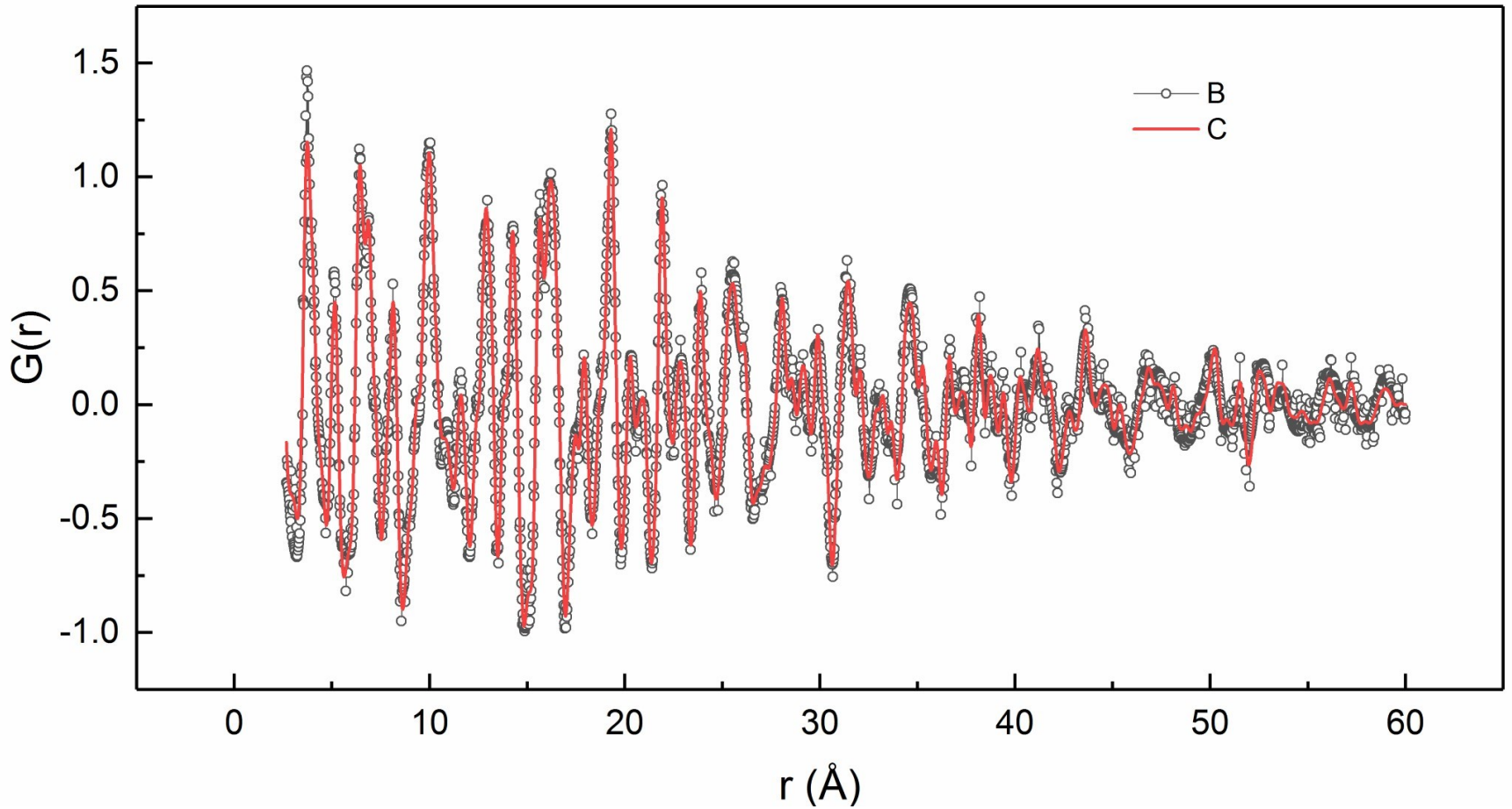

Wragg et al. in preparation

POST UPGRADE DATA

These data allow the tracking of the evolution of the phases, both with respect to their chemistry and to their microstructure as a function of electrochemical state

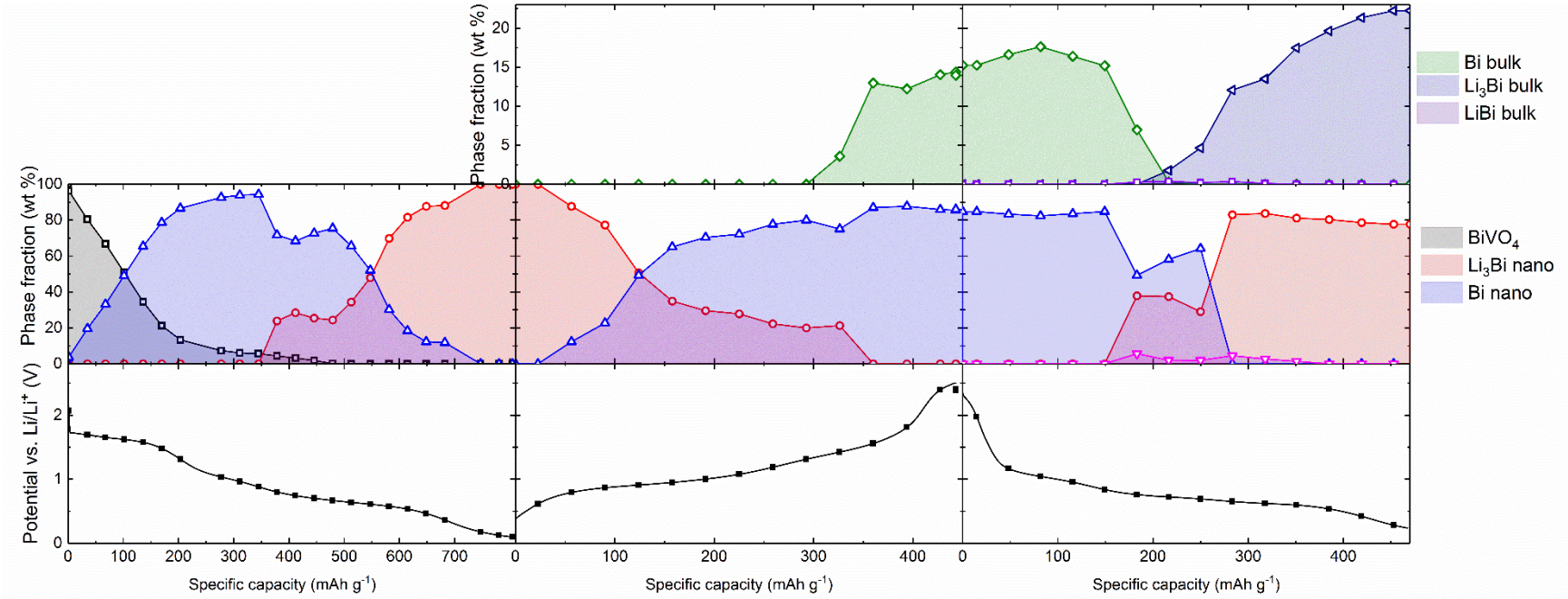

The microstructural model could be verified by TEM

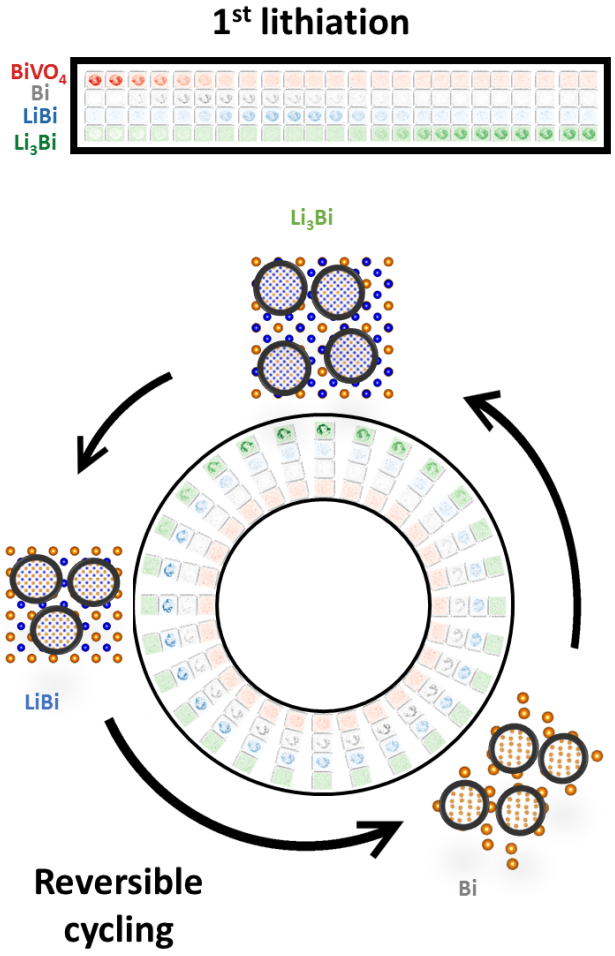

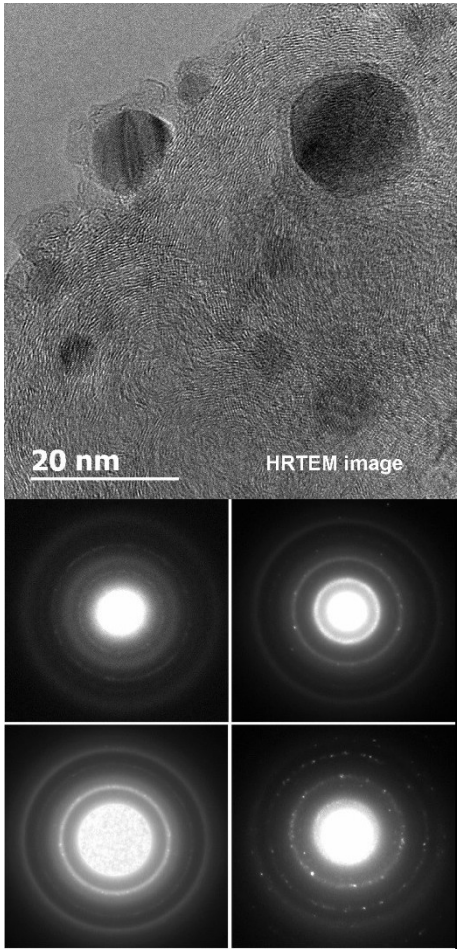

Wragg et al. in preparation

INTERGROWTH OF POLYMER MELTS

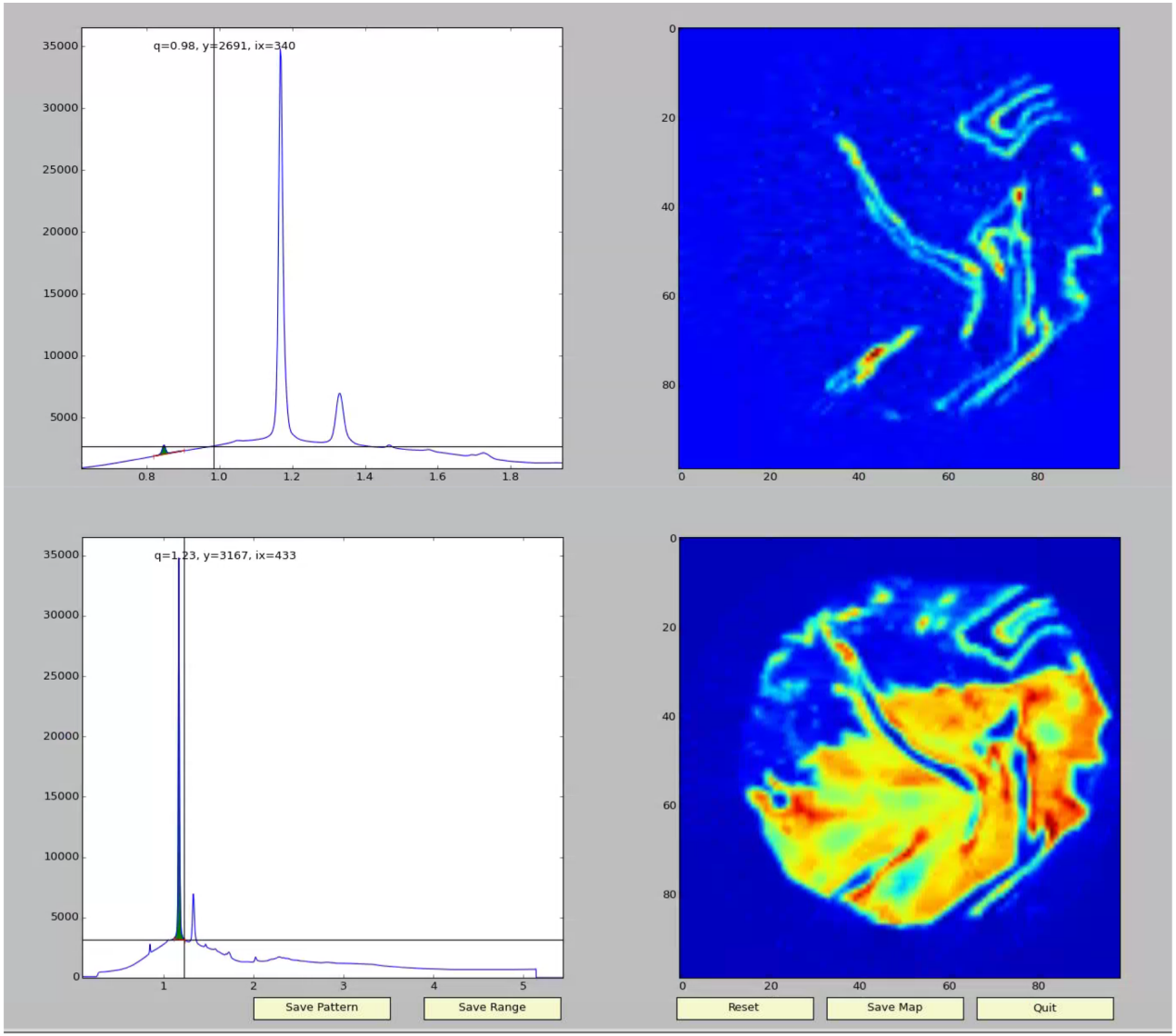

INTERGROWTH OF POLYMER MELTS

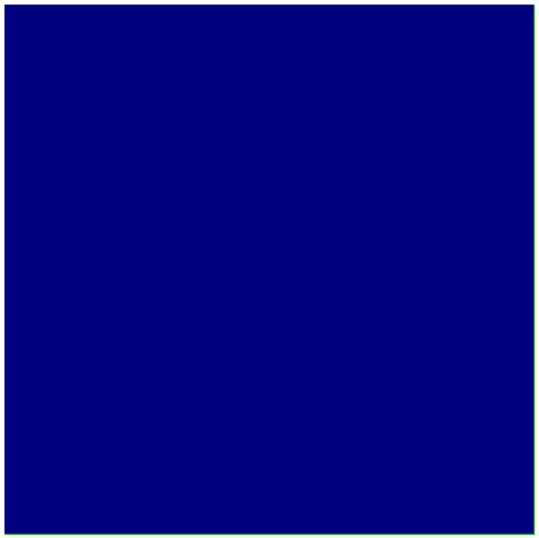

Amorphous Fraction

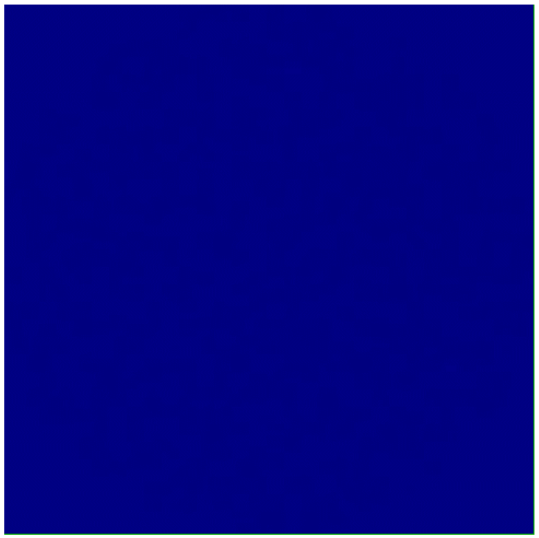

Phase 1

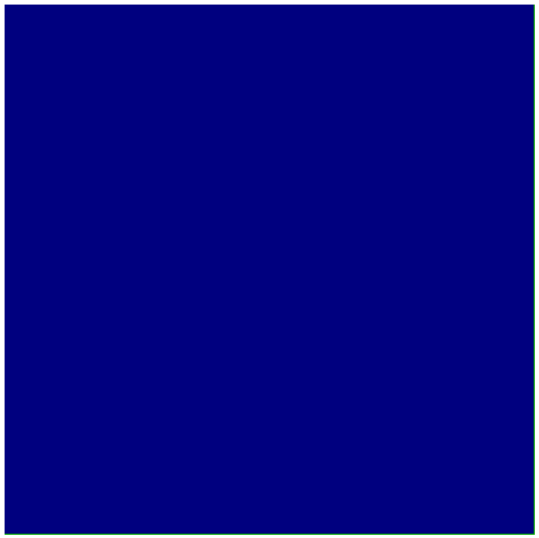

Phase 2

Srnis et al, ACS Applied Polymer Materials, 2019

RESTORATION OF THE MARY ROSE

The Mary Rose was a large (500 crew) ship in the Fleet of Henry VIII of England

RESTORATION OF THE MARY ROSE

The Mary Rose sunk in battle off the south coast of England, and was lost Until 1971…

RESTORATION OF THE MARY ROSE

Rediscoverd in 1971 and recovered in 1982 (half of the hull and 1900 artifacts) and subjected to preservation efforts (sprayed with PEG to stabilize mechanically)

MARY ROSE

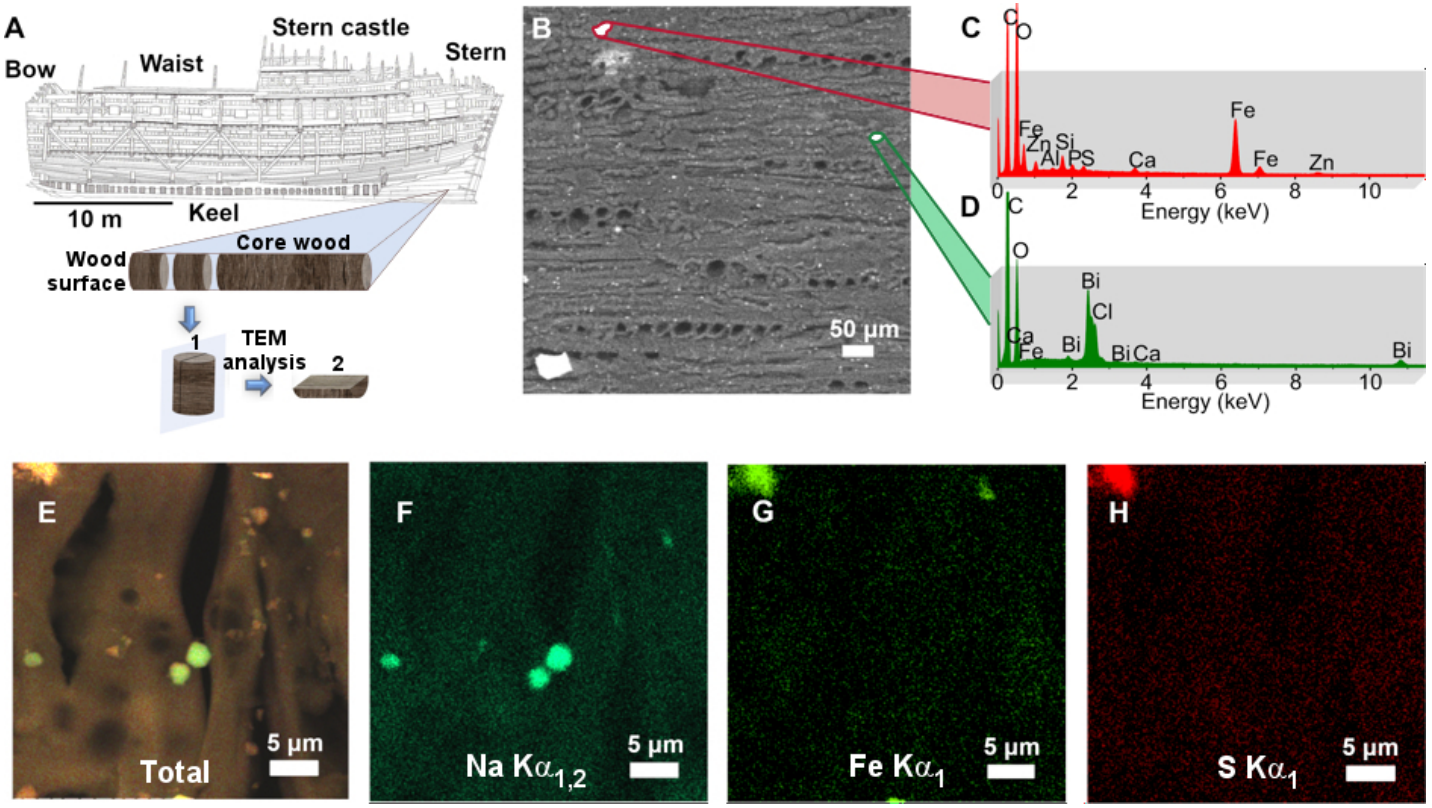

BSE images reveal the presence of iron-sulfur compounds, and sodium salts within the wood structure, though not the complete nature of the particles and therefore insight into their chemistry.

MARY ROSE

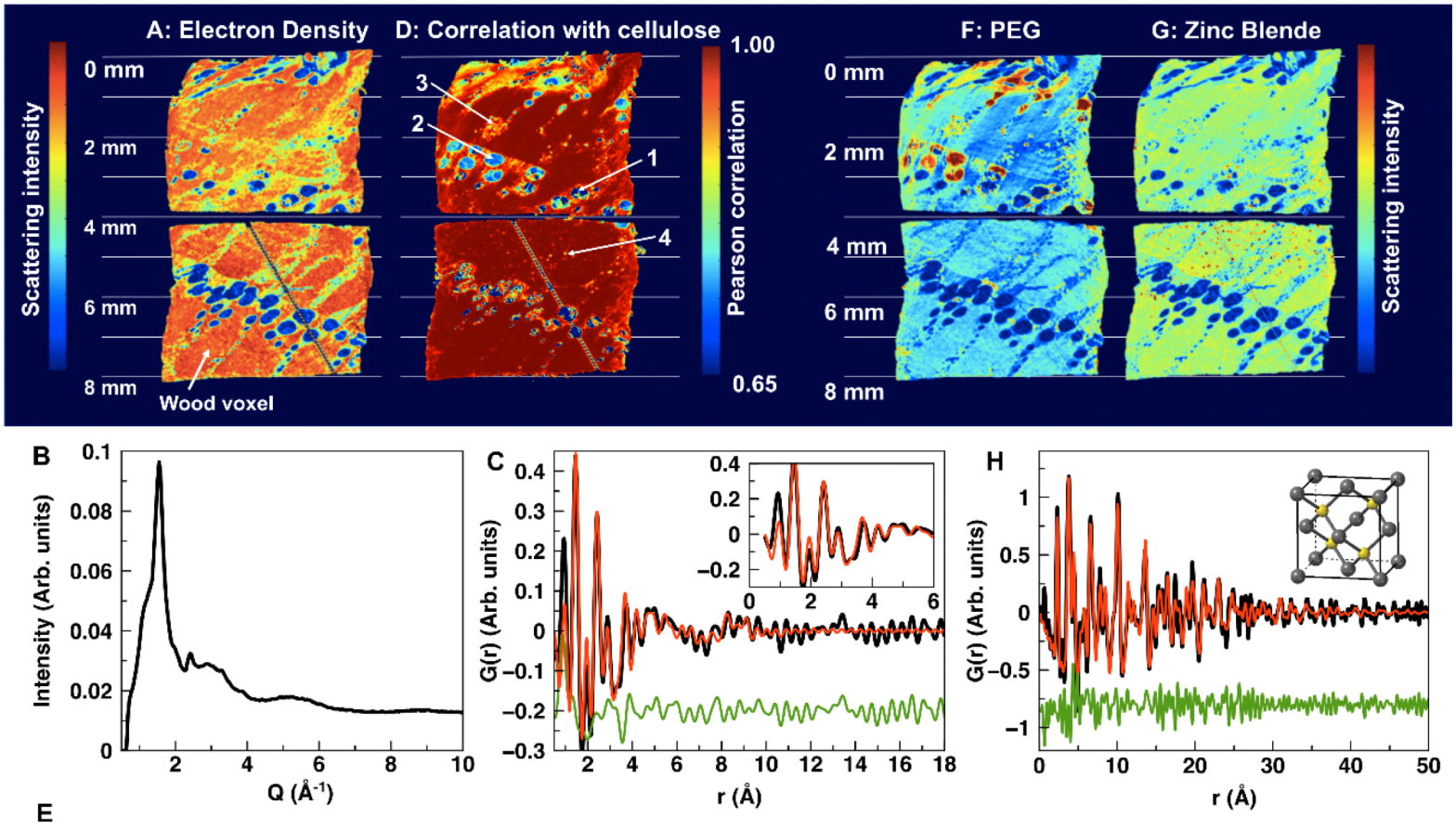

Wood sections were mapped by PDF-CT and a number of crystalline and nanocrystalline phases identified, elucidating the chemistry the hull material continues to undergo

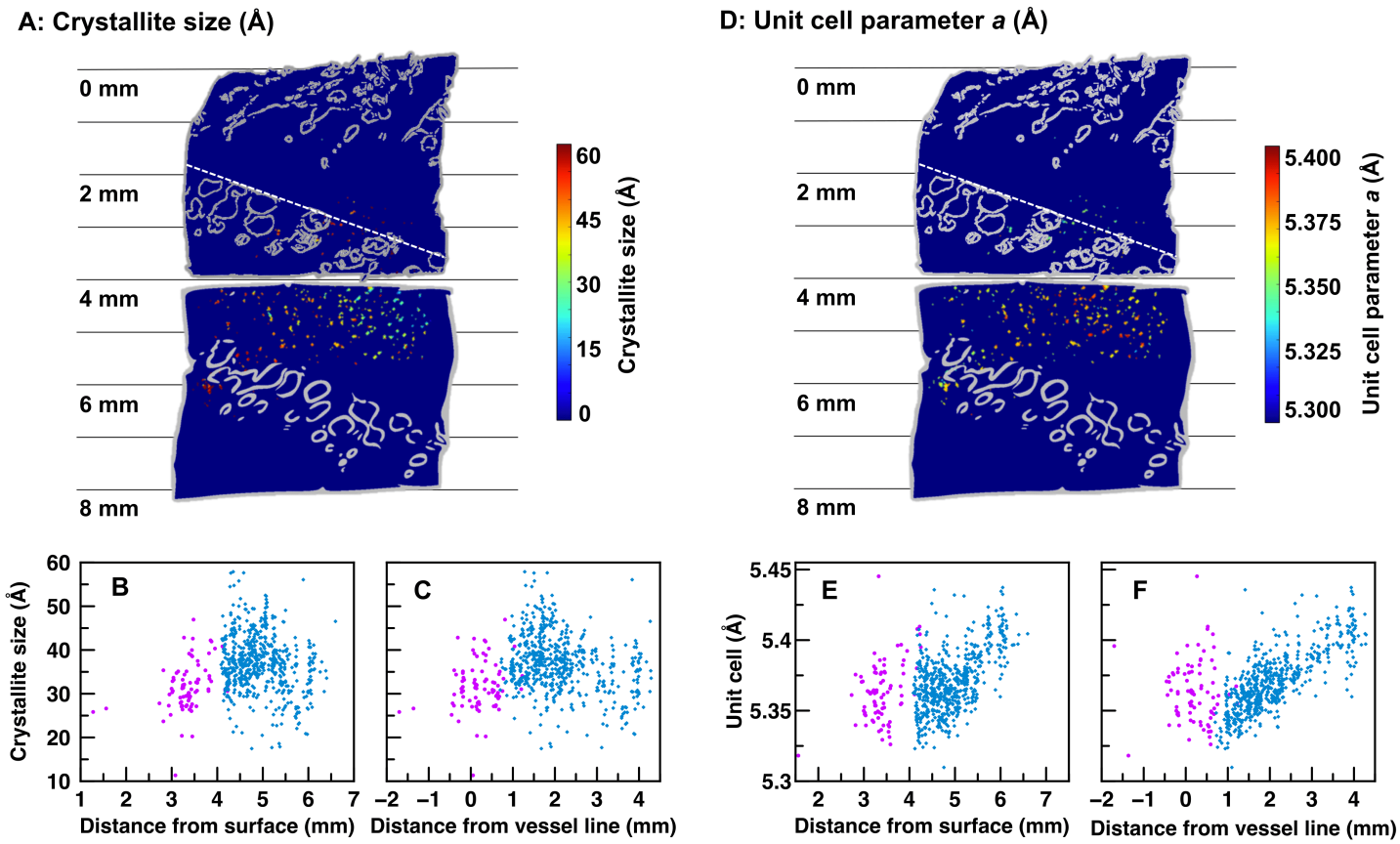

Using image correlation techniques to mine the 4d space, unexpected phases (Zn(Fe)S, crystalline PEG…) and their microstructure distribution characterized.

Corr et al., Nature Lett. In press

CONCLUSIONS

- **These methods have been extensively developed in the last decade**
  - Analytically
  - Experimentally
- **It's now possible to quantitatively characterize amorphous materials even in disadvantageous circumstances**
- **With spatial and temporal resolution**